



Inês Gaspar Melo e Castro Costa de Sousa

Bachelor in Micro and Nanotechnologies Engineering

Plasma Sanitizers on Flexible Substrates

Dissertation submitted in partial fulfillment
of the requirements for the degree of
Master of Science in
Micro and Nanotechnologies Engineering

Orientador: Dr. Diana Filipa Pereira Gaspar
Senior Researcher of Almascience

Co-Orientador: Prof. Dr. Luís Miguel Nunes Pereira
Associate Professor of Universidade NOVA de Lisboa

Júri:

Presidente: Prof. Dr. Rodrigo Martins

Arguente: Prof. Dr. Joana Sarmiento

Vogal: Prof. Diana Gaspar



FACULDADE DE
CIÊNCIAS E TECNOLOGIA
UNIVERSIDADE NOVA DE LISBOA

Plasma Sanitizers on Flexible Substrates

Copyright © Inês Gaspar Melo e Castro Costa de Sousa, Faculdade de Ciências e Tecnologia, Universidade Nova de Lisboa, 2020.

A Faculdade de Ciências e Tecnologia e a Universidade Nova de Lisboa têm o direito, perpétuo e sem limites geográficos, de arquivar e publicar esta dissertação através de exemplares impressos reproduzidos em papel ou de forma digital, ou por qualquer outro meio conhecido ou que venha a ser inventado, e de a divulgar através de repositórios científicos e de admitir a sua cópia e distribuição com objetivos educacionais ou de investigação, não comerciais, desde que seja dado crédito ao autor e editor.

“Whether You Think You Can Or Think You Can’t, You’re Right.”

–By Henry Ford

Acknowledgment

Finishing this master's thesis marks the end of a chapter in my life. It is an important step for me that would not be possible without the support of some people who accompanied me, who motivated me, and always believed in my abilities.

I am incredibly grateful to my thesis advisor, Professor Diana Gaspar, and my co-advisor, Professor Luís Pereira, for all that they taught me and for making everything happen without ever allowing discouragement to settle, even when things were not going well. They trusted me, advised me, allowed me to get out of my comfort zone, and have guided me in the best possible way, providing me with all the tools to work along this thesis.

I would also like to thank Professor Aaron and his team because, despite the warnings that this time brought us, they were always available to help and advise me during this thesis.

Many thanks to Professor Cristina Gaspar, who also helped me by providing that inkjet printing generators were made.

I want to show some appreciation to Professor Rodrigo Martins, who, together with Professor Elvira Fortunato, founded this course and gave us the opportunity to follow our dreams and work hard to be the Engineers of the future.

I also want to thank Sara Silvestre for all the advice and time she spent helping me doing the shadow masks. Moreover, to Inês Cunha, Paul Gray, Goncalo Narciso, Xavier Mascarenhas, and Pedro Centeno, who were always available to clarify my doubts and make me laugh when I needed to.

I want to thank and dedicate this work to my family, parents, sister, grandparents. Without their support and help, none of this would be possible.

To all the incredible friends I made during my academic career. Carolina, Ivânia, Maria Francisca and Tânia, I am very lucky to have you in my life, you are the best friends that anyone could ask for. Francisca and Tânia, I am thrilled to have entered this adventure together, and it is promised here that we all have to go on a trip to the United States. Thanks to Xavier and Tomás for all these years of great help and support that you have given me, we have always done everything together, and I have always learned a lot from you. To my Bruno, Dmytro, Filipe, Juju, and Zé for being incredible people and excellent friends, I loved spending these years with you, and I hope that many more adventures will come. To my dear ones Alentejano, Chaby, Diogo, Luís, Mariana and Ricky, also a big thanks for all the friendship and good times that provided me.

Finally, a big thanks to my best friends ever, Mafalda, Rita, Quaresma, and Natacha, who were always there to help me overcome all problems and always ready to listen to me. Also, Tatiana, Gandum, Ameixa, Palas, Guida, Kiko, Alex, and Freches, thank you for everything. Besides, a special thanks to Tiago, who was the one who supported me most during this final phase.

1. Abstract

Technologies related to low-temperature plasma have gained tremendous importance in recent years due to the numerous advantages they present. These types of treatments allow modifying surfaces without changing their volume properties, in a durable way and according to affordable processes. The mixture of reactive species that cold plasma produces also makes it possible to disinfect surfaces and treat biological tissues. However, the existing cold plasma production techniques are expensive, polluting, and use rigid components that cannot conform to irregular surfaces. To overcome those limitations, this dissertation's objective consists of production, optimization, and testing plasma generators that take advantage of the principle of dielectric barrier discharge (DBD).

The generators developed were produced by two methods, a laser made shadow mask and inkjet printing process, and consist of a structure with one or two electrodes. Three different types of paper were used as the DBD dielectric layer: two commercial papers used for printed electronics, Felix Schoeller smart type 3 and Powercoat™ XD 125, and a third one mostly used for drawing purposes, Canson vegetal paper.

It has been proven that generators patterned by a laser made shadow mask and by inkjet printing can generate plasma in a vacuum chamber, in a pressure range of 0.55 to 10.5 Torr (23 to 1400 Pa) and with a power range from 2 to 16W. It is shown that generators with two electrodes can confine plasma better than the ones using a single electrode. Also, it was observed that the gas atmosphere, patterning method, and structure of the paper influences the lifetime of the paper-based generators. Moreover, it was noticed that the generators made with vegetal paper and powercoat XD paper withstand for a longer period of time.

The use of plasma generators for surface modification was tested on different surfaces. The wettability of cork, vegetal paper, and spinach leaf surfaces was assessed for different plasma times.

Keywords: low-temperature plasma, dielectric barrier discharge, plasma generators, reactive species, surface modification.

2. Resumo

As tecnologias relacionadas com o plasma de baixa temperatura ganharam muita importância nos últimos anos devido às inúmeras vantagens que apresentam. Estes tipos de tratamentos permitem modificar superfícies sem alterar suas propriedades em volume, de forma duradoura e de acordo com processos acessíveis. A mistura de espécies reativas que o plasma frio produz também permite desinfetar superfícies e tratar tecidos biológicos. No entanto, as técnicas de produção existentes são caras, poluentes e utilizam componentes rígidos incapazes de se conformar sob as mais diversas irregularidades.

Com o intuito de responder às limitações apresentadas, o objetivo da presente dissertação consiste na produção, otimização e teste de geradores de plasma que tiram partido do princípio da descarga de barreira dielétrica (DBD). Os geradores desenvolvidos foram produzidos por gravação de padrões a laser e por impressão a jato de tinta, e são compostos por uma estrutura com um ou dois eletrodos. Três tipos de papéis diferentes foram utilizados como camada dielétrica do DBD, dois papéis comerciais usados para eletrônica impressa, Felix Schoeller smart type 3 e Powercoat™ XD 125, e um terceiro usado principalmente para desenho (papel vegetal Canson).

Foi provado que os geradores padronizados por uma máscara feita a laser e por impressão a jato de tinta podem gerar plasma numa câmara de vácuo segundo uma gama de pressão de 0.55 a 10.5 Torr (23 a 1400 Pa) e com uma gama de potência de 2 a 16W. Comprovou-se também que os geradores com dois eletrodos conseguem confinar melhor o plasma do que os geradores com um único eletrodo. Foi ainda observado que o tipo de gás, o método de padronização e a estrutura do papel influenciam o tempo de vida útil dos geradores. Para além disso, observou-se que os geradores produzidos com papel vegetal e papel powercoat XD conseguem suportar maiores períodos de tempo a gerar plasma.

O uso de geradores de plasma para modificação de superfície foi testado em diferentes superfícies. A molhabilidade das superfícies da cortiça, do papel vegetal e das folhas de espinafre foi avaliada para diferentes tempos de plasma.

Palavras-chave: plasma de baixa temperatura, descarga de barreira dielétrica, geradores de plasma, espécies reativas, impressão por laser, modificação de superfícies.

3. Abbreviations

AC	Alternating Current
ATR	Attenuated Total Reflectance
COVID-19	Severe Acute Respiratory Syndrome Coronavirus
DBD	Dielectric Barrier Discharge
DC	Direct Current
DPI	Dots Per Inch
EDX	Energy Disperse X-ray
FS	Felix Schoeller smart paper type 3
FTIR	Fourier Transform Infrared Spectroscopy
LTP	Low-Temperature Plasma
OES	Optical Emission Spectroscopy
RF	Radio frequency
RFID	Radio Frequency Identification Devices
RMS	Root Mean Square
RONS	Reactive Oxygen and Nitrogen Species
SCCM	Standard Cubic Centimeters per Minute
SEM	Scanning Electron Microscope
TGA	Thermogravimetric Analysis
ULS	Universal Laser System
VEG	Canson Vegetal Paper
XD	Powercoat™ XD 125
XDR	X-ray Diffraction

4. Symbols

P	Pressure
P%	Porosity
P_{base}	Base Pressure
P_{gas}	Gas Pressure
V	Voltage
W	Watt
θ	Bragg Angle
<i>ρ_{cellulose}</i>	Cellulose Density
<i>ρ_{sample}</i>	Apparent Density of the Sample

| Contents

1 	Introduction	1
1.1	The Fourth State of Matter	1
1.2	Dielectric Barrier Discharge	2
1.3	LTP Applications	2
1.4	Plasma Generators.....	3
1.4.1	Paper-based Plasma Generators.....	4
2 	Materials and Methods	6
2.1	Characterization techniques.....	6
2.1.1	X-Ray Diffraction	6
2.1.2	Thermogravimetry	6
2.1.3	Porosity	6
2.1.4	Scanning Electron Microscopy	6
2.1.5	Fourier Transform Infrared Spectroscopy.....	6
2.2	Production of the plasma generators	6
2.2.1	Shadow mask patterning by laser engraving	6
2.2.2	Electron beam evaporation deposition	7
2.2.3	Inkjet printing method	7
2.3	Plasma Generation	7
2.3.1	Optical Emission Spectroscopy	7
2.3.2	Contact Angle.....	7
3 	Results and Discussion	8
3.1	Characterization techniques of the papers	8
3.1.1	Papers characterization	8
3.1.2	Paper structure and thermal properties.....	9
3.2	Plasma generator configurations.....	10
3.3	Plasma generation process.....	10
3.4	Plasma generation study.....	11
3.4.1	Argon Atmosphere.....	12
3.4.2	Air Atmosphere	17
3.4.3	Influence of the atmosphere on the plasma generation	18
3.5	Stability of the plasma and Plasma Reactive Species study	19
3.6	Inkjet printing tests.....	21

3.6.1	Inkjet FS generator (600DPI two layers)	22
3.6.2	Inkjet FS generator (700DPI)	24
3.6.3	Silver deposition on shadow mask patterning by laser engraving	24
3.7	Surface modification tests.....	25
4 	Conclusions and Future perspectives	29
5 	Bibliography.....	30
	Annex.....	34
A.1	Parameters of the deposition of aluminum in the generator's design by a laser made shadow mask.....	34
A.2	Images of the Jiusion digital microscope of the generator's design by a laser made shadow mask	35
A2.1	Generator with Felix Scholler paper	35
A2.2	Generator with Canson Vegetal paper	35
A2.3	Generator with Powercoat™ XD paper	36
B.1	Properties of the inkjet printing method	37
B.2	Images of the Jiusion digital microscope of the generators produced by inkjet printing 38	
B2.1	Generator with Vegetal paper	38
i	Inkjet VEG 200DPI (first layer) and 300DPI (second layer).....	38
ii	Inkjet VEG 200DPI (first layer) and x2 300DPI (second layer)	38
iii	Inkjet VEG 400 DPI	39
B2.2	Generator with Felix Scholler paper	39
i	Inkjet FS 600DPI (two layers)	39
ii	Inkjet FS 700 DPI	40
C.	Properties of the different papers	41
C.1	Felix Scholler type 3 smart paper datasheet.....	41
C.2	Powercoat™ XD 125 datasheet.....	42
D.	Plasma generation optimization study.....	43
D.1	Argon Atmosphere: Generator with FS paper	43
D.2	Argon Atmosphere: Generator with VEG paper	44
D.3	Argon Atmosphere: Generator with XD paper	45
E.	Plasma generation study	46
E.1	Argon Atmosphere: Generator with XD paper	46
E.2	Air Atmosphere: SEM images from the generator with VEG paper	47

E.3	Air Atmosphere: SEM images from the generator with XD paper.....	47
E.4	Air Atmosphere: ATR-FTIR of the generators before and after plasma	48
E.5	Comparison between argon and air atmosphere: DC-bias versus Power graph.....	48
F.	Plasma generation time tests and OES.....	49
F.1	Optical emission spectroscopy: Generator with XD paper	49
G.	Inkjet printing tests	50
G.1	(200DPI (first layer) and x2 300DPI (second layer))	50
G.2	400 DPI	50
G.3	SEM images from the inkjet generator with FS (700 DPI).....	51
G.4	OES graphs from the inkjet generators with FS	51
G.5	Test from silver laser-based pattern engraving generators.....	52
G.6	SEM images from the top view of silver generators.....	53
G.7	OES graphs from the silver generators	54
G.8	Photos of silver FS generator	55
G.9	Photos of silver VEG generator	55
G.10	Photos of silver XD generator	56
H.	Surface modification study	57
H.1	Photos of the surfaces studied in the vacuum chamber	57
H.2	Time optimization tests on spinach leaf	58
H.3	Contact angle as function of plasma treatment time graph.....	58

| List of Figures

Figure 1.1 - Order in which state transitions occur by increasing temperature/energy [8].	1
Figure 1.2- Plasma generators: (A) DBD device; (B) plasma jet [48].	3
Figure 1.3 - Cheng-Che Et al plasma generator on a paper substrate among various orientations [49]	5
Figure 1.4- Aaron et al. plasma generator structure (A) and generators with and without applied potential (B) [50].	5
Figure 2.1 - (A) Sheet of paper was covered with Kapton; (B) Pattern engraved on the Kapton; (C) Kapton's interior was removed for aluminum deposition. The 50-cent coin was used for scale purposes (diameter of 24.25mm).	6
Figure 2.2 – Photos of the generators: (A) Before the aluminum deposition; (B) After the aluminum deposition; (C) Kapton removed.	7
Figure 3.1 - SEM images of the top view of the different papers: (A) FS; (B) VEG; (C) XD.	8
Figure 3.2 - XRD characterization of FS, VEG, and XD; TGA curves of FS, VEG, and XD.	9
Figure 3.3 - Schematics of the generator configurations used: (1) One electrode; (2) Two electrodes.	10
Figure 3.4 – Schematic representation of the apparatus used for the plasma generation experiments: vacuum chamber with a generator placed on the glass support, connected with the generator and the OES system.	10
Figure 3.5 - VEG generators with (A) one electrode and (B) two electrodes during the plasma generation.	11
Figure 3.6 - Plasma generation test with the Felix Scholler generator in an argon atmosphere. DC-bias represented in blue. The duration of the plasma generation was 8 minutes.	12
Figure 3.7 - (A) FS generator before plasma generation; (B) and (C) FS generator after plasma generation; (D) Thermal analysis of the FS generator after plasma. Study made in argon atmosphere.	12
Figure 3.8 - SEM images from FS generator of the top and cross-sectional views before and after the plasma generation. Study in argon atmosphere. Plasma time of 8 minutes.	13
Figure 3.9 - Plasma generation test with the vegetal paper generator in argon atmosphere. DC-bias represented in blue. Plasma time of 50 minutes	13
Figure 3.10 - VEG generator before plasma generation; (B) VEG generator after plasma generation; (D) Thermal analysis of the VEG generator after plasma. Study in argon atmosphere.	14
Figure 3.11 - SEM images from VEG generator of the top and cross-sectional views before and after the plasma generation. Study in argon atmosphere.	14
Figure 3.12 - XD generator before plasma generation; (B) XD generator after plasma generation; (D) Thermal analysis of the XD generator after plasma. Study in argon atmosphere.	15
Figure 3.13 - SEM images from XD generator of the top and cross-sectional views before and after the plasma generation. Study in argon atmosphere.	15
Figure 3.14 - ATR-FTIR spectrum before and after the plasma generation in argon of the papers: FS paper 8 minutes of plasma, (B) VEG paper 50 minutes of plasma, and (C) XD paper 44 minutes of plasma.	16
Figure 3.15 - Plasma generation test with the VEG generator in air atmosphere. DC-bias represented in blue. Plasma time of 6 minutes.	17
Figure 3.16 - Picture from the thermal camera. Thermal analysis from a generator with VEG paper in air atmosphere.	17
Figure 3.17 - Plasma generation test with the XD generator in air atmosphere. DC-bias represented in blue. Plasma time of 6 minutes.	18

Figure 3.18 - Picture from the thermal camera. Thermal analysis from the generator with XD paper in air atmosphere.	18
3.19 - Photographs of paper generators of VEG paper after plasma generation time test. DC-bias represented in blue.	19
Figure 3.20 - Picture from the thermal camera. Thermal analysis from a generator with VEG paper in argon after time generation tests.	19
Figure 3.21 - OES spectrum of VEG generator during time tests.	20
Figure 3.22 - Photographs of paper generators of XD paper after plasma generation time test. DC-bias represented in blue.	21
Figure 3.23 - Picture from the thermal camera. Thermal analysis from a generator with XD paper in argon after time generation tests.	21
Figure 3.25 - Plasma generation tests with the inkjet FS generator (600DPI two layers). DC-bias represented in blue.	22
Figure 3.26 - Photograph of inkjet FS generator (600DPI): (A) before plasma, (B), and (C) after plasma generation.	22
Figure 3.27 - SEM images from inkjet generator FS (600DPI) of the top view before and after the plasma generation.	23
Figure 3.28 - OES spectrum of FS inkjet generator 600DPI.	23
Figure 3.29 - Plasma generation tests with the inkjet FS generator (700DPI). DC-bias represented in blue. ...	24
Figure 3.30 - Photograph of inkjet FS generator (700DPI): (A) before and (B) after plasma generation.	24
Figure 3.31 - SEM images from cork surface top view before and after 45 seconds of plasma generation. ...	27
Figure 3.32 - SEM images from vegetal paper surface top view before and after 45 seconds of plasma generation.	27
Figure 3.33 - SEM images from spinach leaf top view before and after 45 seconds of plasma generation.	27
Figure 3.34 - ATR-FTIR spectrum before and after 45 seconds of plasma generation of the different surfaces: (A) cork; (B) vegetal paper and (C) spinach leaf.	28
Figure A.1 - Images of the Jusion digital of FS generator design by a laser made shadow mask. ...	35
Figure A.2 - Images of the Jusion digital of VEG generator design by a laser made shadow mask.	35
Figure A.3 - Images of the Jusion digital of XD generator design by a laser made shadow mask. ...	36
Figure B.1 - Photographs of the generators made by inkjet printing. A 5-cent coin for scale purposes (21.25mm in diameter).	37
Figure B.2 - Images of the Jusion digital of VEG 200DPI generator made by inkjet method.	38
Figure B.3 - Images of the Jusion digital of VEG 200DPI and 300 DPI generator made by inkjet method.	38
Figure B.4 - Images of the Jusion digital of VEG 400DPI generator made by inkjet method.	39
Figure B.5 - Images of the Jusion digital of FS 600DPI generator made by inkjet method.	39
Figure B.6 - Images of the Jusion digital of FS 700DPI generator made by inkjet method.	40
Figure C.1 - Felix Scholler type 3 smart paper datasheet.	41
Figure C.2- Powercoat™ XD 125 datasheet.	42
Figure D.1 - Plasma generation optimization test with a FS generator in an argon atmosphere.	43

Figure D.2 - Photograph of the FS generator after the optimization test in an argon atmosphere.	43
Figure D.3 - Plasma generation optimization test with a VEG generator in an argon atmosphere. ..	44
Figure D.4 -- Photograph of the VEG generator after the optimization test in an argon atmosphere.	44
Figure D.5 - Plasma generation optimization test with a XD generator in an argon atmosphere.	45
Figure D.6 - Photograph of the XD generator after the optimization test in an argon atmosphere. ..	45
Figure E.1 - Plasma generation test with a XD generator in an argon atmosphere.	46
Figure E.2 - SEM images from VEG generator of the top view before and after the plasma generation in air atmosphere.....	47
Figure E.3 - SEM images from XD generator of the top view before and after the plasma generation in air atmosphere.....	47
Figure E.4 - ATR-FTIR spectrum before and after the plasma generation in argon of the papers:...	48
Figure E.5 - DC-bias vs Power graph: comparison between argon and air atmosphere.....	48
Figure F.1 - OES spectrum of XD generator during time tests.....	49
Figure G.1 - SEM images from VEG inkjet (200DPI and x2 300 DPI) generator of the top view before plasma generation.	50
Figure G.2 - SEM images from VEG inkjet (400 DPI) generator of the top view before plasma generation.....	50
Figure G.3 - SEM images from inkjet generator FS (700DPI) of the top view after the plasma generation.....	51
Figure G.4 - OES spectrum of FS inkjet generator 700DPI.	51
Figure G.5 - Plasma generation tests with the silver FS generator.	52
Figure G.6 - Plasma generation tests with the silver VEG generator.	52
Figure G.7 - Plasma generation tests with the silver XD generator.....	52
Figure G.8 - SEM images from silver FS generator of the top view before and after the plasma generation.....	53
Figure G.9 - SEM images from silver VEG generator of the top view before and after the plasma generation.....	53
Figure G.10 - SEM images from silver XD generator of the top view before and after the plasma generation.....	54
Figure G.11 - OES spectrum of silver generators: (A) FS , (B) VEG and (C) XD.....	54
Figure G.12 - Photograph of silver FS generator before and after plasma generation.	55
Figure G.13 - Photograph of silver VEG generator before and after plasma generation.....	55
Figure G.14 - Photograph of silver XD generator before and after plasma generation.	56
Figure H.1 - Photographs of the different surfaces in the vacuum chamber.....	57
Figure H.2 - Photographs of spinach leaf: (A) Without treatment; (B) with 5 minutes of vacuum; (C) with 2 min of plasma treatment.....	58
Figure H.3 - Graph of Contact angle in function of plasma treatment time.	58

| List of Tables

Table 3.1 - Properties of the different papers: FS, VEG, and XD.	9
Table 3.2 - Plasma generation parameters: pressure, power, P_{base} , P_{gas} , and argon flux.	11
Table 3.3 - Contact angle measurements in cork, vegetal paper, and spinach leaf samples without treatment, with vacuum, and with a plasma treatment of 15,30 and 45 seconds.	26
Table A.1- Parameters of the deposition of aluminum in the generator's design by a laser made shadow mask.	34
Table A.2- Data on the thickness, diameter, and height of the generator's design by a laser made shadow mask.	34
Table B.1 - Properties of the inkjet printing method with generators made with VEG and FS papers.	37
Table B.2 - Diameter and height of the generators made by inkjet printing method.	37

Motivation and Objectives

Nowadays, more and more information is gathered on low-temperature plasma treatments for medical and sanitizer purposes and surface modification. This approach provides a non-contact, painless and harmless treatment for the management of lesions in large areas due to its regenerating properties and is capable of eliminating microorganisms, such as bacteria and viruses [1]. It is important to bear in mind that delivering health care and sanitation at an affordable expense is one of the most important problems facing this century, according to the 2030 Agenda for Sustainable Development [2]. In this way, technologies that can improve the life quality at a reduced cost, such as plasma technology, would be of immense commercial and social benefit. Likewise, providing treatment of surfaces such as cork, paper, fabric, metal, food, and many others in a sustainable way and without chemicals or high temperatures is also extremely necessary due to the growing daily need for this type of treatment in the most varied modern industries. However, current manufacturing methods are costly, polluting, and use rigid components that cannot conform to irregular and intricate shapes. Therefore, this thesis emerges following the growing need to develop low-cost, conformable, disposable, and efficient low-temperature plasma generators made of recyclable material.

Currently, there is a strong interest in the scientific and industrial community in using cellulose-based materials for electronic applications. Cellulose-based papers are lightest, biodegradable, cheap substrates, and the main biopolymer on earth, of immense global economic importance [3]. Paper-based electronics are projected to positively impact environmental emissions caused by electronic waste [4]. In this way, cellulose-based papers seem to be an excellent bet for the development of plasma generators. Thereby, the objectives of this thesis are related to the fabrication of plasma generators with a focus on:

- Development of paper-based plasma generators according to the working principle of dielectric barrier discharge;
- Optimization of the generators' production process (shadow mask design by laser engraving and inkjet printing);
- Test of the plasma generators produced and study the best characteristics of each one;
- Study of the plasma produced by the paper generators and the generation parameters: pressure, power, DC-bias, and reactive species produced by the plasma;
- Study of surface modification caused by the generators in cork, vegetal paper, and spinach leaf.

1| Introduction

1.1 The Fourth State of Matter

The different types of matter can be identified as solid, liquid, gas, and, last but not least, plasma. Plasma is the fourth fundamental state of matter and was first described in 1920 by the chemist Irving Langmuir [5]. It is an ionized gas composed of a lot of species (including ions, electrons, radicals, non-radicals, ultraviolet photons, among others). In contrast to the other three states, plasma does not exist in normal conditions on the earth's surface but can be found in everyday life in particular circumstances (like fluorescent lamps and plasma monitors). However, in the universe, it is the most abundant state (99%) found in various natural phenomena (like lightning and northern lights) [6].

Most of the transitions to the different states occur in the following order: solids-liquids-gases-plasma (**Figure 1.1**). Plasma is generated when sufficient energy is supplied to gas to expel at least one electron from the outer shells of the gas constituents. So, the atomic layer breaks down, forming negatively and positively charged particles like electrons and ions, respectively. Although the plasma incorporates both positive and negative particles, it has a neutral character, as there are equal amounts of particles with opposite charges [7].

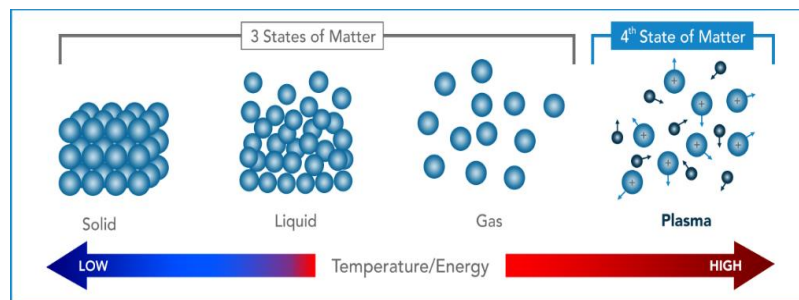


Figure 1.1 - Order in which state transitions occur by increasing temperature/energy [8].

Unlike the gaseous state that is electrically neutral, the plasma state is the best conductor of electricity and can respond to magnetic fields, being the highest energy state. Therefore, there are two different types of plasma depending on the environment and the conditions under which they are created: thermal or high-temperature (hot) plasma and low-temperature (cold) plasma. Hot plasmas (usually arc discharges and torches) are of the equilibrium type, which means all their particles share the same energy [9]. Low-temperature plasmas (LTP) exhibit electron energies far superior to other ions and neutral molecules. Because of the comparatively cold ions and neutrals, its temperature remains below 50°C and does no thermal damage to the items it comes into contact with [10]. This type of plasma is obtained using less energy than the hot plasma and generally by dielectric barrier discharge, corona discharge, brightness discharge, and spark discharge [11].

This function opened the possibility of using plasma to treat heat-sensitive materials, including biological materials such as cells and tissues.

In the scope of this thesis, only LTP will be addressed.

1.2 Dielectric Barrier Discharge

Among the multiple plasma generation sources, the dielectric barrier discharge (DBD) enables the obtention of one of the most cost-efficient LTPs. DBDs consist of electrical discharges that support themselves in electrode configuration, and their concepts are characterized in the discharge path through a dielectric material. An electrical discharge is the release and transmission of electricity in a gaseous medium due to the gas's ionization [12].

In its basic architecture, a DBD plasma source is composed of two electrodes, a dielectric material and the gap between electrodes is filled with gas [13]. The discharge gap (distance between the electrodes when the reaction occurs) is generally in the range of 0.1 to 10 mm for operating an LTP [14]. This process typically operates with most types of gases and mixtures as well as different waveforms of the alternating current (AC) over a wide range of pressure and frequency [15].

Plasma is generated when energy (usually high AC voltage) is applied to the active electrode so that the area around the electrodes forms an electric field to ionize the gas. In this process, electrons with higher energy are formed [16]. So, plasma sustainability depends on the voltage across the gap, which must exceed the gas's breakdown voltage. When this voltage is attained, the gas loses its dielectric properties and turns into a conductor. Plasma formation is explained by the transfer of energy and momentum from the charged particles to the neutral gas components [17].

A DBD unique property is that a dielectric layer covers at least one of the electrodes, and sometimes both. The dielectric layer is the key to the proper functioning of the discharge. A dielectric is an electrical insulator that, under the action of an external electric field above the limit of its dielectric strength, allows the flow of electric current. This layer is vital in DBD devices because it can limit the current flow and the temperature of the discharge, prevent the occurrence of a plasma arc (forming a glow discharge) and distributes the discharge over the whole electrode area uniformly [18]. Dielectric materials such as glass, quartz, ceramics, enamel, mica, plastics, silicon rubber, or Teflon are commonly utilized in this context [19].

Primarily, DBDs were mainly utilized in industrial ozone generators and then are also implemented in surface modification, pollution control, plasma chemical vapor deposition, and plasma display screens [20]. More recently, DBD plasma at atmospheric pressure has found new applications in sterilization and medical sectors [21].

1.3 LTP Applications

As an emerging technology, LTP becomes useful for many applications because they produced a potent mixture of highly reactive chemical species, that when in contact with a surface, can change its properties, both chemically and physically. In the plasma process, free electrons collide with neutral gas molecules transferring energy and momentum. These collisions and transfers of energy from the reactive species interact with exposed solid surfaces, which leads to the modification of its surface [22].

Currently, processes that allow disinfecting and sterilizing have gained tremendous attention. A sustainable alternative to traditional solutions that resort to high temperatures, chemical processes, such as autoclave and ethylene oxide, is LTP, which is seen as a promising tool for killing microorganisms. This plasma ability to kill bacteria such as *B. subtilis*, *E. coli*, *Salmonella Enteritidis*, and viruses like Tulane, HIV-1, among others, has been widely studied [23]–[25]. Therefore, the LTP characteristics become important in today's biggest concern, the fight against

severe acute respiratory syndrome coronavirus (COVID-19). This disease triggered a once-in-a-century pandemic, and tests have shown that this virus is viable on many surfaces for many hours. Surface contamination presents severe risks of COVID-19 transmission, and it is essential to interrupt the transmission chain by creating new approaches to inactivation such as LTP due to its promising past in the inhibition of viruses [26].

One of the most important LTP utility is applied to medicine, for example, in treating wounds, skin diseases, or cancer [27]. The interaction of LTP and biological cells is mediated by reactive oxygen and nitrogen species (RONS). RONS are composed of superoxide (O_2^-), hydroxyl (OH), hydrogen peroxide (H_2O_2), atomic oxygen (O), and nitric oxide (NO). For example, the OH radicals are one of the cell membrane's key components. The H_2O_2 is regulated by its powerful oxidative properties that influence lipids, proteins, and DNA. The NO serves as an intracellular messenger and regulator of biological functions and is also responsible for managing immune deficiency, cell proliferation, phagocytose activation, collagen synthesis regulation, and angiogenesis [28].

Also, this future-oriented technology is exceptionally versatile and can be used in a vast range of industries. In food manufacturing, companies are pursuing new methods to satisfy market demand, along with the quality and protection of finished food products. Cold plasma technology is ideal for applications that are also efficient in extracting biological contaminants, changing packaging products, enhancing food safety and functionality, agrochemical removals, seed germination, and reducing biochemical loads from wastewater [29]. Other types of treatments include hardening of tools, dies, or metals, manufacture of semiconductor integrated circuits, anti-corrosion, thermal or electrical coatings, enhance biocompatibility and improve functionalization adhesion [30], [31].

LTP treatments bring the advantages that no solvent treatment or drying steps are needed, resulting in a significant reduction of the process's environmental impact and lower operating costs. Another benefit of this plasma therapy is that the resulting surface properties depend on easily customizable discharge parameters such as electrical power, treatment duration, gas composition, and gas pressure. As a result, this mechanism can be well regulated, rendering LTP treatment a flexible and multifunctional process that can be effectively applied [32], [33].

1.4 Plasma Generators

Considering all the benefits that plasma treatments offer, ways of producing plasma generators have been abundantly studied. In addition to DBD devices, several techniques and instruments are used to generate LTP, like plasma jet [34], as shown in **Figure 1.2**.

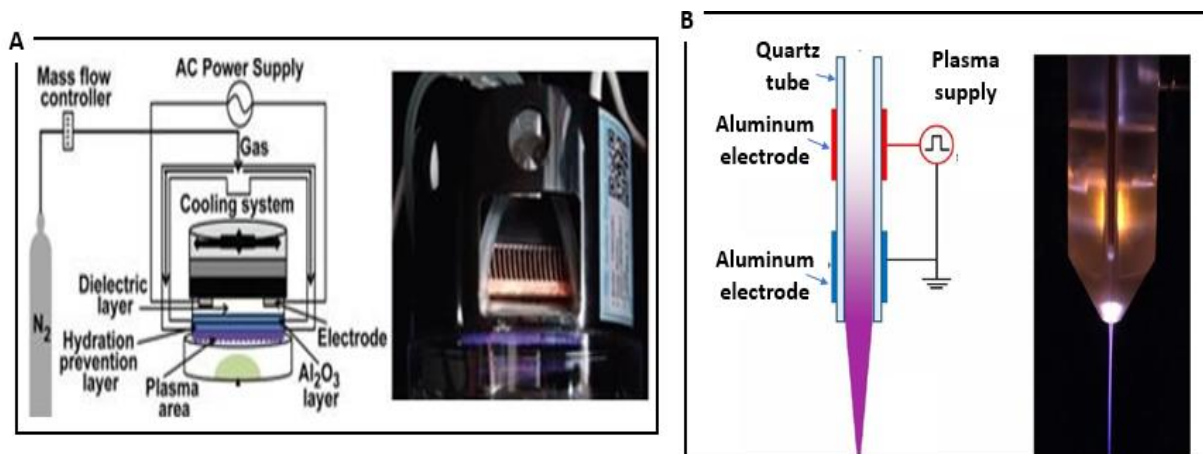


Figure 1.2- Two plasma generators configurations: (A) DBD device; (B) plasma jet [34].

In 2020, Ghorashi and his team produced a plasma jet device. This device consists of two concentric electrodes through which the medium gas flows: one is radiofrequency (RF) biased, and the second one is grounded. A quartz tube is placed between the electrodes to prevent arcing. The discharged gas is ignited by applying RF power to the inner electrode, and the ionized gas flows through a nozzle. This research aims to develop an ideal cold plasma generating device to inactivate *Aspergillus flavus* from the nuts' surface [35].

Also, in 2020, Sharma *et al.* developed a DBD device to disinhibit COVID-19. The plasma is produced between 90 mm diameter copper electrodes and a Petri dish of 100 mm (where the samples are placed) between the electrodes. The high voltage power supply produced uniform DBD plasma at 15 kV-20 kHz [36].

These plasma generators generally use rigid components, which cannot bend or conform under the most diverse shapes. Scalable, flexible, and portable plasma generators can be beneficial in different environments. Therefore, it became essential to develop new techniques to produce LTP with the characteristics previously described.

1.4.1 Paper-based Plasma Generators

In recent decades, cellulose-based technologies have gained tremendous significance, and it is easy to mention some of its many advantages such as three-dimensional fibrous structure, biocompatibility, biodegradable displaying hierarchical fibers porous structure, lightweight, ease of processing and modification, low-cost and availability all over the world [37], [38].

Nowadays, devices are manufactured from non-renewable and toxic materials. Electronics made of paper has incredible economic and environmental improvement that allow modern recyclable electronic devices such as paper displays, smart packaging, radio frequency identification devices (RFID) tags, disposable electrochemical sensors, solar cells, and many others [39]–[41].

Amongst the most interesting electrical properties of paper are volume and surface resistivity, dielectric loss factor, charging potential, decay rate, dielectric constant, and dielectric breakdown strength [42]. The dielectric properties of paper depend on its molecular constitution, physical structure, and chemical composition.

The dielectric constants of different materials are reported in Table 1.1. All dielectric materials are insulators, but a good dielectric is a material that is easily polarized. The amount of polarization which occurs when a certain voltage is applied to a material influences the amount of electrical energy that is stored in the electric field. The paper offers a perfect balance in terms of dielectric constant values because some voltage (but not too much) is necessary for it to start conducting which helps to control the plasma discharge [43], [44]. In this way, making LTP paper-based plasma devices seems to be an excellent bet in the field of cheap and biodegradable electronics.

Table 1.1 - Dielectric constant of different materials [44].

Material	Dielectric constant
Air (dry)	1.0
Bakelite	4.9
Mylar	3.2
Nylon	3.4
Paper	3.7
Paraffin-impregnated paper	3.5
Polypropylene	2.2
Polystyrene	2.6
Polyvinyl chloride	3.4
Porcelain	6.0
Pyrex glass	5.6
Strontium titanate	233.0
Water	80.0

In 2016, Cheng-Che Et al. manufactured a plasma generator on a paper substrate using the screen-printing technique. For the generator's production, patterns were set on a mask and then transferred to a photosensitive emulsion coated screen. A ceiling projector with a halogen lamp was used as a light source for exposure. Thus, a negative stencil of the electrode geometry is formed on the screen. Then, carbon paste was used as ink to paint the paper substrate and define the electrode. This works demonstrated that plasmas are sustained using a DC power source in a helium atmosphere, and that plasma can be maintained stably on a paper substrate when the paper is flat, rolled, or folded along various orientations (**Figure 1.3**). For all configurations, plasmas can sustain for more than 15 minutes with only minor damage on the paper substrate [45].

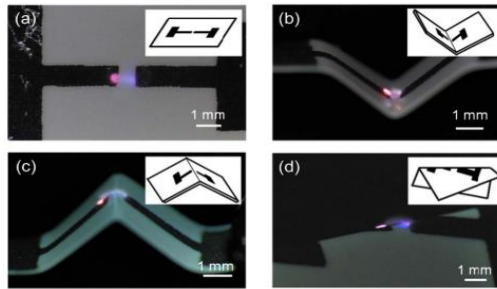


Figure 1.3 - Cheng-Che Et al plasma generator on a paper substrate among various orientations [45]

Aaron D. Mazzeo and his research group proposed in 2017 disposable plasma generators made from layered and patterned sheets of metallized paper obtained by laser engraving capable of eliminating bacteria. The plasma generators produced (**Figure 1.4**) rely on the working principle of DBD. For the generation of the plasma, they produced sinusoidal signals with frequencies ranging from 1 to 8 kHz, and high oscillating voltages of $\pm 1 \pm 10$ V. The paper-based generators are conformable to curved surfaces, compatible with user interfaces, and suitable for sanitization of microbes aerosolized onto a surface, deactivating more than 99% of *Saccharomyces cerevisiae* and *Escherichia coli* cells [46].

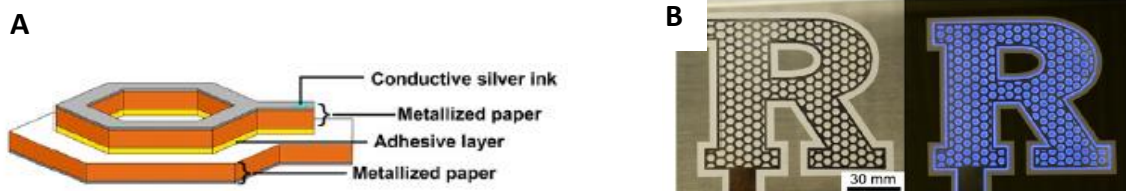


Figure 1.4- Aaron et al. plasma generator structure (A) and generators without (white) and with applied potential (blue) (B) [46].

According to the dielectric barrier discharge principle (DBD), the present thesis aims to develop, optimize, and test plasma generators on paper substrates. The DBD plasma sources produced are composed of one or two aluminum electrodes, separated by a dielectric layer, that in this case, is a paper substrate that gas can penetrate due to paper porosity. The characteristics of the three different papers utilized (Felix Schoeller smart paper type 3, Powercoat™ XD 125, and Canson Vegetal Paper, also known as tracing paper) were studied and compared to perceive how the dielectric influences plasma generation. The generators were produced by shadow mask design by laser engraving and by inkjet printing. A comparison between the two production methods was made in order to understand each method's advantages. Besides, the plasma generation parameters are also studied, such as pressure, power, DC-bias voltage, atmosphere (argon and air), and reactive species released by the plasma. Finally, the impact of the plasma produced by these generators on the modification of surfaces such as cork, vegetal paper, and spinach leaf will also be evaluated.

2| Materials and Methods

2.1 Characterization techniques

2.1.1 X-Ray Diffraction

X-ray diffraction (XRD) is a non-destructive technique that assesses the crystallographic structure of the different papers [47]. The results were recorded using an X-ray diffractometer (PANalytical X'Pert PRO MPD) in Bragg-Brentano geometry with a Cu K α radiation source ($\lambda = 1.506 \text{ \AA}$), in a 2θ range from 10° to 90° .

2.1.2 Thermogravimetry

The thermogravimetric analysis (TGA) was made using a Simultaneous Thermal Analyzer (TGADSC- STA 449 F3 Jupiter), from room temperature to 550°C with a heating rate of $5^\circ\text{C}/\text{min}$, under nitrogen atmosphere. Studying the TGA of the papers is important because the paper (dielectric layer of the generator) will increase its temperature during the plasma generation. Thus, perceive if the temperature influences the generator's functioning enriches this thesis.

2.1.3 Porosity

The paper's porosity is crucial because it allows the gas to penetrate its bulk volume and pass through the substrate to provide plasma [46]. The cellulose substrates have porosity (P) according to **equation 1**: $P(\%) = \left(1 - \frac{\rho_{\text{sample}}}{\rho_{\text{cellulose}}}\right) \times 100$. Where $\rho_{\text{cellulose}}$ is the cellulose density (1.6 g cm^{-3}), and ρ_{sample} the apparent density of the sample (g cm^{-3}) [48].

2.1.4 Scanning Electron Microscopy

The Scanning Electron Microscope (SEM) was used to analyze the morphology of the generators produced in this work. They were imaged with an SEM Hitachi TM 3030Plus Tabletop equipped with Energy Disperse X-ray (EDX) measurements.

2.1.5 Fourier Transform Infrared Spectroscopy

The Fourier Transform Infrared Spectroscopy (FTIR) is a technique capable of examining each generator's molecular groups. The Thermo Nicolet 6700 FTIR was the system utilized in the mode of attenuated total reflectance (ATR), measuring wavelengths between 525 and 4500 cm^{-1} with a data spacing of 1.928 cm^{-1} .

2.2 Production of the plasma generators

2.2.1 Shadow mask patterning by laser engraving

In this production method, each type of paper was first covered with Kapton (**Figure 2.1A**). Then, a laser was used for engraving the desired pattern on the Kapton. This system is computer-controlled and functions as a printer where the desired pattern is imported and then is engraved into the substrate. The pattern used was based on the honeycomb design that allowed plasma generation along the edges of the hexagonal grid and was provided by Professor Aaron Mazzeo [46]. The laser system utilized was the Universal Laser System (ULS) VLS3.5. The power and speed conditions of the laser were 3W and 0.0508 m/s , respectively. Then, after the pattern was engraved on the Kapton (**Figure 2.1B**), the polymeric layer was removed, keeping only the regions that would be used as shadow mask to pattern the plasma generators (**Figure 2.1C**).

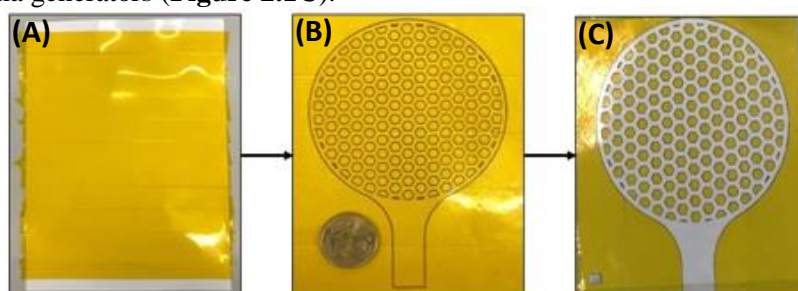


Figure 2.1 - (A) Sheet of paper was covered with Kapton; (B) Pattern engraved on the Kapton; (C) Kapton's interior was removed for aluminum deposition. The 50-cent coin was used for scale purposes (diameter of 24.25mm).

2.2.2 Electron beam evaporation deposition

Electron beam evaporation deposition was the technique selected to produce the electrodes by the deposition of aluminum on top of the paper using the Kapton as a shadow mask. The deposition of aluminum was carried out according to the conditions described in **Table A.1**. The substrate's aspect immediately after the deposition of aluminum can be seen in **Figure 2.2B**, and the final aspect after the Kapton removal can be seen in **Figure 2.2C**. The data related to the generators produced by this method and the experimental conditions used for the evaporation process can be found in **Annex A**.

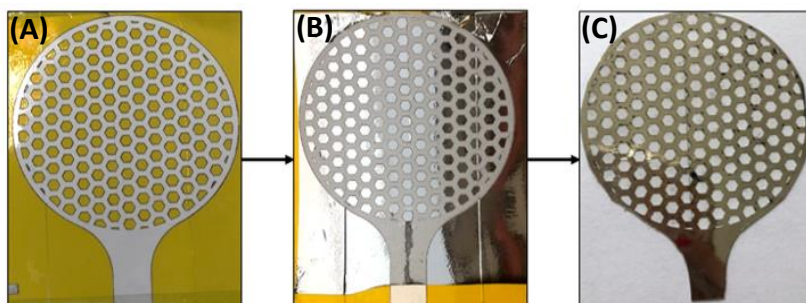


Figure 2.2 – Photos of the generators: (A) Before the aluminum deposition; (B) After the aluminum deposition; (C) Kapton removed.

2.2.3 Inkjet printing method

The second method for producing the generators is inkjet printing. This method consists in the deposition of drops of ink poured from a nozzle onto a substrate [49]. It is computer controlled and prints the desired pattern on the substrate. Due to the time-consuming process for this particular design, the honeycomb pattern's original size was reduced for half compared to the previous method. The silver ink used was Sicrys™ I50T-13. After that, curing was carried out at 150°C on a hot plate for 30 minutes. The generators were produced with different resolutions in Felix Schoeller paper and Canson vegetal paper. The resolution is given by dots per inch (DPI) and is the measure of how many dots of ink a printer can place within an inch [49]. The samples were also covered with another Al layer on the backside of the generators to act as the second electrode. The characteristics of the printing method and these generators are found in **Annex B**.

2.3 Plasma Generation

The DBD generators were tested in a vacuum chamber using a 13.56 MHz rf generator, where argon and air were introduced to evaluate the paper generator's response under different atmospheres. First, a piece of Kapton was glued to the tip on the back of the generator. In this way, the crocodile is connected only to the front electrode (power electrode). Then, an aluminum tape is glued to the back of the generator and connected to the vacuum chamber. Thus, the back electrode works as the grounded electrode. Glass support was used to glue the generator, keep it in the desired position, and allow adequate visualization of what is happening inside the chamber. After the plasma generation, a thermal analysis was performed using a thermal camera and the computer software PIROSOFT Compact. Note that the recorded temperatures are approximate values since the measurement is made immediately after opening the chamber.

2.3.1 Optical Emission Spectroscopy

The Optical Emission Spectroscopy (OES) equipment used to determine the plasma's reactive species was the Ocean Optics HR4000 spectrometer (with a range of 200 to 1100 nm). The computer software was the Ocean Optics SpectraSuit, and the integration time of the measures was 2 seconds.

2.3.2 Contact Angle

The equipment used to make contact angle experiments was the Contact Angle DATA PHYSICS SCA 20. This technique was used to evaluate how plasma affects the wettability of different surfaces (such as spinach leaf, paper, and cork). The liquid used for the measurements was water, the syringe utilized to dispense the water was the Hamilton 500 µL, and each drop dispensed had 1 µL.

3| Results and Discussion

In this chapter, all the work done regarding the plasma generators testing is presented and discussed. Firstly, section 3.1 describes the properties of the three papers used as the DBD dielectric layer. In section 3.2, the plasma generation process will be explained. Sections 3.3 and 3.4 are devoted to the optimization of generators design by shadow mask and the study of plasma generation in air and argon atmospheres. The plasma generation tests, and detection of reactive species will be discussed in section 3.5, while in section 3.6 will be presented the inkjet generators tests and a comparison between production methods. Finally, the study of surface modification by the plasma is demonstrated in section 3.7.

3.1 Characterization techniques of the papers

Since the main objective of this thesis combines the production of plasma generators and their optimization, three different types of paper were used as the dielectric of the DBD generators: Felix Schoeller smart paper type 3 (referred to as FS), Canson vegetal paper (referred to as VEG), and Powercoat™ XD 125 (referred to as XD). So, it was necessary to characterize each paper and understand the differences between them to perceive how the dielectric influences the plasma generation. Papers are generally composed of cellulose fibers (a heterogeneous mixture of plant material such as cellulose, hemicellulose, lignin, among others). A wide variety of chemicals can be used in the paper forming process, giving them different characteristics [50]. The Felix Schoeller is a paper-based substrate composed of a hydrophilic nanoporous surface coating, indicated for printed electronics, with a mesoporous surface that contains a pore size of about 15 nm with a barrier coating underneath [51]. The Canson vegetal paper is a low opacity paper that allows light to pass through, suitable for drawing. It is made from sulfite pulp by reducing the fibers to a fine subdivision state and hydrolyzing them by prolonged beating in water [52]. Powercoat XD is a smooth paper with a specially adapted coating that provides a surface indicated for printing electronic circuits [53].

3.1.1 Papers characterization

The SEM micrographs in **Figure 3.1** presents the morphology of the different papers. The FS (**Figure 3.1A**) has a smooth, compact, and homogeneous structure due to the nanoporous coating and the resin layer before the paper layer. VEG has a high-density structure of intertwined cellulose fibers, with different shapes and sizes, where the high concentration of small size fibers fills the gaps and surface between the larger fibers (**Figure 3.1B**). The XD also exhibits a coating and shows a matrix formed by large and small fibers (**Figure 3.1C**). The thickness, grammage, and apparent density were obtained through each paper's datasheet and factory information (**Annex C**). The thickest paper is FS (175 μm), followed by XD (128 μm), and the thinner is VEG (65 μm), with a porosity (determined by **Equation 1**) of 39%, 37%, and 45%, respectively. FS has RMS roughness of 0.80 μm ([54]), VEG of 3.90 μm ([55]), and XD of 1.50 μm . The characteristics of the papers are listed in **Table 3.1**.

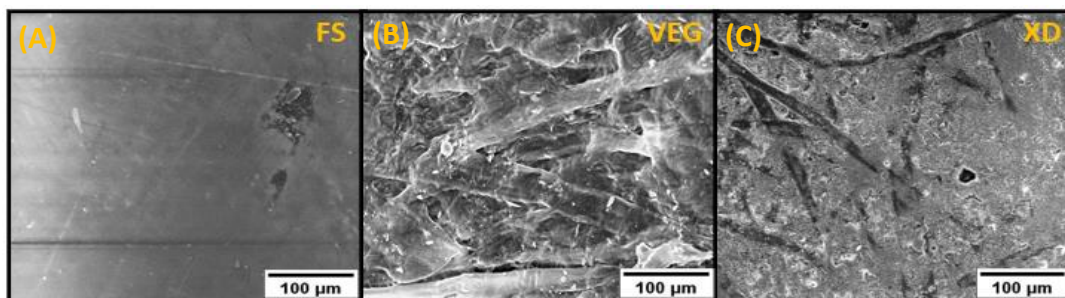


Figure 3.1 - SEM images of the top view of the different papers: (A) FS; (B) VEG; (C) XD.

Table 3.1 - Properties of the different papers: FS, VEG, and XD.

Properties of the papers	Felix Schoeller	Canson Vegetal	Powercoat XD 125
Thickness (μm)	175	65	128
Grammage (g m^{-2})	170	90	129
Apparent Density (g cm^{-3})	0.97	0.87	1.00
Porosity (%)	39.2	45.6	37.4
Roughness RMS (μm)	0.80	3.90	1.50

3.1.2 Paper structure and thermal properties

XRD patterns of the different papers (**Figure 3.2 A**) shows peaks at 2θ around 14.90° , 16.30° , and 22.7° , which are associated with $(1\bar{1}0)$, (110) , and (002) crystallographic planes of cellulose I [56]. In FS and XD diffractograms is observed a peak at 29.70° , which corresponds to the (004) plane of calcite (CaCO_3). Calcite is a calcium carbonate mineral that makes paper brighter and bulkier [57]. In FS's XRD pattern, another peak is visible around 21.50° , corresponding to the (110) plane of aragonite, that can also match to the calcium carbonate mineral used in coatings and fillers in the paper production process [58]. The XD's pattern exhibits peaks around 12.50° and 24.60° , corresponding to the (001) and (002) planes of kaolinite ($\text{Al}_2(\text{OH})_4\text{Si}_2\text{O}_5$), a clay mineral that improves color and brightness and allows for better printability [59].

Information regarding thermal stability was obtained by TGA (**Figure 3.2 B**). The FS, VEG, and XD TGA curves show an initial weight loss of 3.81%, 7.66%, and 5.38%, respectively. This loss occurs close to 100°C and is related to the desorption of free water from cellulose fibers [60]. In the TGA of VEG is observed that cellulose thermal degradation starts around 270°C and continues until 350°C , followed by a weight loss of 71.39%. In the XD case, the weight loss was 68.27%, related not only to the degradation of cellulose but also to the coating layer. In the TGA of the FS paper, a first abrupt mass loss of 40.17% occurs as the temperature increases up to 370°C , which corresponds to the degradation of the nanoporous layer and the resin layer simultaneously with cellulose degradation. Next, two more mass losses occur, 24.37% up to 463°C and 10.99% up to 600°C .

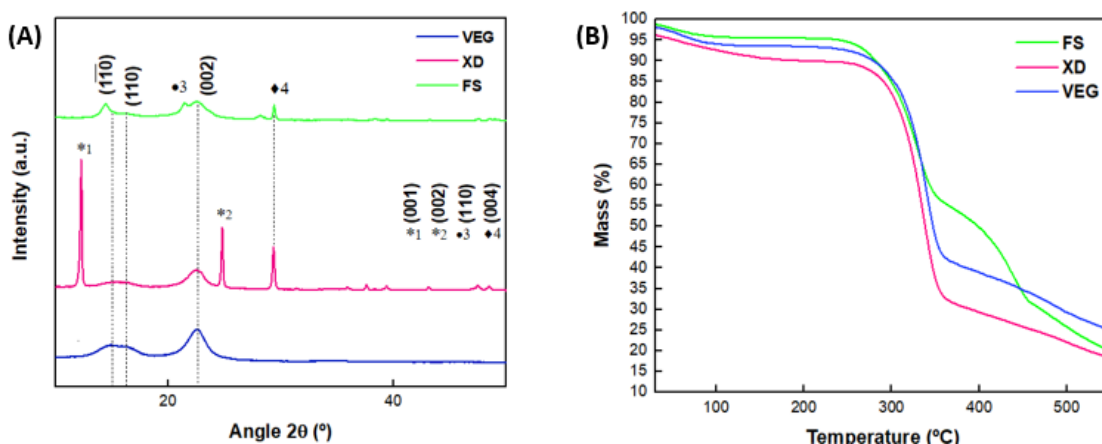


Figure 3.2 - XRD characterization of FS, VEG, and XD; TGA curves of FS, VEG, and XD.

Knowing the range of temperatures in which the paper substrates remain thermally stable is a crucial point to consider since, in this process, the generators are heated during the production of the plasma. Therefore, given the cold plasma application, below 50°C , the mass losses are mostly associated with water presence.

3.2 Plasma generator configurations

Two different generator configurations were produced in order to verify which one would be the most suitable to generate plasma. In the first configuration, aluminum was deposited only at the generator's front (single-electrode configuration). In the second configuration, in addition to the front aluminum deposition, a similar aluminum deposition was also effectuated on the back of the generator (but not patterned), presenting two conductive layers (two electrodes) with the dielectric layer (paper) in the middle, as shown in figure **Figure 3.3**.



Figure 3.3 - Schematics of the generator configurations used: (1) One electrode; (2) Two electrodes.

3.3 Plasma generation process

The plasma generators produced in this thesis work according to the principle of dielectric barrier discharge (DBD). The plasma is originated from the discharge between two electrodes separated by the paper substrate (dielectric layer). For that to happen, RF power is applied to the generator's active electrode, and when the gas that permeates the bulk volume of the dielectric paper exceeds its breakdown voltage, it ionizes and forms a glowing plasma. During this process, free electrons are accelerated and ionize the gas through collisions, and an electronic avalanche is generated, leading to an accumulation of charged particles on the paper [61]. In **Figure 3.4** is seen the schematic used to perform the plasma generation experiments.

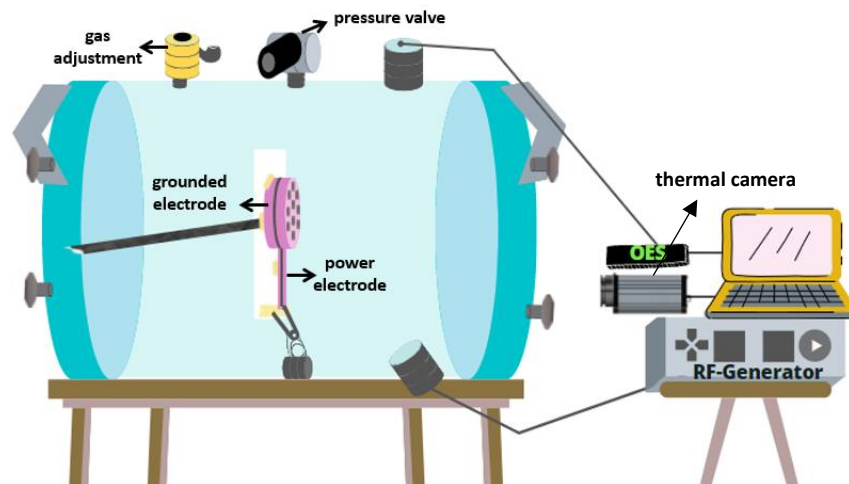


Figure 3.4 – Schematic representation of the apparatus used for the plasma generation experiments: vacuum chamber with a generator placed on the glass support, connected with the generator and the OES system.

The plasma generation tests that will be presented below were done in an argon atmosphere, and the tested generators were patterned by a laser made shadow mask. This first trial was made in VEG generators with a configuration of one and two electrodes with the following conditions: working pressure (P) of 0.55 Torr, power of 5 watts (W), base pressure (P_{base} - equivalent to the pressure when starting to make vacuum) of 0.18 Torr, gas pressure (P_{gas} - equivalent to pressure when gas is introduced in the chamber) of 0.38 Torr, argon flow of 20 sccm, and 2 minutes of testing time.

After conducting these tests, it is possible to conclude that the generators with two electrodes confine the plasma better. In **Figure 3.5A**, it is observed that the plasma is spread both in the front and behind the generator, while in **Figure 3.5B**, the plasma is most evident in the dielectric material, not seen at the rear nor spread over the camera. A possible explanation for this may be related to the gap distance (space between electrodes where the DBD principle occurs). In the configuration with two electrodes, this is a well-defined space with a thickness equal to the paper's thickness, while in the configuration with only one electrode, this space is not well defined. Beyond what is possible to see in the photographs, some considerations found in the literature reveal a greater use of DBD with two electrodes where is reported stability, homogeneity, and greater intensity of reactive species for this configuration [62]–[65].

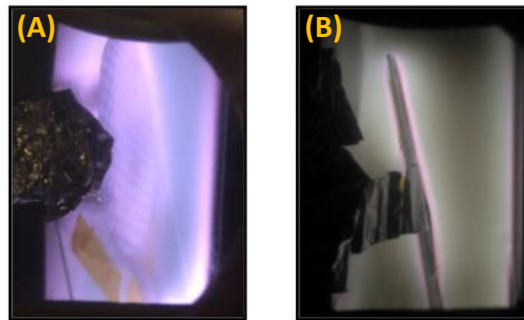


Figure 3.5 - VEG generators with (A) one electrode and (B) two electrodes during the plasma generation.

The plasma being confined is an important parameter since it is possible to direct the plasma to the surface area to be treated without affecting surrounding areas. Therefore, the two-electrode configuration was adopted to develop this master thesis.

3.4 Plasma generation study

In order to understand which are the most indicated values of the plasma generation parameters, such as pressure, power, and gas flux, optimization tests were performed. The optimization tests were done in an argon atmosphere, and the tested generators in these subsections were patterned by the shadow mask made by laser method. The generators were tested with different pressures [0.55; 1; 2; 4; 8; > 10.501] Torr and powers [2; 5; 10; 15; 20; 25] W. For each set of pressure, the rf power was increased, stabilizing in periods of 2 minutes, and photos were taken with a mobile phone at each step to analyze the plasma status. Also in each set of pressure and power, the DC-bias was measured. The DC-bias is the parameter that controls the ion energy distribution of the plasma. When a high frequency powers an electrode, the oscillating RF potential responds with this DC voltage formation on the generator surface due to the difference in mobility between ions and electrons [66]

After conducting these tests, it was possible to notice that the power range chosen was very high because both the XD generator and the FS generator started to fail for applied powers of 20W and 25W (0.55 Torr). The diagram of photos taken at each tested conditions of pressure and power of the first plasma generations and respective photographs after generation are found in **Annex D**.

Therefore, these preliminary tests allowed to establish the protocol to characterize the paper-based generators (**Table 3.2**). In the end of each test, a thermal analysis of the temperature achieved by the generator was made. This study was done first in argon and then in the air, and finally, a comparison of plasma generation is made in both atmospheres.

Table 3.2 - Plasma generation parameters: pressure, power, P_{base} , P_{gas} , and argon flux.

Pressure (P) (Torr)	Power (W)	P_{base} (Torr)	P_{gas} (Torr)	Argon (sccm)
[0.55; 1; 2; 4; 8; > 10.501]	[2; 5; 10; 16]	0.18	0.38	20

3.4.1 Argon Atmosphere

The plasma generation tests presented in this subsection were performed in an argon atmosphere. Argon (Ar) is a colorless, tasteless, odorless, noncorrosive, noninflammable, and nontoxic gas, and it is the most abundant noble gas and the third major component of the air. Noble gases are not very reactive since they have a very stable electron configuration [67].

The results obtained in the plasma generation test with the Felix Scholler (FS) paper are shown in **Figure 3.6**. This generator started to shut down at 16W, after 8 minutes of plasma generation. It is observed that the DC-bias increased with increasing power.

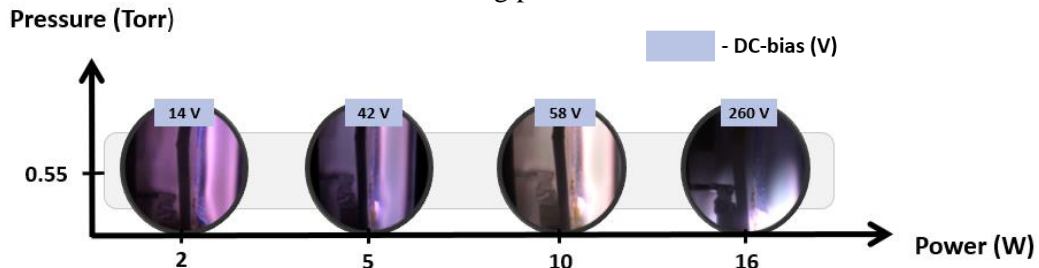


Figure 3.6 - Plasma generation test with the Felix Scholler generator in an argon atmosphere. DC-bias represented in blue. The duration of the plasma generation was 8 minutes.

The generator's status can be seen in **Figure 3.7(A-C)**. A degradation of the generator is observed once some parts of the aluminum peeled off. A possible explanation for this phenomenon can be an excessive heating may have occurred due to the existence of defects or even the degradation of the resin/nanoporous layer leading to the ceasing of the plasma generation.

The recorded temperature range (immediately recorded after the vent of the chamber) is between 19.7°C and 34.8°C (**Figure 3.7D**). It is expected that during the plasma, this temperature should reach higher values. The thermal image proves that there was a higher temperature in the areas where the aluminum was removed.

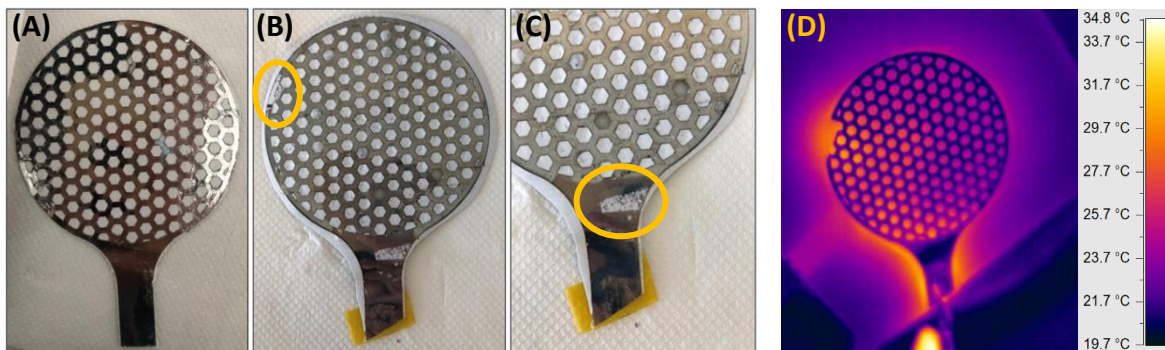


Figure 3.7 - (A) FS generator before plasma generation; (B) and (C) FS generator after plasma generation; (D) Thermal analysis of the FS generator after plasma. Study made in argon atmosphere.

SEM images from the top and cross-sectional views are shown in **Figure 3.8**. The edges of the interface between paper and metal seem more straight after generation, indicating a potential etching of the edges. The surface after the plasma is significantly degraded, with certain parts destroyed in the aluminum and the paper area, as already seen in **Figure 3.7**. According to the cross-view, it is possible to observe that the paper fibers' definition is much more evident before generating plasma. After the generation of plasma, the fibers are more compacted, as if the voids of the matrix were partially filled. Through the analysis of EDX, the components identified in the sample were aluminum (Al), silicon (Si) a constituent of the paper, carbon (C), calcium (Ca), and oxygen (O), which reveals that the plasma does not alter the chemical composition of the generator.

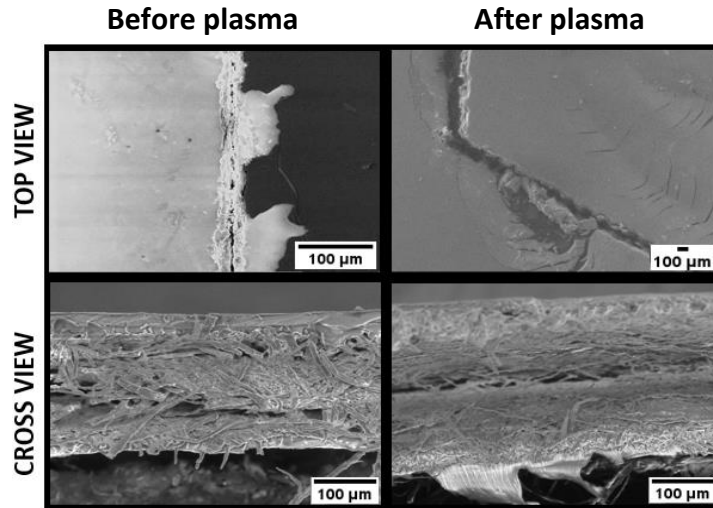


Figure 3.8 - SEM images from FS generator of the top and cross-sectional views before and after the plasma generation. Study in argon atmosphere. Plasma time of 8 minutes.

The results obtained in the plasma generation test with the Canson Vegetal paper (VEG) substrate are shown in **Figure 3.9**. For a specific pressure, the rf power was increase untill 16 W (2 min at each power value), and then it was repeated for increasing pressures to extract the values of DC Bias and the photographs during plasma generation. This generator was able to sustain the plasma for nearly 50 minutes. It is demonstrated that the DC-bias increases with increasing power (as seen in the FS generator case) and decreases with increasing pressure. Its dependency on pressure is related to the mean free path of electrons that determines the average distance a particle travels before a collision occurs. A smaller mean free path results in a decrease in DC voltage, and its inverse proportional to the pressure is described by the kinetic theory of gas (ideally, $PV=nRT$ where P, V, and T are the pressure, volume, and temperature, n is the amount of substance and R is the ideal gas constant). Gas pressure is created by the collisions between the molecules of gas and the collisions of those molecules with the chamber walls. A higher amount of collisions explains an increase in pressure and a reduction in voltage [68].

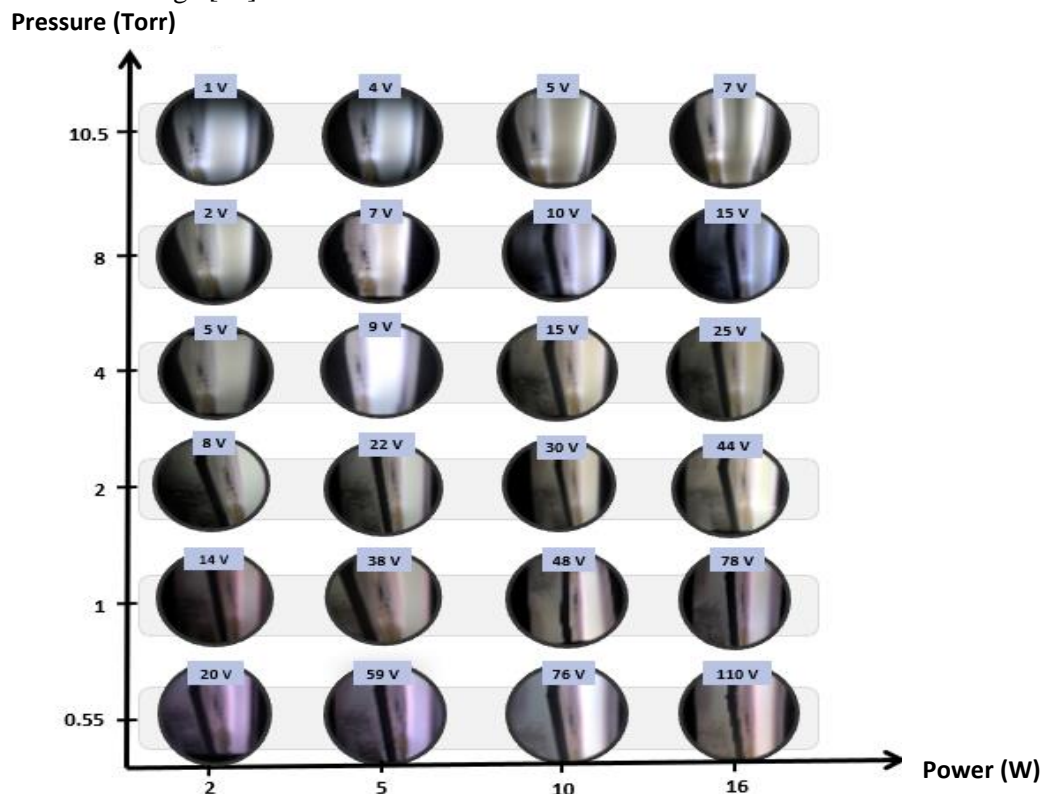


Figure 3.9 - Plasma generation test with the vegetal paper generator in argon atmosphere. DC-bias represented in blue. Plasma time of 50 minutes

The appearance of the VEG generator can be seen in **Figure 3.10(A-B)**. Visually, there are no differences between the images, which indicates that the generator was not damaged during plasma generation. The recorded temperature range is between 31.3°C and 54.5°C (**Figure 3.10C**) due to the long working time. The temperature distribution reached higher values and is more uniform than what was observed for the FS generator, corroborating the inexistence of macroscopic defects.

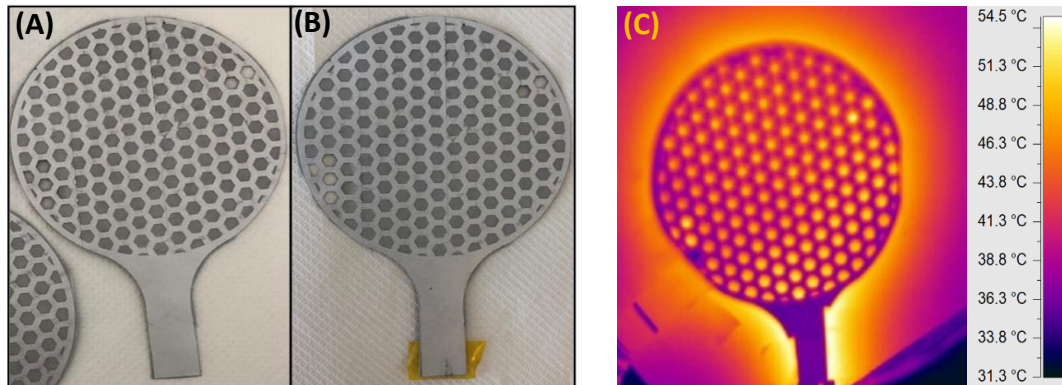


Figure 3.10 - VEG generator before plasma generation; (B) VEG generator after plasma generation; (D) Thermal analysis of the VEG generator after plasma. Study in argon atmosphere.

SEM images from the top and cross-sectional views are shown in **Figure 3.11**. Before the plasma generation, the top micrographs show defined fibers with an evident separation between aluminum and paper areas. After the plasma, it was verified that the plasma made the surface of the generator smoother and more compact, with the aluminum-paper interface less evident. The smoothing of the surface can be justified by the plasma's ability to remove microfibrils, small fragments, or dust present on the paper's surface. Regarding the cross-view, after the plasma generation, the paper fibers' definition is more evident, contrary to what happened in the FS case. The EDX analysis of this paper reveals that the components in this sample were the same before and after plasma: aluminum (Al), silicon (Si), carbon (C), and oxygen (O).

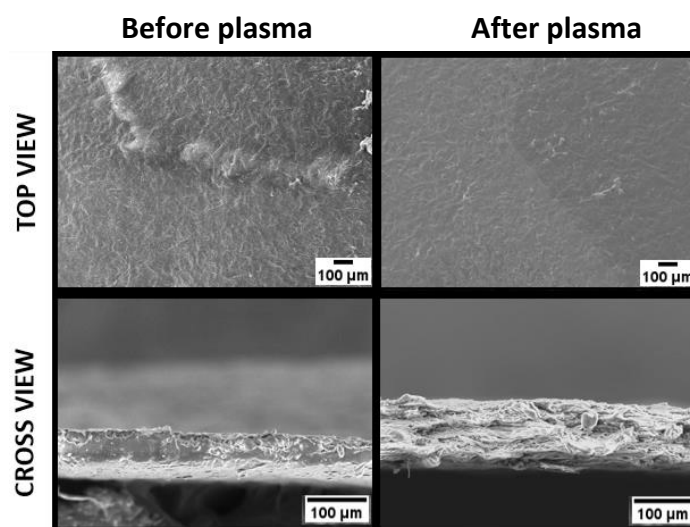


Figure 3.11 - SEM images from VEG generator of the top and cross-sectional views before and after the plasma generation. Study in argon atmosphere.

The graph of the pressure in function of the power obtained in the plasma generation test with the Powercoat™ XD 125 (XD) paper substrate is shown in **Figure E.1** in **Annex E**. In this case, it was possible to generate plasma for about 44 minutes until it shut down. As discussed before, the DC-bias increases with increasing power and decreases with increasing pressure.

There are no evident differences between the generator before and after generating plasma (**Figure 3.12(A-B)**), which indicates that it was not degraded. Similarly to what was observed for the VEG generator, the recorded temperature range is between 20.6°C and 50.6°C (**Figure 3.12C**), as expected due to the larger time elapsed during the plasma. The uniformity in temperature distribution allows to conclude that there are no hotspots.

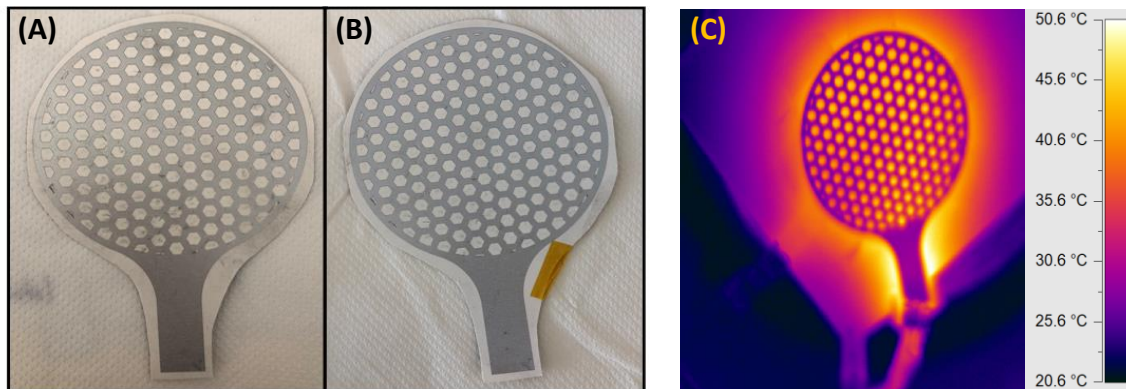


Figure 3.12 - XD generator before plasma generation; (B) XD generator after plasma generation; (D) Thermal analysis of the XD generator after plasma. Study in argon atmosphere.

SEM images from the top and cross-sectional views are demonstrated in **Figure 3.13**. Considering the top view, it appears that before the plasma generation, the details of the surface are well defined, without visible degradation. After the plasma, the surface became smoother and presented a slight degradation level. In the cross-view, before the plasma, the paper's laminated structure is evident, while after the plasma, the same is not verified. Fiber matrix presents appear to become denser after the plasma, suggesting a modification of the generator's surface and bulk due to the plasma. The interaction of reactive plasma species with the generator surface can lead to surface etching and modification of some of the paper's different layers, which may justify the visualized changes. However, no significant chemical modification was observed before and after the plasma since, for both cases, the elements identified in the EDX analysis were aluminum (Al), silicon (Si), calcium (Ca), carbon (C), and oxygen (O).

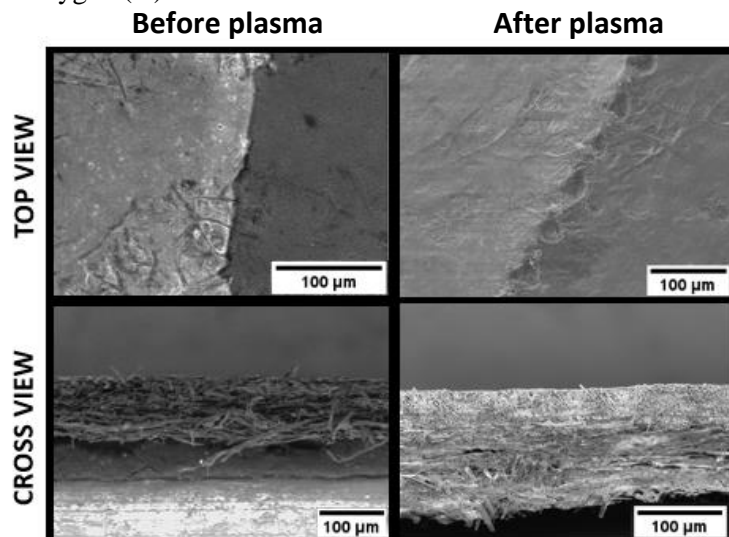


Figure 3.13 - SEM images from XD generator of the top and cross-sectional views before and after the plasma generation. Study in argon atmosphere.

3.4.1.1 FTIR analysis

The ATR-FTIR analysis of the different papers is presented in **Figure 3.14**. It is possible to observe, for all cases, absorption bands characteristic of cellulose, such as hydrogen-bonded OH stretching at $3600\text{--}3000\text{ cm}^{-1}$, the C–H stretching at 2962 cm^{-1} and the C–O stretching at 1255 and 1064 cm^{-1} .

The hemicellulose characteristic peak can be observed at the $1.200\text{--}900\text{ cm}^{-1}$ range. Hemicellulose is a polysaccharide group with an intricate absorption pattern. This area is dominated by ring vibrations that overlap with the stretching vibrations of the C–OH side groups and the C–O–C glycosidic bond vibration. Lignin peaks can also be observed between $1000\text{--}500\text{ cm}^{-1}$ [69]–[71].

From the three papers, the VEG graph (**Figure 3.14B**) has the most evident peak at 1640 cm^{-1} corresponding to O–H bending vibration, which is related to the absorbed water [72].

In the XD case (**Figure 3.14C**), other two peaks are seen, one at 1730 cm^{-1} and another at 1415 cm^{-1} corresponding to calcite, a constituent of this type of paper [58].

It is concluded that, after the plasma, all spectra exhibited an increase in the intensity of the absorbance bands (the peaks are at larger absorbance values). This fact may indicate that plasma has increased the functional groups present on paper [73].

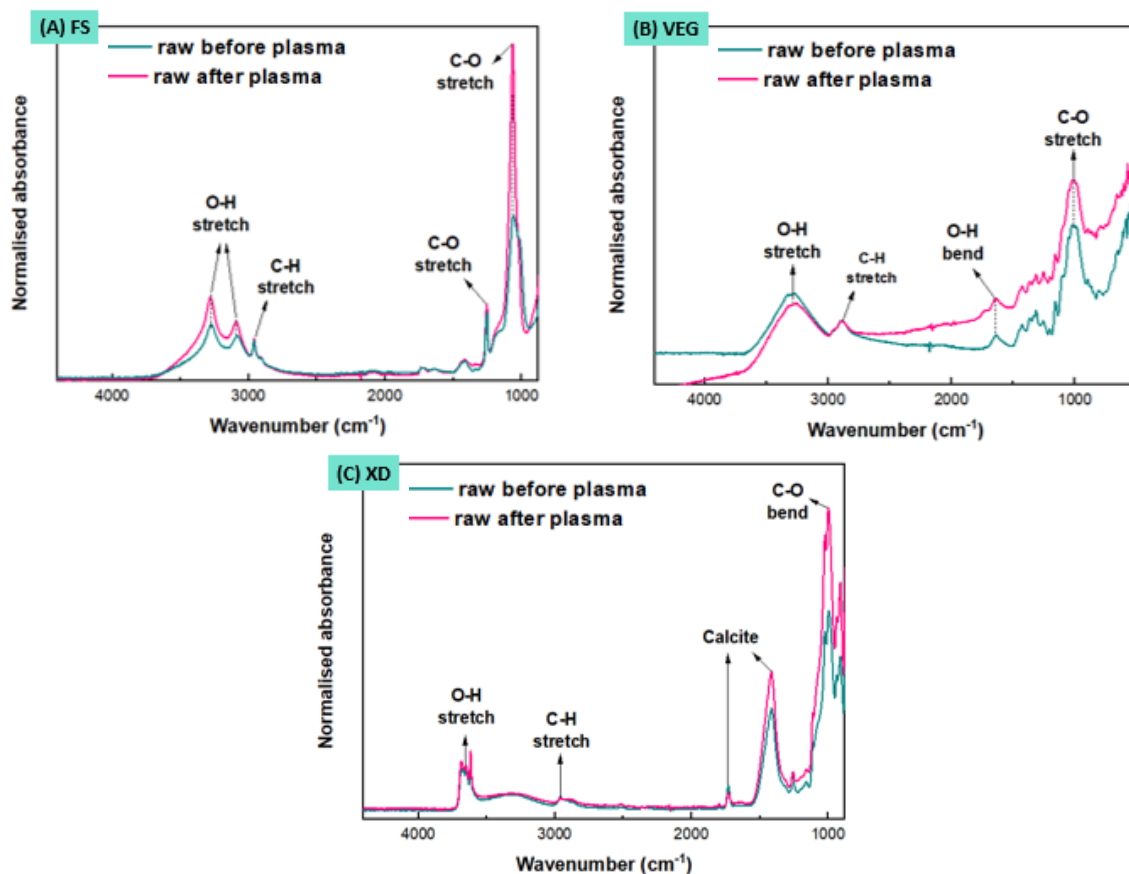


Figure 3.14 - ATR-FTIR spectrum before and after the plasma generation in argon of the papers: FS paper 8 minutes of plasma, (B) VEG paper 50 minutes of plasma, and (C) XD paper 44 minutes of plasma.

After performing the previous tests, it was concluded that the VEG and XD generators were the ones that sustained a more stable plasma generation for a longer time (more than 40 minutes). The VEG generator showed no evident damage after plasma, while the XD showed a slight degradation. VEG does not have any coating, is formed only by the fiber matrix layer, showing that simpler papers are better to produce paper-based generators.

The FS sustained the plasma only for 8 minutes and was significantly degraded. The degradation seems to be related to the nanoporous coating and the resin layer presented on the FS structure that may conduct to the aluminum delamination. Typically, DBD can generate two types of plasma: volume plasma and surface plasma, depending on the device's configuration [46]. Volume plasma usually has an air gap between the two electrodes, and thus the volume plasma could cause the substantial degradation of the resin and nanoporous coating, leading to the cracking and peel-off of the aluminum layers and consequently compromising the functioning of the device.

3.4.2 Air Atmosphere

These devices' ultimate goal would be its use on atmospheric pressure using air as the ionizable gas. In this way, plasma generation tests were also performed in an air atmosphere. Note that, as the generator made with FS did not support well the generation of plasma in the argon atmosphere, it was not tested in air.

The air is the gas mixture that forms the earth's atmosphere and is made up of about 78% nitrogen (N) and 21 % oxygen (O₂), and also has small concentrations of other gases, such as carbon dioxide (CO₂), neon (Ne) and hydrogen (H). Reactive gases of air are tropospheric ozone, carbon monoxide, volatile organic compounds, reactive nitrogen gases, and reactive sulfur gases [74].

The results obtained in the plasma generation test with the VEG paper are shown in **Figure 3.15**. This generator was generating plasma for about 6 minutes and then stopped working. The recorded temperature range is between 22.9°C and 27°C, and the temperature distribution is uniform, corroborating the lack of hotspots.

According to the SEM images visualized in **Figure E.2** of this VEG generator's top view, it is possible to infer that the plasma resulted in the smoothing of the surface. However, as the generation time was smaller than for argon atmosphere the changes in surfaces are less evident. The EDX analysis reveals that the components in this sample were the same before and after plasma.

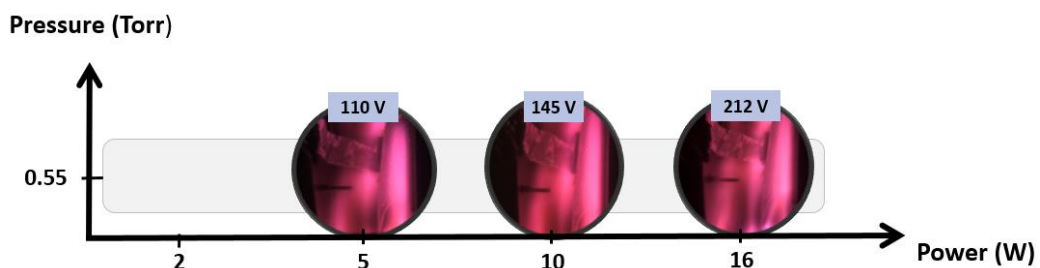


Figure 3.15 - Plasma generation test with the VEG generator in air atmosphere. DC-bias represented in blue. Plasma time of 6 minutes.

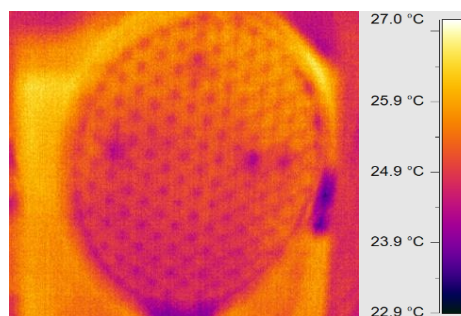


Figure 3.16 - Picture from the thermal camera. Thermal analysis from a generator with VEG paper in air atmosphere.

The results obtained in the plasma generation test with the XD generator is shown in **Figure 3.17**. The generator held up to generate plasma for about 6 minutes. The recorded temperature range is between 38.7°C and 48.3°C (**Figure 3.18**). In this case, an increase in temperature is observed, which can be explained by defects on the generator's surface.

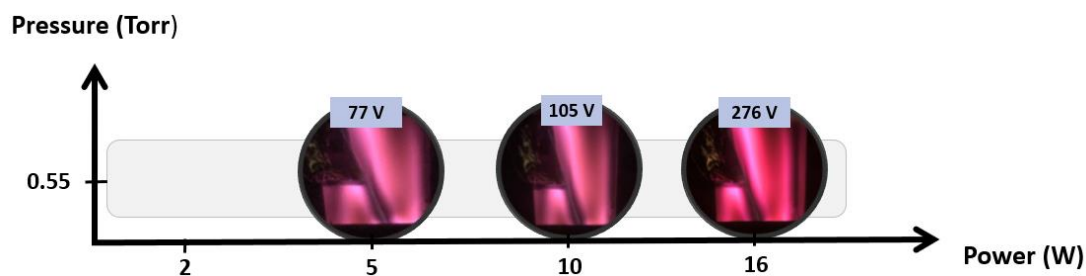


Figure 3.17 - Plasma generation test with the XD generator in air atmosphere. DC-bias represented in blue. Plasma time of 6 minutes.

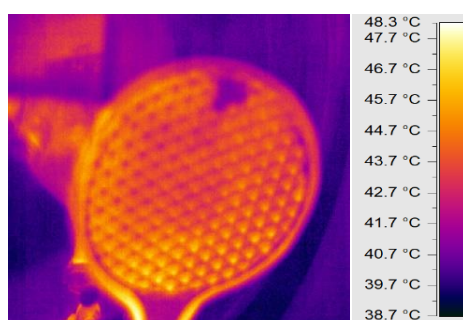


Figure 3.18 - Picture from the thermal camera. Thermal analysis from the generator with XD paper in air atmosphere.

According to the SEM images presented in **Figure E.3** of the top view of this XD generator, it is possible to verify, besides the smoothing of the surface after the plasma generation, some degradation of the generator. Once again, it becomes evident that papers with layers of coating are more susceptible to degradation. Through the analysis of EDX, the components identified in the sample were aluminum (Al), silicon (Si), carbon (C), and oxygen (O) before the generation of plasma. After plasma generation, all elements were present except the Si, which suggests that air plasma, led to a preferential removal of Si in the paper.

3.4.3 Influence of the atmosphere on the plasma generation

The analysis of the graphs related to the ATR-FTIR analysis (**Figure E.4**) shows results similar to the ones observed with generators in the argon atmosphere (**3.4.1**). However, in the air case, a lower intensity of the absorption bands is observed, denouncing a smaller increase in the functional groups. This may be related to the fact that air generators have only been able to withstand the generation of plasma for a small fraction of time (6 minutes), while in argon, the generation time was longer.

It was verified that, in the air case, the plasma generation only started when 5 W was applied (for the pressure of 0.55 Torr). The generators stopped working at a pressure of 0.55 Torr and a power of 16W for both cases, indicating that plasma tests done in argon atmospheres have withstood a much wider range of pressures and power than in air. Additionally, this shows that the atmosphere changes the lifetime of the generator.

Furthermore, for the same pressure and power set, the measured DC-bias was much higher in the air atmosphere than in the argon atmosphere, as seen in the graph of **Figure E.5**. Reactive gasses are easily adsorbed or absorbed by exposed surfaces due to their high chemical activity. Being a more

reactive gas means lower electron density and higher electron temperature, making the value of DC-bias higher [66].

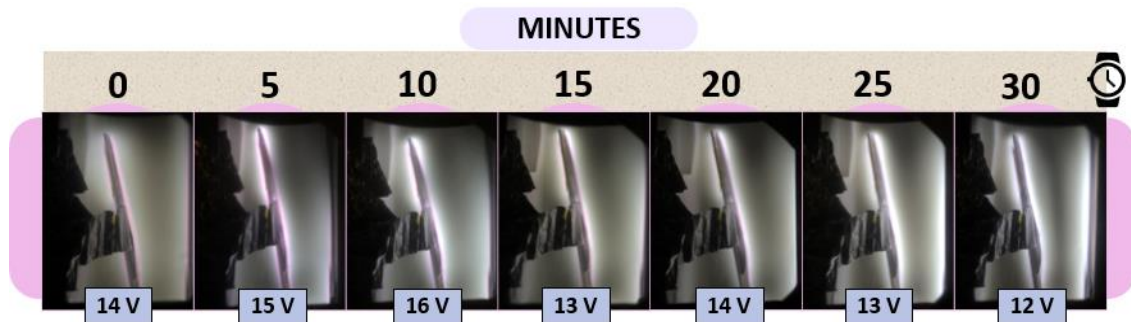
Thereby, as this air environment is much more reactive than the argon atmosphere, the plasma production was halted. As a future goal is to approach atmospheric pressure, an atmosphere that reaches higher pressure values is needed - atmospheric pressure corresponds to 1 atm, equivalent to 750 Torr [75]. Thus, the argon atmosphere was chosen to accomplish the remaining tests.

3.5 Stability of the plasma and Plasma Reactive Species study

As mentioned previously, these generators' interest in sterilization is related to the reactive species that can be formed in the plasma. Although not being the main focus of this work, the Optical Emission Spectroscopy (OES) of the Ar plasma was made to evaluate the reactive species present in the plasma, but also to try to understand if other elements resulting from the paper degradation were detected.

Thus, it was fixed a power of 16 W and a testing time of 30 minutes. These tests were done with the exhaustion valve closed (pressure > 10.5 Torr) while the Ar flow was kept constant (20 sccm). However, it was found that at this pressure, it was not possible to generate the plasma because the generators turned off after a few seconds. Therefore, a pressure of 9 Torr (the highest pressure that the generators could sustain the plasma) was used during the remaining tests. The OES acquisition was made every 5 minutes.

The VEG generator data during the 30 minutes of plasma generation was recorded in **Figure 3.19**. As time passed, the intensity of light emitted by the plasma increased. The DC-bias fluctuated between 12 and 16V, increasing up to 10 minutes of generation and decreasing. The recorded temperature range is between 32.9 °C and 72.1°C (**Figure 3.20**). The uniformity of the temperature distribution reveals that there were no macroscopic defects on the surface.



3.19 - Photographs of paper generators of VEG paper after plasma generation time test. DC-bias represented in blue.

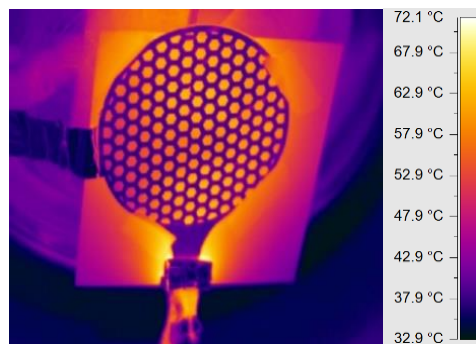


Figure 3.20 - Picture from the thermal camera. Thermal analysis from a generator with VEG paper in argon after time generation tests.

The OES spectrum of the VEG generator is shown on the graph of **Figure 3.21**. The OES spectrum shows emissions from the OH radical in the range of 305–310 nm related to water release from paper. The characteristic atomic argon lines (labeled as Ar I) are observed in 690-850 nm, while at 911 nm is shown a line of singly ionized Ar (Ar II). These elements are common in argon plasmas [34], [75], [76].

The results testify that the concentration of species is higher at the initial instant and then decreases at 5 minutes. The highest value was reached after 30 minutes of testing. Thereby, it appears that with the increasing of the plasma generation time, the concentration of all detected reactive species increases. It is also important to refer that the reactive species present are the same over time, revealing that the paper does not release new species when generating the plasma.

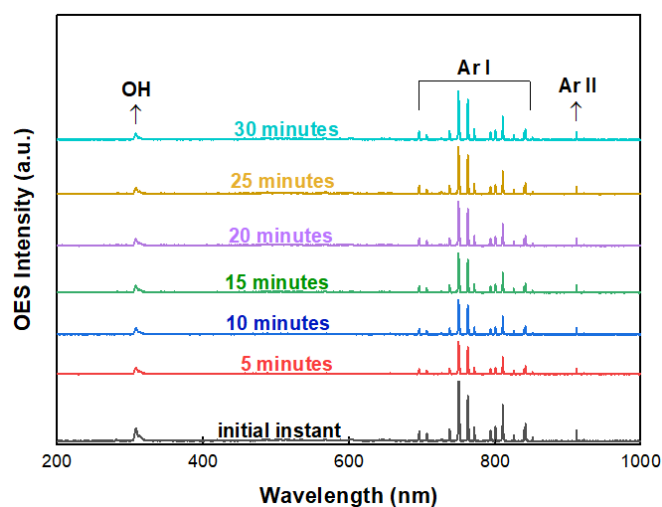


Figure 3.21 - OES spectrum of VEG generator during time tests.

The XD generator data during 30 minutes of plasma generation is visualized on **Figure 3.22**. As time passed, oscillations in the intensity of the light emitted from the plasma were observed. For example, at 10 minutes, there was a greater intensity than at 20 minutes. The observed DC-bias fluctuated between 11 and 14V.

The recorded temperature range is between 31.9°C and 71.7°C (**Figure 3.23**). Note that, in the case of time tests, the temperature was higher than the observed in the previous study (**3.4.1**) because higher pressure and power values were maintained throughout this test. Besides, defects on the generator, such as areas of the paper that fell during the generator's production, may have led to increased temperature in those areas.

The XD OES spectrum is similar to the previous VEG generator (**Figure F.1**), and also no elements present in the paper were identified in the plasma.

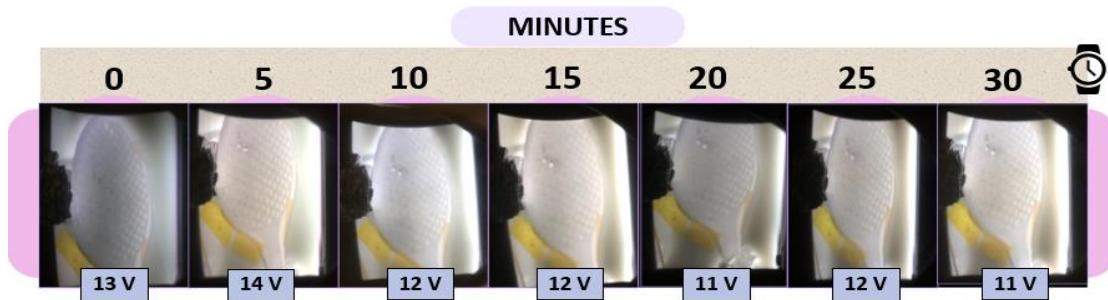


Figure 3.22 - Photographs of paper generators of XD paper after plasma generation time test. DC-bias represented in blue.

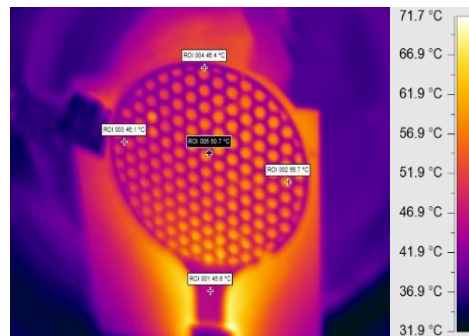


Figure 3.23 - Picture from the thermal camera. Thermal analysis from a generator with XD paper in argon

3.6 Inkjet printing tests

In addition to the generators produced via patterning by shadow masks, another production method was used to make DBD generators, the inkjet printing. In this way, it was possible to compare the two production methods and understand each method's advantages. However, in the inkjet printing case, some parameters had to be changed. The generators' size had to be reduced to almost half due to the amount of ink and time required to print the large-scale generators, which was unsustainable. Besides, instead of aluminum electrodes, as seen in the previous method, the printing ink used to produce the front electrode was silver. In the back of this generators, aluminum was deposited by e-beam evaporation to form the back electrode.

The tests on printed generators were done with a constant power of 8W, and the pressure was increased every 2 minutes. The base pressure used was 0.18 Torr, the gas pressure was 0.45 Torr, and the argon flow was 20 sccm.

First, the tests started with the inkjet generators produced with vegetal paper. Through the SEM images of these generators taken before plasma generation (viewed in **Figure 3.24** and **Annex G**), it is possible to infer that the printing in this paper does not present great quality since there are many flaws in the silver lines, which may have led to the formation of non-conductive paths. Besides, it was noticed that silver was being released from the paper when attempting to produce plasma. For these reasons, inkjet VEG paper generators do not work.

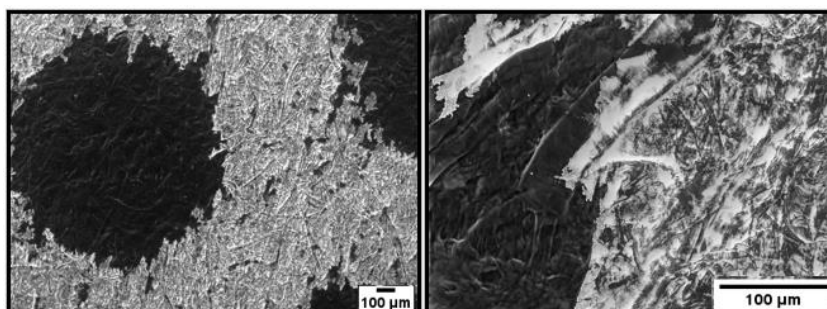


Figure 3.24 - SEM images from VEG inkjet (200DPI and 300 DPI) generator of the top view before plasma generation. after time generation tests.

Despite the poor performance previously observed, some inkjet generators made in the FS paper were tested. This type of paper is suitable for printing electronics, and therefore, FS generators were produced by inkjet printing with good quality and proper definition. In the next subsections, the plasma generation tables with this generation data are represented. During plasma generation, an OES analysis was performed every 2 minutes.

3.6.1 Inkjet FS generator (600DPI two layers)

The generators printed in two steps with 600 DPI were able to generate plasma for 12 minutes, reaching a pressure of 10 Torr (**Figure 3.24**). In the images of the generation, it is notorious that there is a brighter zone, where there was a higher concentration of plasma and consequently greater heating.

The generator's pictures taken after the plasma demonstrate that it was burned and degraded at the front and the back (**Figure 3.26(B-C)**). The fact that there was a greater heating and the generator burned may be related to the printing defects on the surface, leading to the formation of hotspots, compromising the generator's lifetime.

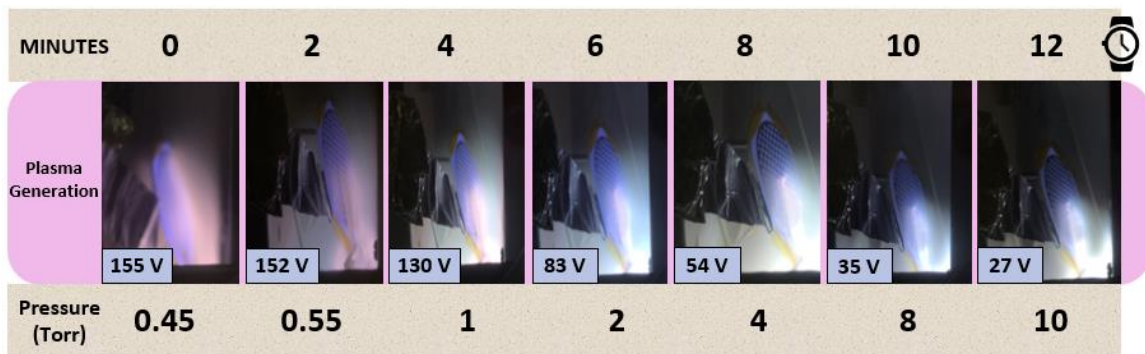


Figure 3.24 - Plasma generation tests with the inkjet FS generator (600DPI two layers). DC-bias represented in blue.

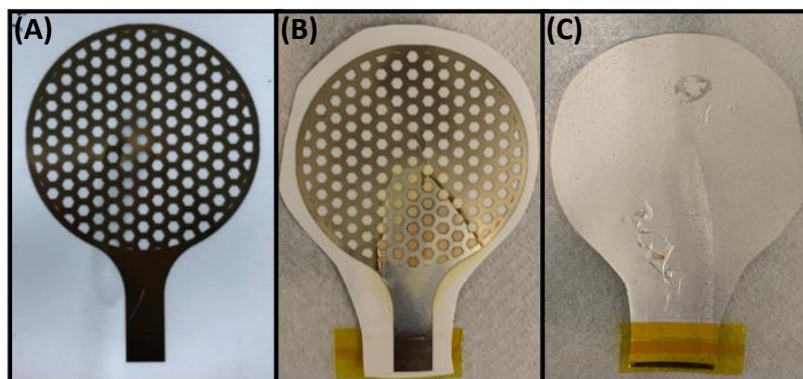


Figure 3.25 - Photograph of inkjet FS generator (600DPI): (A) before plasma, (B), and (C) after plasma generation.

The SEM images in **Figure 3.27** show that this paper's printing presents more continuous, and therefore conductive lines than in the case of VEG inkjet generator.

As the FS is a specific paper for electronic printing, as opposed to VEG paper, the FS is a better substrate to produce inkjet plasma generators. However, there is still a lack of coverage that could be resolved by printing other silver layers, giving greater conductivity and increasing the generator's life.

These SEM images also show significant degradation after the plasma, with cracks in the paper and silver zones. The printing defects must have led to excessive heating that promoted the appearance of cracks that consequently compromised the generator's structure.

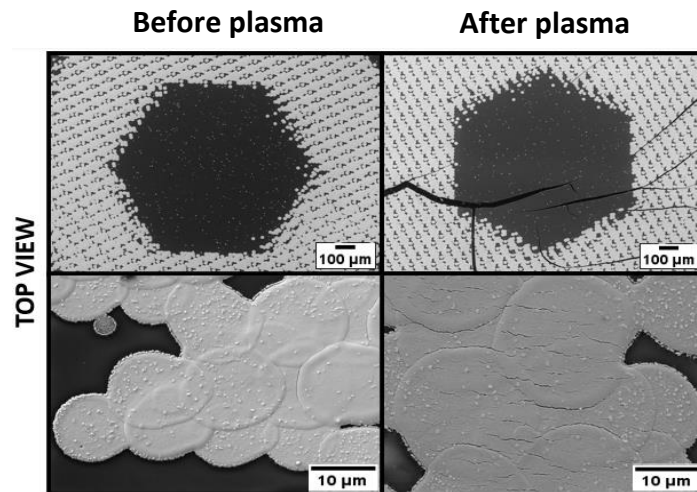


Figure 3.26 - SEM images from inkjet generator FS (600DPI) of the top view before and after the plasma generation.

The OES spectrum (**Figure 3.28**) shows the same species observed in previous studies: emissions from the OH radical in the range 305–310 nm, the ArI in the range of 690-850 nm, and an ArII peak at 911 nm. However, the reactive species' intensity is lower in the initial instant, then increases up to 4 minutes, but a decrease occurs from 6 to 12 minutes. The decrease of the intensity of the spectral lines with the increase in pressure could be explained by a reduction in the energetic electrons present. Furthermore, these decrease in the species' intensity may also be related to the generator degradation over time, compromising its operation. Once again, the species present were the same over time, so neither the paper nor ink lead to new species' release.

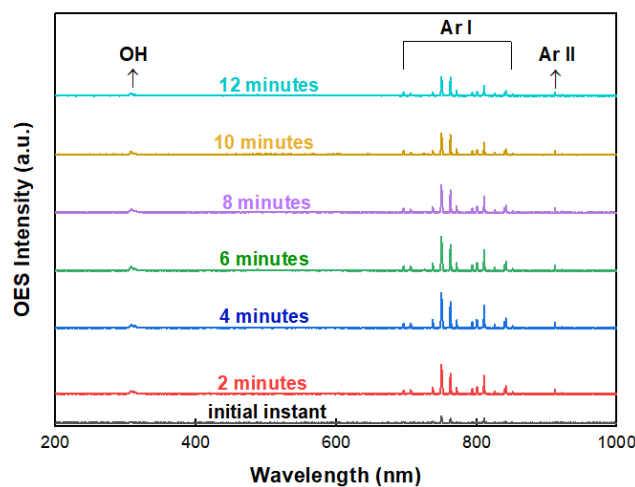


Figure 3.27 - OES spectrum of FS inkjet generator 600DPI.

3.6.2 Inkjet FS generator (700DPI)

The generators printed with 700 DPI started to shut down at 8 minutes of the generation when the pressure reached 4 Torr (**Figure 3.29**). The pictures of the generator show its poor print quality, and it is also verified that after the plasma, the generator was burnt (**Figure 3.30**).

SEM images (**Figure G.3**) demonstrate low quality and defective ink printing, with ink flaws. For these reasons, the generators did not operate for a long time, nor did they show much intensity of reactive species (**Figure G.4**) as the previous generator (**3.6.1**).

In the previous case, two layers of ink were printed, which promoted greater conductivity. In this case, only one layer was printed, which made the generator less conductive, despite the higher resolution. This problem could be overcome by printing other layers of ink that would improve coverage and increase conductivity.

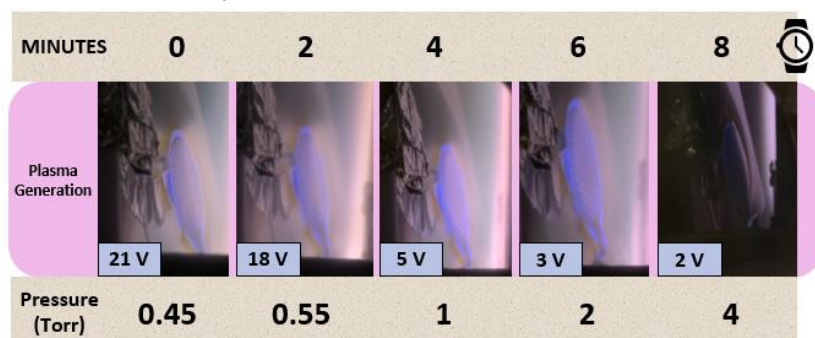


Figure 3.28 - Plasma generation tests with the inkjet FS generator (700DPI). DC-bias represented in blue.

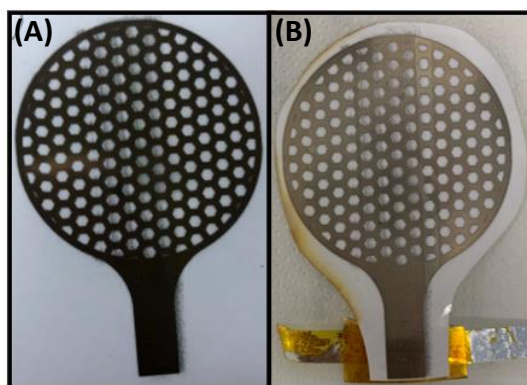


Figure 3.29 - Photograph of inkjet FS generator (700DPI): (A) before and (B) after plasma generation.

3.6.3 Silver deposition on shadow mask patterning by laser engraving

In the inkjet generators method, the ink used to form the electrodes was silver. Thus, to perform a better comparison between production methods, silver was deposited by e-beam evaporation in generators made with shadow mask patterning by laser engraving, instead of aluminum. In these tests, the plasma generation parameters were the same as the used for inkjet tests except for the power utilized, which this time was 16W, once the size of the generator was larger.

The tables with the plasma generation data can be found in **Annex G section G.5**. Interestingly, the silver generator that did not last as long linked to generating plasma was the VEG generator, which turned off when it reached 10 minutes of generation and a pressure of 8 Torr. Both the FS and the XD silver generators endured generating plasma during the 12 minutes reaching the maximum pressure (10 Torr), and archive higher DC-bias values. All generators were burned after the plasma generation.

SEM images shown in **Annex G section G.6** demonstrated, in all cases, poor coverage of the silver with many parts without silver. The paper fibers become more defined, and the surface smoother after the plasma. However, silver showed crimped areas in FS (**Figure G.8**) and XD (**Figure G.10**). This proves the generators' damage that probably was related to surface defects due to the poor silver deposition, which leads to the overheating of the device compromising its structure.

OES spectra of the silver generators represented in **Figure G.11** show that the reactive species' are the same over time, but the intensity is lower in the initial instant, increases up to 4 minutes, and decreases in the remaining test time. The generators started to degrade and burn, which may have compromised the devices' functioning and, consequently, the plasma generation.

For these reasons, it is possible to infer that the generators produced by inkjet printing, despite they allow miniaturization and are interesting for design, have low uniformity and insufficient step coverage, which means that they are not so good for generating plasma as the generators produced by shadow masks. In addition, the printing parameters vary widely from substrate to substrate, and to make a print perfectly suited to the different papers, it is necessary to make optimizations, which would lead to a huge waste of time and money. The shadow mask method, despite being a method that has some limitations in the miniaturization, allowed to make plasma generators more efficient.

Also, it is seen that aluminum shadow mask generators worked better than silver generators. The differences between generators with silver and aluminum electrodes can be justified by the fact that the physical and chemical characteristics of the electrode material affect the input power, which can increase the energy of the ionized electrons. The intensity of the plasma and the discharge is related to the electrode material because different electrode materials have different electrical properties (such as electrical resistivity and conductivity), which can affect the plasma discharge [77]. In addition, in order for the silver not to be released from the generator, it would be necessary to deposit a layer that promotes adhesion. Therefore, aluminum generators evidenced better coverage. Also, aluminum VEG and XD generators made by shadow mask presented a longer lifetime and practically no degradation.

3.7 Surface modification tests

In addition to the interest shown in plasma generators for sterilization and disinfection purposes, they can also be used for surface modification. Thereby, contact angle measurements were performed to analyze the impact of the plasma produced by the DBD generators on the surface wettability.

In this investigation, three different surface samples were studied: cork, vegetal paper, and spinach leaf. One square of each sample was cut and placed on a glass holder. Five similar glass holders were made: one served as standard (no treatment was made), another was subjected to vacuum, and in the rest, plasma treatment was performed for 15, 30, and 45 seconds.

The DBD plasma generator used was a VEG generator made by the shadow mask method. This was the generator chosen to perform these tests because it was the generator that got the best results since it was able to generate plasma for a more extended period of time and did not show degradation.

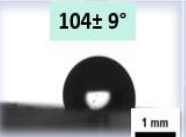
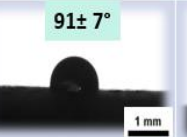
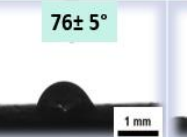
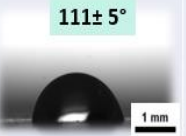
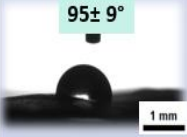
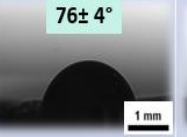
The plasma generation time was optimized according to preliminary tests carried out with the spinach leaf (**Annex H section H.2**). In turn, the glass holders were placed on the chamber support (**Figure H.1**). Vacuum tests were accomplished for 1:30 minutes, which was the time until a pressure base of 0.18 Torr was reached. These tests are used to understand if the vacuum causes any changes in the surfaces. Therefore, in the plasma generation tests, the base pressure used was 0.18 Torr. Next, it was waited until 0.70 Torr to start plasma, with an argon flow of 1000 sccm and 16W of power.

During the plasma treatments, the surfaces are bombarded by ionized gas, which induces chemical reactions on the material's surface to be treated.

The contact angle results are shown in **Table 3.3**. It is observed a significant difference when comparing the samples with and without plasma treatment. The contact angle hardly changes with vacuum treatment, proving that the vacuum did not modify the surfaces. However, the water contact angle decreased as the plasma treatment time increased, as seen in the graph of **Figure H.3**. Without treatment and vacuum treatment, the angles are greater than 90°, indicating that the surfaces are hydrophobic. With 45 seconds of treatment, all angles decrease to values lower than 90°, becoming hydrophilic surfaces [78]. These events show the plasma's efficiency in modifying the surface since the low contact angle implies a greater wetting of the surface.

For the surface's wettability to increase, the surface energy must increase, which may occur by incorporating polar groups on the surface. In addition, the increase in wettability can also be related to the increase in surface roughness [79]. Plausible reasons for this to happen are the cleavage of original functional groups, mechanical alteration of the surface, and hydrophilic functional groups created by plasma on the different surfaces [80],[81].

Table 3.3 - Contact angle measurements in cork, vegetal paper, and spinach leaf samples without treatment, with vacuum, and with a plasma treatment of 15, 30 and 45 seconds.

	Without treatment	Vacuum (no plasma)	Plasma treatment 15 seconds	Plasma treatment 30 seconds	Plasma treatment 45 seconds
 Cork	122± 6° 	104± 9° 	91± 7° 	76± 5° 	51± 7° 
 Vegetal paper	115± 13° 	111± 5° 	53± 9° 	43± 8° 	39± 5° 
 Spinach leaf	95± 9° 	92± 10° 	76± 4° 	65± 9° 	60± 10° 

The SEM images of untreated surfaces and with 45 seconds of plasma treatment were evaluated. The SEM cork images (**Figure 3.31**) demonstrate that the thickness of the cell walls of the treated sample is smaller than the one that had no treatment. The cork walls became narrower, and the walls' hexagonal prisms more open, suggesting that the plasma treatment is responsible for the erosion of the cell walls.

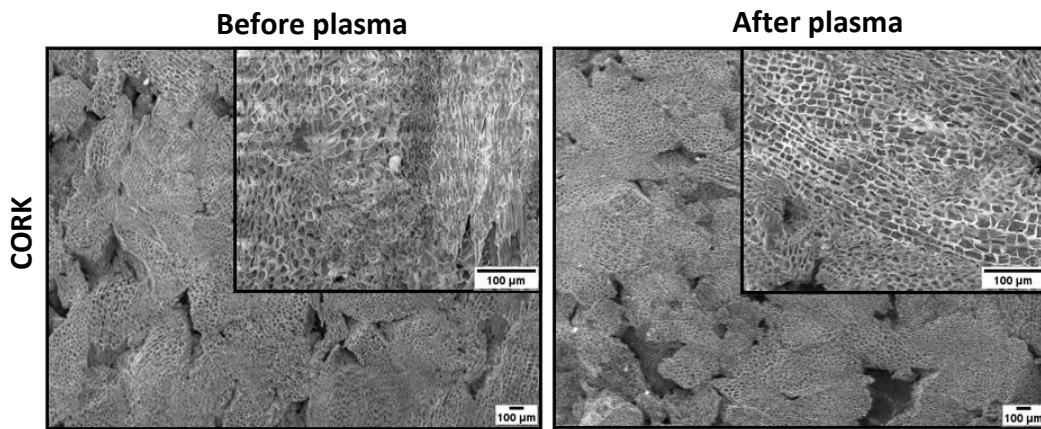


Figure 3.30 - SEM images from cork surface top view before and after 45 seconds of plasma generation.

In the vegetal paper case (**Figure 3.32**), there are no significant differences between the structures with and without treatment. Without plasma treatment, a tangle of fibers is observed, and with treatment, the fibers have become more defined.

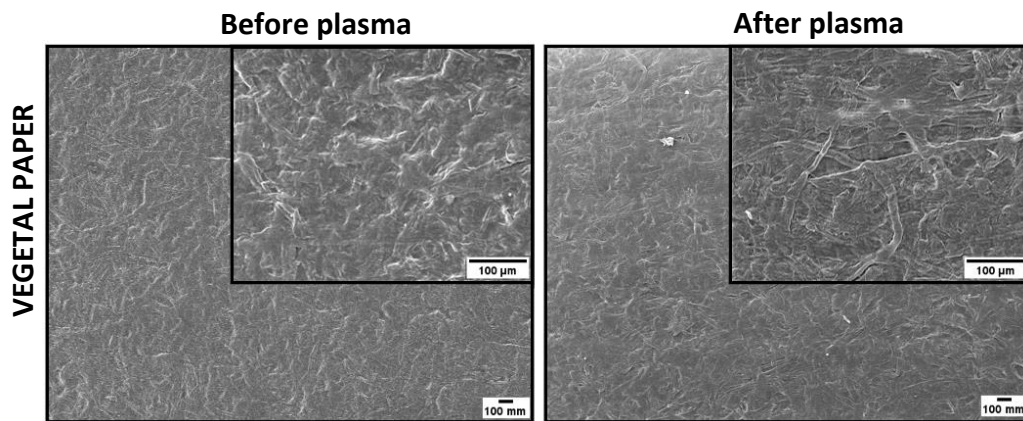


Figure 3.31 - SEM images from vegetal paper surface top view before and after 45 seconds of plasma generation.

In the SEM micrographs of the spinach leaf (**Figure 3.33**), before plasma generation, the cutin is observed. A plant cutin is a protecting film covering the leaves' epidermis that consists of lipid and hydrocarbon polymers impregnated with wax [82]. After the plasma, it appears that the cutin has been destroyed. It is noticed that the stomata were exposed along the entire surface of the leaf. The stomata are apertures in the epidermis and have the function of constituting a channel for the exchange of gases and the plant's transpiration [83]. These facts suggest that the plasma treatment has been executed for too long since the leaf's protective layer has been removed.

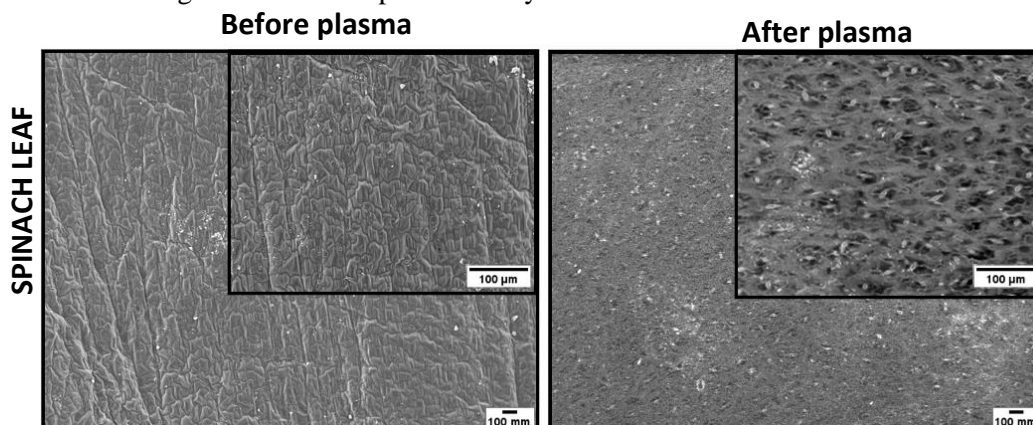


Figure 3.32 - SEM images from spinach leaf top view before and after 45 seconds of plasma generation.

In addition to the previous information, ATR-FTIR of samples without treatment and with 45 seconds of plasma was analyzed and represented in **Figure 3.34**.

The infrared absorption of cork (**Figure 3.34A**) reveals peaks at 2917, 2850, and 1730 cm^{-1} related to suberin chains, at 1600-1350 cm^{-1} related to lignin around 1100 cm^{-1} associated with polysaccharides [84]. The FTIR from the vegetal paper (**Figure 3.34B**) shows the same peaks seen previously on the VEG plasma generator (subsection 3.4). In the spinach leaf case (**Figure 3.34C**), the ATR-FTIR peaks at 3270 cm^{-1} from O-H stretching and at 1632 cm^{-1} from O-H absorption, related to cellulose and water presence. Cutin and cellulose showed interfering absorptive bands at 1018 cm^{-1} (C-O stretching) [85].

It is verified that, after the plasma, the peaks of the absorption bands are at higher absorbance values, as noted in previous cases, which is probably related to the fact that the plasma increases the amount of functional groups present in the surfaces.

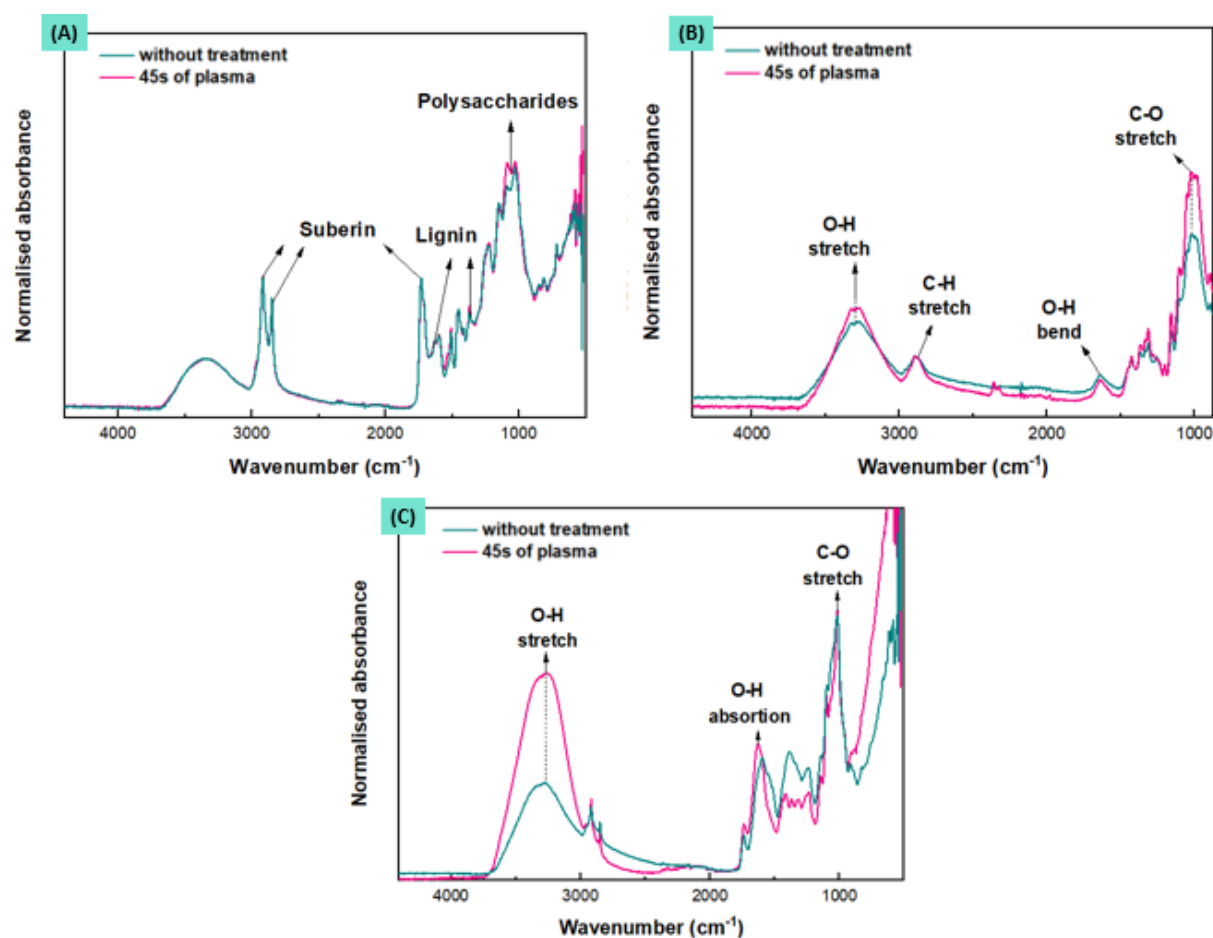


Figure 3.33 - ATR-FTIR spectrum before and after 45 seconds of plasma generation of the different surfaces: (A) cork; (B) vegetal paper and (C) spinach leaf.

4| Conclusions and Future perspectives

During this dissertation, a method of producing paper-based plasma generators that rely on the principle of dielectric barrier discharge was presented. It has been demonstrated that DBD plasma generators patterned by a laser made shadow mask can be produced by a low-cost method that can generate plasma in a vacuum chamber. The paper-based generators have been shown to have the advantage of generating a bulk homogenized volume plasma and a surface plasma, with the stable plasma area ensuring that the gas is treated uniformly. It is also more efficient and with lower energy consumption than other plasma techniques [10], [86].

It was successfully demonstrated that generators with two electrodes confine the plasma better than generators with only one electrode.

The generators patterned by a laser made shadow mask produced with vegetal paper endured the generation of plasma in a greater power range and lasted for a more extended period of time. Other works related to paper generators show generators that presented some degradation with only 15 minutes of generation [45]. In this thesis, it was successfully proved that VEG generators can generate plasma for more than 50 minutes with no visible damage. In addition, these generators are reusable since they have been tested more than once.

The Powercoat XD generators patterned by a laser made shadow mask also proved to be a good substrate option, holding up almost as well as the VEG generator and showing minor damage after the plasma generation.

In the tests performed (except in the time tests when the generators had 30 consecutive minutes to generate plasma), the temperature range is within the specified for cold plasma (below 50°C). This indicates that the generators can contact biological tissues without causing damage.

Furthermore, it was concluded that the type of atmosphere changes the lifetime of the generators and that the argon atmosphere proved to be a more suitable atmosphere than air.

Inkjet printing proved to be a suitable choice to miniaturize the generators' size. Despite the poor robustness of the plasma, it was found that the best paper to produce inkjet generators is the FS because it is devoted to printed electronics, unlike VEG. However, VEG and XD generators produced by laser engraving achieved better results than all the generators produced by inkjet.

In all plasma generation tests performed, it was checked that the DC-bias increases with increasing power and decreases with increasing pressure. Furthermore, the type of gas used in the process would also give the DC-bias a different outcome.

Besides the development and study of the paper-based generators, they were used for surface modification. It was observed that the longer plasma exposure time, the smaller the surface contact angle due to the increase of the surfaces' wettability. Thus, it is concluded that water contact angle results in this study suggested that the DBD plasma produced could effectively improve surface hydrophilicity and, consequently, modify surfaces in a very short time (15-45 seconds).

By concluding this dissertation with great and promising results, it is possible to continue studying and improving paper-based plasma generators' utility. One of the most demanding research topics would be performing this generation of plasma at atmospheric pressure without requiring high power. Upon reaching this goal, it will be possible to make intelligent dressings that heal wounds instantly and simultaneously flexible, conformable, reusable, and biodegradable. Besides, it will be possible to make portable surface modifiers and disinfectants. This will also pave the way for the development of new applications of these cost-effective plasmas.

5| Bibliography

- [1] A. Sakudo, Y. Yagyu, and T. Onodera, “Disinfection and sterilization using plasma technology: Fundamentals and future perspectives for biological applications,” *Int. J. Mol. Sci.*, vol. 20, no. 20, 2019, doi: 10.3390/ijms20205216.
- [2] T. A. Tsalis, K. E. Malamateniou, D. Koulouriotis, and I. E. Nikolaou, “New challenges for corporate sustainability reporting: United Nations’ 2030 Agenda for sustainable development and the sustainable development goals,” *Corp. Soc. Responsib. Environ. Manag.*, no. January, pp. 1–13, 2020, doi: 10.1002/csr.1910.
- [3] R. Martins, I. Ferreira, and E. Fortunato, “Electronics with and on paper,” *Phys. Status Solidi - Rapid Res. Lett.*, vol. 5, no. 9, pp. 332–335, 2011, doi: 10.1002/pssr.201105247.
- [4] Y. Zhang *et al.*, “Flexible electronics based on micro/nanostructured paper,” *Adv. Mater.*, vol. 30, no. 51, pp. 1–39, 2018, doi: 10.1002/adma.201801588.
- [5] A. Greek *et al.*, “Plasma (physics).”
- [6] K. T. A. L. Burm, “Plasma: The fourth state of matter,” *Plasma Chem. Plasma Process.*, vol. 32, no. 2, pp. 401–407, 2012, doi: 10.1007/s11090-012-9356-1.
- [7] E. Vardges Rostomyan, “Introduction: Plasma Parameters and Simplest Models,” *Plasma Sci. [Working Title]*, pp. 1–17, 2020, doi: 10.5772/intechopen.91222.
- [8] “hazardous waste treatment | metal recovery solutions | production processes.”
- [9] K. H. Ip, B. H. Stuart, P. S. Thomas, and A. S. Ray, “Thermal characterization of the clay binder of heritage Sydney sandstones,” *J. Therm. Anal. Calorim.*, vol. 92, no. 1, pp. 97–100, 2008, doi: 10.1007/s10973-007-8743-y.
- [10] S. Duarte and B. H. D. Panariello, “Comprehensive biomedical applications of low temperature plasmas,” *Arch. Biochem. Biophys.*, vol. 693, no. August, p. 108560, 2020, doi: 10.1016/j.abb.2020.108560.
- [11] A. Gao, S. Yang, D. Lu, X. Qi, and Q. Li, “Comparing Acid Red B Dye Decolorization by Glow and Spark Discharge Plasma in Atmospheric Pressure Air,” *IOP Conf. Ser. Earth Environ. Sci.*, vol. 555, no. 1, 2020, doi: 10.1088/1755-1315/555/1/012068.
- [12] K. G. Kostov, R. Y. Honda, L. M. S. Alves, and M. E. Kayama, “Characteristics of dielectric barrier discharge reactor for material treatment,” *Brazilian J. Phys.*, vol. 39, no. 2, pp. 322–325, 2009, doi: 10.1590/S0103-97332009000300015.
- [13] S. Bhosle *et al.*, “Electrical modeling of an homogeneous Dielectric Barrier Discharge (DBD),” *Conf. Rec. - IAS Annu. Meet. (IEEE Ind. Appl. Soc.)*, vol. 4, pp. 2315–2319, 2005, doi: 10.1109/IAS.2005.1518783.
- [14] U. Kogelschatz, “Dielectric-barrier Discharges : Their History , Discharge Physics , and Industrial Applications,” vol. 23, no. 1, pp. 1–46, 2003.
- [15] A. Yehia, “The electrical characteristics of the dielectric barrier discharges,” vol. 063520, 2016, doi: 10.1063/1.4954300.
- [16] S. N. Kane, A. Mishra, and A. K. Dutta, “Preface: International Conference on Recent Trends in Physics (ICRTP 2016),” *J. Phys. Conf. Ser.*, vol. 755, no. 1, 2016, doi: 10.1088/1742-6596/755/1/011001.
- [17] N. Benard and E. Moreau, “On the vortex dynamic of airflow reattachment forced by a single non-thermal plasma discharge actuator,” *Flow, Turbul. Combust.*, vol. 87, no. 1, pp. 1–31, 2011, doi: 10.1007/s10494-011-9325-4.
- [18] X. X. U, “Dielectric barrier discharge ㄹ properties and applications,” pp. 237–242, 2001.
- [19] C. L. Hunks and D. J. Hunzmun, “REPORT Section 3 . Electrical Insulating Materials and Capacitors RADIATION EFFECTS INFORMATION CENTER AERONAUTICS ADMINISTRATION,” *Security*, no. July 1971, 2018.
- [20] U. Kogelschatz, B. Eliasson, and W. Egli, “From ozone generators to flat television screens: History and future potential of dielectric-barrier discharges,” *Pure Appl. Chem.*, vol. 71, no. 10, pp. 1819–1828, 1999, doi: 10.1351/pac199971101819.
- [21] M. Tanino, W. Xilu, K. Takashima, S. Katsura, and A. Mizuno, “Sterilization using Dielectric Barrier Discharge at Atmospheric Pressure,” vol. 10, pp. 102–107, 2007.
- [22] S. L. Kaplan and P. W. Rose, “Plasma surface treatment of plastics to enhance adhesion,” *Int. J. Adhes. Adhes.*, vol. 11, no. 2, pp. 109–113, 1991, doi: 10.1016/0143-7496(91)90035-G.
- [23] S. Mořovská *et al.*, “Cold atmospheric pressure ambient air plasma inhibition of pathogenic bacteria on the surface of black pepper,” *Food Res. Int.*, vol. 106, no. 2017, pp. 862–869, 2018, doi: 10.1016/j.foodres.2018.01.066.
- [24] S. C. Min, S. H. Roh, B. A. Niemira, J. E. Sites, G. Boyd, and A. Lacombe, “Dielectric barrier discharge atmospheric cold plasma inhibits Escherichia coli O157:H7, Salmonella, Listeria monocytogenes, and

- Tulane virus in Romaine lettuce,” *Int. J. Food Microbiol.*, vol. 237, pp. 114–120, 2016, doi: 10.1016/j.ijfoodmicro.2016.08.025.
- [25] O. Volotskova, L. Dubrovsky, M. Keidar, and M. Bukrinsky, “Cold atmospheric plasma inhibits HIV-1 replication in macrophages by targeting both the virus and the cells,” *PLoS One*, vol. 11, no. 10, pp. 1–9, 2016, doi: 10.1371/journal.pone.0165322.
- [26] Z. Chen and R. E. Wirz, “Cold atmospheric plasma for COVID-19,” no. April, pp. 1–7, doi: 10.20944/preprints202004.0126.v1.
- [27] B. Haertel, T. von Woedtke, K. D. Weltmann, and U. Lindequist, “Non-thermal atmospheric-pressure plasma possible application in wound healing,” *Biomol. Ther.*, vol. 22, no. 6, pp. 477–490, 2014, doi: 10.4062/biomolther.2014.105.
- [28] M. Laroussi, “Plasma Medicine: A Brief Introduction,” *Plasma*, 2018, doi: 10.3390/plasma1010005.
- [29] S. Hati, M. Patel, and D. Yadav, “Food bioprocessing by non-thermal plasma technology,” *Curr. Opin. Food Sci.*, vol. 19, pp. 85–91, 2018, doi: 10.1016/j.cofs.2018.03.011.
- [30] F. Rezaei *et al.*, “Investigation of plasma-induced chemistry in organic solutions for enhanced electrospun PLA nanofibers,” *Plasma Process. Polym.*, vol. 15, no. 6, pp. 1–18, 2018, doi: 10.1002/ppap.201700226.
- [31] C. Liu, N. M. D. Brown, and B. J. Meenan, “Dielectric barrier discharge (DBD) processing of PMMA surface: Optimization of operational parameters,” *Surf. Coatings Technol.*, vol. 201, no. 6, pp. 2341–2350, 2006, doi: 10.1016/j.surfcoat.2006.04.001.
- [32] H. U. Lee *et al.*, “Role of reactive gas in atmospheric plasma for cell attachment and proliferation on biocompatible poly ϵ -caprolactone film,” *Appl. Surf. Sci.*, vol. 254, no. 18, pp. 5700–5705, 2008, doi: 10.1016/j.apsusc.2008.03.049.
- [33] G. Buyle, J. Schneider, M. Walker, Y. Akishev, A. Napartovich, and M. Perucca, “Plasma Systems for Surface Treatment,” *Plasma Technol. Hyperfunct. Surfaces Food, Biomed. Text. Appl.*, pp. 33–61, 2010, doi: 10.1002/9783527630455.ch2.
- [34] J. Chauvin, F. Judée, M. Yousfi, P. Vicendo, and N. Merbahi, “Analysis of reactive oxygen and nitrogen species generated in three liquid media by low temperature helium plasma jet,” *Sci. Rep.*, vol. 7, no. 1, 2017, doi: 10.1038/s41598-017-04650-4.
- [35] A. H. Ghorashi, M. A. R. Tasouji, and A. Kargarian, “Optimum cold plasma generating device for treatment of *Aspergillus flavus* from nuts surface,” *J. Food Sci. Technol.*, vol. 57, no. 11, pp. 3988–3994, 2020, doi: 10.1007/s13197-020-04429-y.
- [36] S. K. Sharma and A. Sharma, “Sterilization of Microorganisms Contaminated Surfaces and its Treatment with Dielectric Barrier Discharge Plasma,” *Trans. Indian Natl. Acad. Eng.*, vol. 5, no. 2, pp. 321–326, 2020, doi: 10.1007/s41403-020-00124-8.
- [37] D. Tobjörk and R. Österbacka, “Paper electronics,” *Adv. Mater.*, vol. 23, no. 17, pp. 1935–1961, 2011, doi: 10.1002/adma.201004692.
- [38] H. Ba *et al.*, “Foldable flexible electronics based on few-layer graphene coated on paper composites,” *Carbon N. Y.*, vol. 167, pp. 169–180, 2020, doi: 10.1016/j.carbon.2020.05.012.
- [39] B. Wang and L. L. Kerr, “Dye sensitized solar cells on paper substrates,” *Sol. Energy Mater. Sol. Cells*, vol. 95, no. 8, pp. 2531–2535, 2011, doi: 10.1016/j.solmat.2011.02.032.
- [40] L. Yang, A. Rida, R. Vyas, and M. M. Tentzeris, “RFID tag and RF structures on a paper substrate using inkjet-printing technology,” *IEEE Trans. Microw. Theory Tech.*, vol. 55, no. 12, pp. 2894–2901, 2007, doi: 10.1109/TMTT.2007.909886.
- [41] J. Hu *et al.*, “Advances in paper-based point-of-care diagnostics,” *Biosens. Bioelectron.*, vol. 54, pp. 585–597, 2014, doi: 10.1016/j.bios.2013.10.075.
- [42] H. El Omari, A. Zyane, A. Belfkira, M. Taourirte, and F. Brouillette, “Dielectric Properties of Paper Made from Pulps Loaded with Ferroelectric Particles,” *J. Nanomater.*, vol. 2016, 2016, doi: 10.1155/2016/3982572.
- [43] G. I. Torgovnikov, “Dielectric Properties of Wood-Based Materials,” pp. 135–159, 1993, doi: 10.1007/978-3-642-77453-9_8.
- [44] J. B. Whitehead and E. W. Greenfield, “Dielectric Properties of Cellulose Paper—I,” *Trans. Am. Inst. Electr. Eng.*, vol. 53, no. 10, pp. 1389–1396, 1934, doi: 10.1109/T-AIEE.1934.5056528.
- [45] G. H.-Q. Lateral and O. Bulk, “JMEMS Letters,” *J. Microelectromechanical Syst.*, vol. 21, no. 2, pp. 253–255, 2012.
- [46] J. Xie, Q. Chen, P. Suresh, S. Roy, J. F. White, and A. D. Mazzeo, “Paper-based plasma sanitizers,” *Proc. Natl. Acad. Sci. U. S. A.*, vol. 114, no. 20, pp. 5119–5124, 2017, doi: 10.1073/pnas.1621203114.
- [47] F. Sima, C. Ristoscu, L. Duta, O. Gallet, K. Anselme, and I. N. Mihailescu, *Laser thin films deposition and characterization for biomedical applications*. Elsevier Ltd, 2016.
- [48] J. Park, J. H. Shin, and J. K. Park, “Experimental analysis of porosity and permeability in pressed paper,” *Micromachines*, vol. 7, no. 3, 2016, doi: 10.3390/mi7030048.

- [49] B. M. Singh, H. M. Haverinen, P. Dhagat, and G. E. Jabbour, "Inkjet Printing — Process and Its Applications," vol. 90014, pp. 673–685, 2010, doi: 10.1002/adma.200901141.
- [50] P. Bajpai and P. Bajpai, "Brief Description of the Pulp and Papermaking Process," *Biotechnol. Pulp Pap. Process.*, pp. 9–26, 2018, doi: 10.1007/978-981-10-7853-8_2.
- [51] R. Coating, R. Paper, and R. Coating, "P _ E:Smart Paper Type 3," 1924, [Online]. Available: https://www.felix-schoeller.com/fileadmin/content/documents/downloads/pe_smart_Type3.pdf.
- [52] S. A. Yates, "The conservation of nineteenth-century tracing paper," *Pap. Conserv.*, vol. 8, no. 1, pp. 20–39, 1984, doi: 10.1080/03094227.1984.9638456.
- [53] C. M. De, "Technical data sheet," vol. 41, no. 0, pp. 2–4, 2014.
- [54] M. Laroussi, "Cold Plasma in Medicine and Healthcare: The New Frontier in Low Temperature Plasma Applications," *Front. Phys.*, vol. 8, no. March, pp. 1–7, 2020, doi: 10.3389/fphy.2020.00074.
- [55] A. T. Vicente *et al.*, "Optoelectronics and Bio Devices on Paper Powered by Solar Cells," *Nanostructured Sol. Cells*, 2017, doi: 10.5772/66695.
- [56] P. Nascimento, R. Marim, G. Carvalho, and S. Mali, "Nanocellulose produced from rice hulls and its effect on the properties of biodegradable starch films," *Mater. Res.*, vol. 19, no. 1, pp. 167–174, 2016, doi: 10.1590/1980-5373-MR-2015-0423.
- [57] X. Chen, X. Qian, and X. An, "Using calcium carbonate whiskers as papermaking filler," *BioResources*, 2011, doi: 10.15376/biores.6.3.2435-2447.
- [58] G. Jovanovski, V. Stefov, B. Šoptrajanov, and B. Boev, "Minerals from Macedonia. IV. Discrimination between some carbonate minerals by FTIR spectroscopy," *Neues Jahrb. fur Mineral. Abhandlungen*, vol. 177, no. 3, pp. 241–253, 2002, doi: 10.1127/0077-7757/2002/0177-0241.
- [59] Y. Cui, Y. Zheng, and W. Wang, "Synthesis of 4A Zeolite from Kaolinite-type pyrite flotation tailings (KPFT)," *Minerals*, vol. 8, no. 8, 2018, doi: 10.3390/min8080338.
- [60] M. Chen, B. Coasne, R. Guyer, D. Derome, and J. Carmeliet, "Role of hydrogen bonding in hysteresis observed in sorption-induced swelling of soft nanoporous polymers," *Nat. Commun.*, vol. 9, no. 1, 2018, doi: 10.1038/s41467-018-05897-9.
- [61] M. Boselli *et al.*, "Study of the role of dielectric material in a dielectric barrier discharge (DBD) plasma source for dermatological applications," pp. 595–598, 2013.
- [62] I. A. De Souza *et al.*, "Study of the influence of variation in distances between electrodes in spectral DBD plasma excitation," *Mater. Res.*, vol. 19, no. 1, pp. 202–206, 2016, doi: 10.1590/1980-5373-MR-2015-0205.
- [63] R. Tyata' and D. Subedi, "An Investigation of the Effect of Electrode Geometry and Frequency of Power Supply in the Homogeneity of Dielectric Barrier Discharge in Air," *Kathmandu Univ. J. Sci. Eng. Technol.*, vol. 6, no. 1, pp. 96–101, 1970, doi: 10.3126/kuset.v6i1.3316.
- [64] C. Miao, F. Liu, Q. Wang, M. Cai, and Z. Fang, "Investigation on the influence of electrode geometry on characteristics of coaxial dielectric barrier discharge reactor driven by an oscillating microsecond pulsed power supply," *Eur. Phys. J. D*, vol. 72, no. 3, 2018, doi: 10.1140/epjd/e2018-80575-3.
- [65] D. Amri, Z. Nawawi, and M. I. Jambak, "The Comparison between types of electrodes in Dielectric Barrier Discharge (DBD) plasma for obtaining potable water: A review," *IOP Conf. Ser. Mater. Sci. Eng.*, vol. 620, no. 1, 2019, doi: 10.1088/1757-899X/620/1/012091.
- [66] J. Upadhyay, D. Im, S. Popović, L. Phillips, and L. Vušković, "Self-bias Dependence on Process Parameters in Asymmetric Cylindrical Coaxial Capacitively Coupled Plasma," *arXiv.org*, vol. physics.ac, no. June, p. 1506.05167v1, 2015.
- [67] F. Nespoli, S. Redaelli, L. Ruggeri, F. Fumagalli, D. Olivari, and G. Ristagno, "A complete review of preclinical and clinical uses of the noble gas argon: Evidence of safety and protection," *Ann. Card. Anaesth.*, vol. 22, no. 2, pp. 122–135, 2019, doi: 10.4103/aca.ACA_111_18.
- [68] M. J. Kushner, "MonteCarlo simulation of electron properties in rf parallel plate capacitively coupled discharges Monte-Carlo simulation of electron properties in rf parallel plate capacitively coupled discharges," vol. 4958, no. 1983, 2006, doi: 10.1063/1.332763.
- [69] J. Coates, "Encyclopedia of Analytical Chemistry -Interpretation of Infrared Spectra, A Practical Approach," *Encycl. Anal. Chem.*, pp. 1–23, 2004, [Online]. Available: <http://www3.uma.pt/jrodrigues/disciplinas/QINO-II/Teorica/IR.pdf>.
- [70] C. Cao, Z. Yang, L. Han, X. Jiang, and G. Ji, "Study on in situ analysis of cellulose, hemicelluloses and lignin distribution linked to tissue structure of crop stalk internodal transverse section based on FTIR microspectroscopic imaging," *Cellulose*, vol. 22, no. 1, pp. 139–149, 2015, doi: 10.1007/s10570-014-0525-7.
- [71] Q. Liu, S. Wang, Y. Zheng, Z. Luo, and K. Cen, "Mechanism study of wood lignin pyrolysis by using TG-FTIR analysis," *J. Anal. Appl. Pyrolysis*, vol. 82, no. 1, pp. 170–177, 2008, doi: 10.1016/j.jaap.2008.03.007.
- [72] Z. Movasaghi, S. Rehman, and I. Rehman, "Fourier Transform Infrared (FTIR) Spectroscopy of

- Biological Tissues,” vol. 4928, no. January, 2018, doi: 10.1080/05704920701829043.
- [73] K. Poonsawat, R. Kiattinun, P. Worakul, P. Thonglor, P. Amnuaycheewa, and S. Dangtip, “FTIR analysis of thermal and plasma treatments on riceberry brown rice,” *J. Phys. Conf. Ser.*, vol. 1144, no. 1, 2018, doi: 10.1088/1742-6596/1144/1/012175.
- [74] A. H. Goldstein and I. E. Galbally, “Known and unexplored organic constituents in the earth’s atmosphere,” *Environ. Sci. Technol.*, vol. 41, no. 5, pp. 1514–1521, 2007, doi: 10.1021/es072476p.
- [75] D. Staack, B. Farouk, A. Gutsol, and A. Fridman, “DC normal glow discharges in atmospheric pressure atomic and molecular gases,” *Plasma Sources Sci. Technol.*, vol. 17, no. 2, 2008, doi: 10.1088/0963-0252/17/2/025013.
- [76] D. Yan, J. H. Sherman, and M. Keidar, “Cold atmospheric plasma, a novel promising anti-cancer treatment modality,” *Oncotarget*, vol. 8, no. 9, pp. 15977–15995, 2017, doi: 10.18632/oncotarget.13304.
- [77] J. Li, C. Ma, S. Zhu, F. Yu, B. Dai, and D. Yang, “A review of recent advances of dielectric barrier discharge plasma in catalysis,” *Nanomaterials*, vol. 9, no. 10, pp. 1–34, 2019, doi: 10.3390/nano9101428.
- [78] F. R. Oliveira, E. A. A. Silva, S. N. Do Carmo, F. Steffens, and A. P. G. D. V. Souto, “Functionalization of natural cork composite with microcapsules after plasma treatment,” *Adv. Mater. Sci. Eng.*, vol. 2014, 2014, doi: 10.1155/2014/685829.
- [79] T. H. C. Costa, M. C. Feitor, C. Alves Junior, and C. M. Bezerra, “Caracterização de filmes de poliéster modificados por plasma de O₂ a baixa pressão,” *Matéria (Rio Janeiro)*, vol. 13, no. 1, pp. 65–76, 2008, doi: 10.1590/s1517-70762008000100008.
- [80] K. S. Kim, K. H. Lee, K. Cho, and C. E. Park, “Surface modification of polysulfone ultrafiltration membrane by oxygen plasma treatment,” *J. Memb. Sci.*, vol. 199, no. 1, pp. 135–145, 2002, doi: 10.1016/S0376-7388(01)00686-X.
- [81] H. Pan *et al.*, “Cold plasma-induced surface modification of heat-polymerized acrylic resin and prevention of early adherence of *Candida albicans*,” *Dent. Mater. J.*, vol. 34, no. 4, pp. 529–536, 2015, doi: 10.4012/dmj.2015-035.
- [82] E. Gutiérrez-Rodríguez, H. J. Lieth, J. A. Jernstedt, J. M. Labavitch, T. V. Suslow, and M. I. Cantwell, “Texture, composition and anatomy of spinach leaves in relation to nitrogen fertilization,” *J. Sci. Food Agric.*, vol. 93, no. 2, pp. 227–237, 2013, doi: 10.1002/jsfa.5780.
- [83] A. . Fallis, “Estomas,” *J. Chem. Inf. Model.*, 2013.
- [84] H. Garcia *et al.*, “Dissolution of cork biopolymers in biocompatible ionic liquids,” *Green Chem.*, vol. 12, no. 3, pp. 367–36, 2010, doi: 10.1039/b922553f.
- [85] J. A. Hardin, C. L. Jones, P. R. Weckler, N. O. Maness, J. W. Dillwith, and R. D. Madden, “Rapid Quantification of Spinach Leaf Cuticular Wax Using Fourier Transform Infrared Attenuated Total Reflectance Spectroscopy,” *Trans. ASABE*, vol. 56, no. 1, pp. 331–339, 2013, doi: 10.13031/2013.42579.
- [86] O. Gabriel, S. Kirner, M. Klick, B. Stannowski, and R. Schlatmann, “Plasma monitoring and PECVD process control in thin film silicon-based solar cell manufacturing,” *EPJ Photovoltaics*, vol. 5, no. February, 2014, doi: 10.1051/epjpv/2013028.

Annex

A. | Annex

This annex will provide additional information regarding the Materials and Methods chapter, which could not be incorporated in the main text for lack of space. The data related to the deposition of aluminum, height, length, and images taken from Jiusion digital microscope of the generator's design by a laser made shadow mask are presented.

A.1 Parameters of the deposition of aluminum in the generator's design by a laser made shadow mask

Table A.1- Parameters of the deposition of aluminum in the generator's design by a laser made shadow mask.

Initial P (mbar)	Initial T (°C)	H2O T (°C)	Density	Z Factor	Thickness (nm)	Growth rate (nm/s)	Current (mA)	Final P (mbar)	Final T (°C)
8.5×10^{-6}	27	9	2.7	8.2	100	0.5	0.12	1.1×10^{-5}	35

Table A.2- Data on the thickness, diameter, and height of the generator's design by a laser made shadow mask. Thickness 1 is referred to generators with one electrode. Thickness 2 is referred to generators with one electrode.

	Felix Schoeller	Canson Vegetal	Powercoat XD
Thickness 1 (μm)	175.2	65.2	128.2
Thickness 2 (μm)	175.1	65.1	128.1
Diameter (cm)	8.5		
Height (cm)	11.5		

A.2 Images of the *Jiusion* digital microscope of the generator's design by a laser made shadow mask

A2.1 Generator with Felix Scholler paper

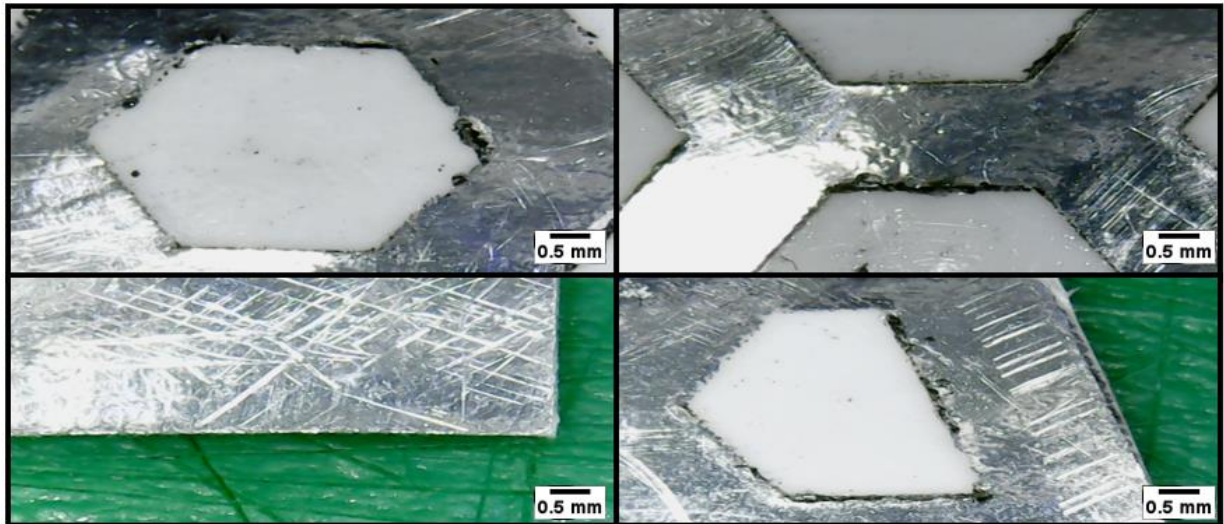


Figure A.1 - Images of the *Jiusion* digital of FS generator design by a laser made shadow mask.

A2.2 Generator with Canson Vegetal paper

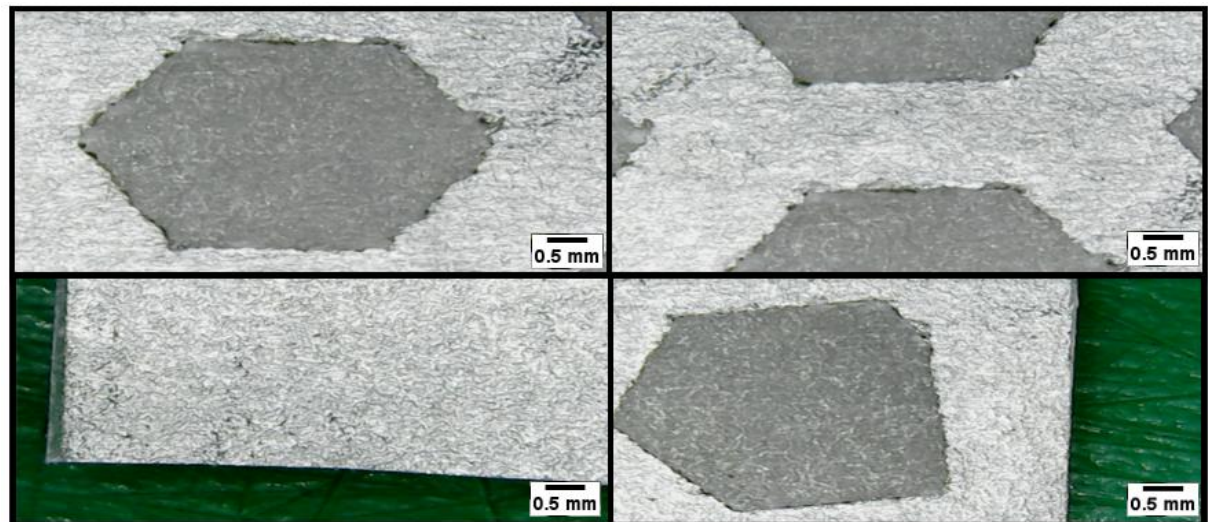


Figure A.2 - Images of the *Jiusion* digital of VEG generator design by a laser made shadow mask.

A2.3 Generator with Powercoat™ XD paper

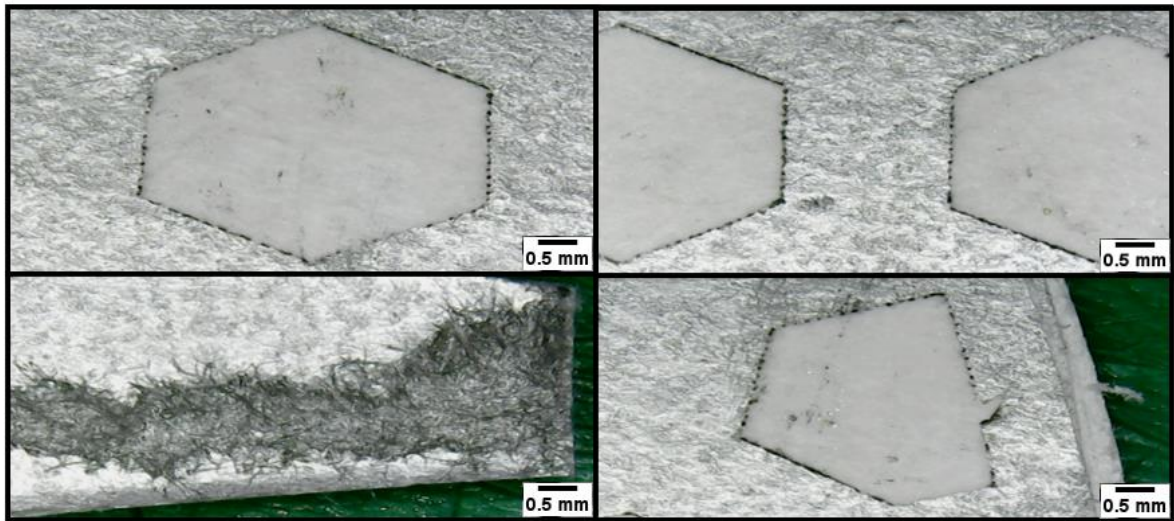


Figure A.3 - Images of the Jusion digital of XD generator design by a laser made shadow mask.

B. | Annex

This annex will provide additional information regarding the Materials and Methods chapter, which could not be incorporated in the main text for lack of space. The data related to the inkjet printing method's properties, height, length, and images taken from the Jiusion digital microscope of the inkjet generators are presented.

B.1 Properties of the inkjet printing method

Table B.1 - Properties of the inkjet printing method with generators made with VEG and FS papers.

	VEG	VEG	VEG	FS	FS
Substrate temperature	45°C	45°C	45°C	45°C	45°C
Resolution	200DPI (first layer) and 300DPI (second layer)	200DPI (first layer) and x2 300DPI (second layer)	400DPI	600DPI (two layers)	700DPI
Print speed	150 mm/s	150 mm/s	150 mm/s	150 mm/s	150 mm/s



Figure B.1 - Photographs of the generators made by inkjet printing. A 5-cent coin for scale purposes (21.25mm in diameter).

Table B.2 - Diameter and height of the generators made by inkjet printing method.

	Canson Vegetal	Felix Schoeller
Diameter (cm)	3.6	3.6
Height (cm)	6	6

B.2 Images of the *Jiusion* digital microscope of the generators produced by inkjet printing

B2.1 Generator with Vegetal paper

i Inkjet VEG 200DPI (first layer) and 300DPI (second layer)

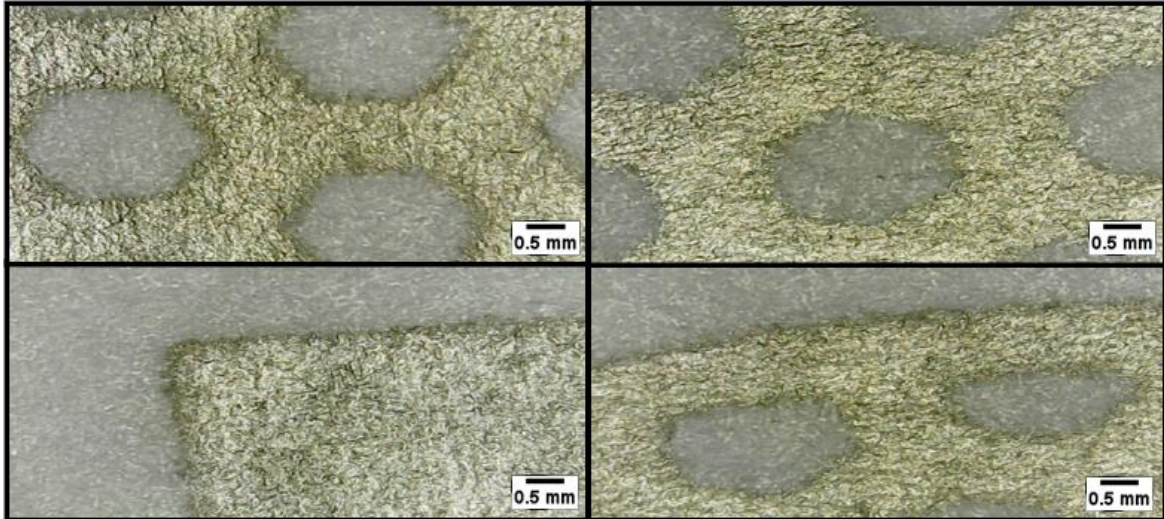


Figure B.2 - Images of the *Jiusion* digital of VEG 200DPI generator made by inkjet method.

ii Inkjet VEG 200DPI (first layer) and x2 300DPI (second layer)

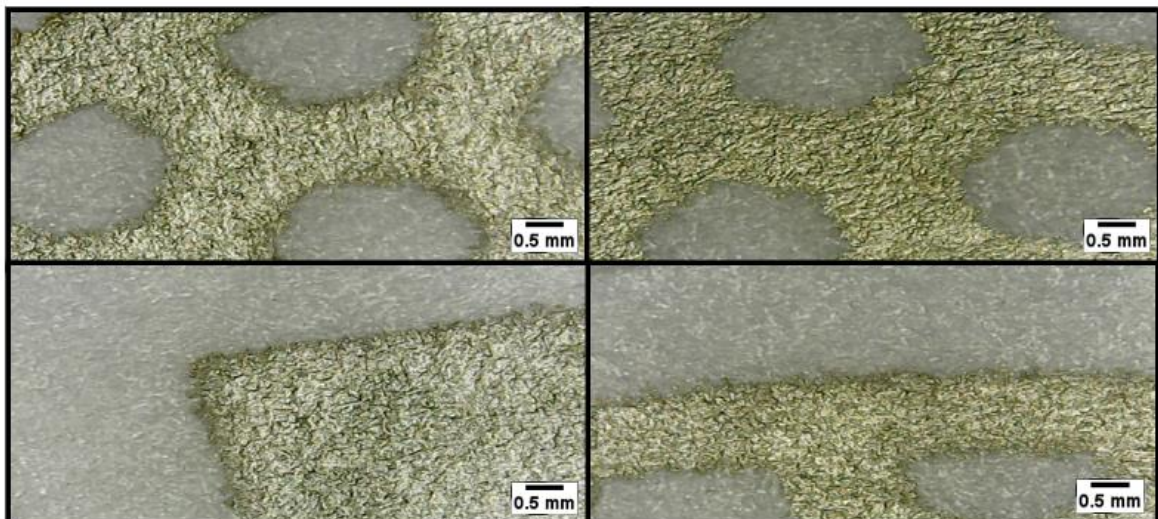


Figure B.3 - Images of the *Jiusion* digital of VEG 200DPI and 300 DPI generator made by inkjet method.

iii Inkjet VEG 400 DPI

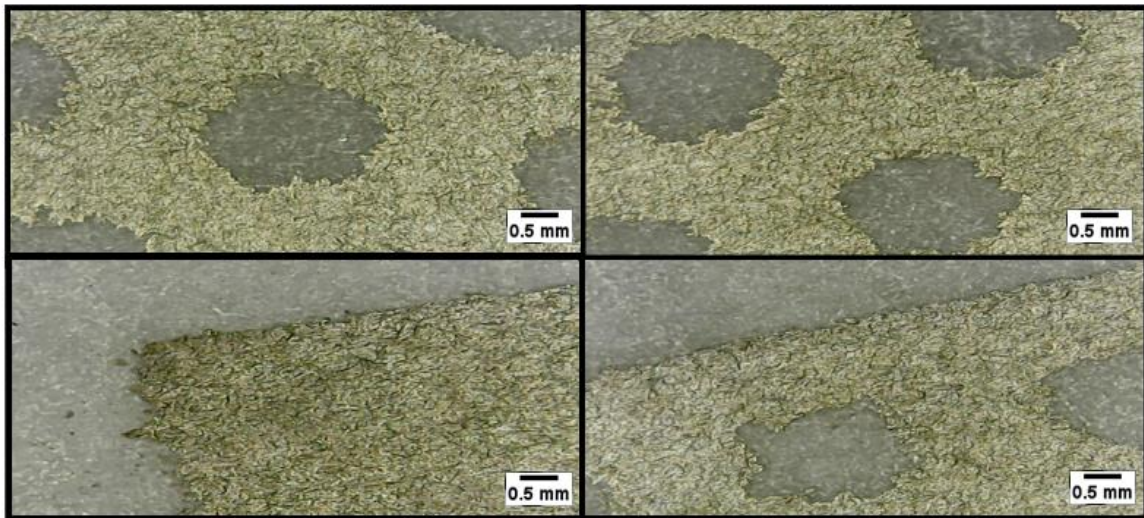


Figure B.4 - Images of the Jusion digital of VEG 400DPI generator made by inkjet method.

B2.2 Generator with Felix Scholler paper

i Inkjet FS 600DPI (two layers)

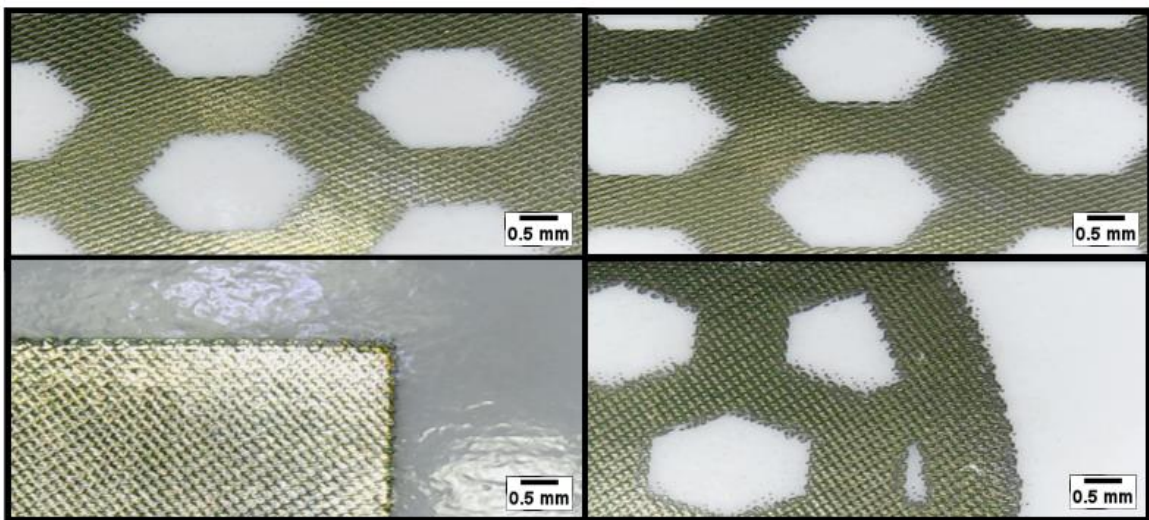


Figure B.5 - Images of the Jusion digital of FS 600DPI generator made by inkjet method.

ii Inkjet FS 700 DPI

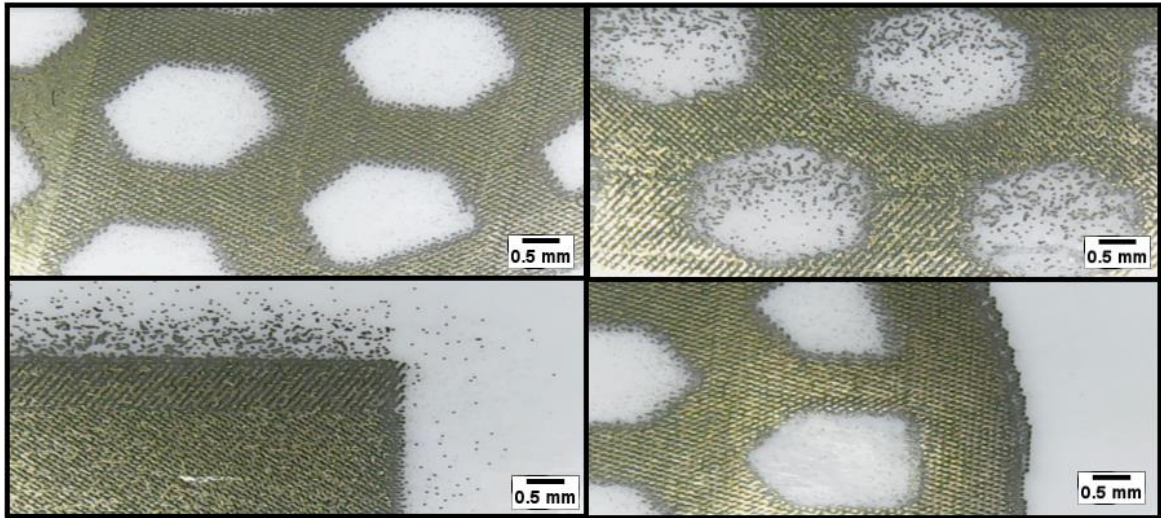


Figure B.6 - Images of the Jusion digital of FS 700DPI generator made by inkjet method.

C. | Annex

C. Properties of the different papers

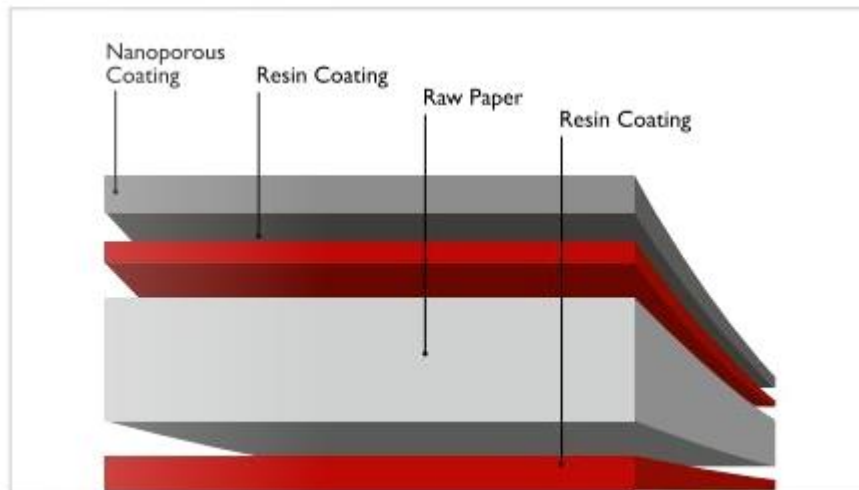
C.1 Felix Scholler type 3 smart paper datasheet

p_e:smart paper type 3

White opaque paper based substrate having hydrophilic nanoporous surface coating.

Classification / Type: Substrate

Electrical Specifications: Insulator



Specifications:

Property	Unit	Type 3	Range	Test Method
Caliper	µm	175	± 10	DIN 20534
Grammage	g/m ²	170	± 10	ISO 536
Gloss front side	60°	50	± 10	DIN 67530
surface free energie front side	mN/m	65	± 10	Schoeller Method
surface free energie reverse side	mN/m	40	± 10	Schoeller Method
Surface resistance front side	Ohm	> 10E09		Schoeller Method
Surface resistance reverse side	Ohm	< 10E13		Schoeller Method
Stiffness MD (10mm/7,5°)	mN	> 120		DIN 53121
Stiffness CD (10mm/7,5°)	mN	> 90		DIN 53122
Temperature resistance	°C	< 100		Schoeller Method
Tensile Strength Dry MD	N/15mm	> 120		ISO 1924-1
Tensile Strength Dry CD	N/15mm	> 60		ISO 1924-1

Figure C.1 - Felix Scholler type 3 smart paper datasheet.

C.2 Powercoat™ XD 125 datasheet

POWERCOAT XD PAPER						
CHARACTERISTICS	APPARATUS	STANDARDS		125g	200g	
Basis Weight g/m ²	Sartorius L2200 Balance	NF EN ISO 536- RNE PC.110- RNE PC.111		129	202	
Thickness µm	M20	NF EN ISO 20534- PC.90 ISO 534- PC.91/PC.101		128	204	
Bulk cm ³ /g				0.99	1.01	
Smoothness Ra (µm)	Bekk (s)			136	80	
	Profilometer Ra (µm)			1500	2000	
Porosity ml/min	Bondson L&W	NF Q 03-076-COFRAC PC.390 ISO 5636/3-COFRAC PC.391		2	35	
Tear mN	Tear tester 60-220	NF EN 21974- RNE PC.60		MD	576	871
				CD	604	932
Tear index mN.m ² /g				MD	4	4
				CD	5	5
Tensile	Tensile tester MTC-100	NF EN ISO 1924- COFRAC PC.20- COFRAC PC.21	Force N	MD	134	88
				CD	70	48
			Elongation mm	MD	3.230	2.935
				CD	7.577	5.897
Stiffness Nmm	Stiffness tester Frank	ISO 2493		MD	1.498	4.044
				CD	0.964	2.371
Burst kPa	Bursting tester EC05	NF Q 03-053- RNE PC0.40 ISO 2758-RNE PC0.41		386	489	
Burst index kPa.m ² /g				3	2	
Brightness	Color Touch CTHA 2045	NF Q 03-039- RNE PC.200 ISO 2470- RNE PC.201		82.6	82.4	
Yellowing after curing (ΔE)	Color Touch CTHA 2045	Internal method	5 minutes at 180°C	2.8	2.6	
Moisture Content %	Oven Gallenkamp Kem Balance	NF EN 20 287-PC.40 ISO 287-PC.41		Wet weight	8.11	12.64
				Dry weight	7.72	12.12
				Moisture content	4.81	4.11
Shrinkage %	Unrestrained at 200°C / 5 min			MD	-0.36	-0.35
				CD	-0.71	-0.70
	Reconditioned at 23°C / 50%RH			MD	-0.10	-0.07
				CD	-0.19	-0.14

Figure C.2- Powercoat™ XD 125 datasheet.

D. | Annex

This annex will be provided additional information regarding the Results and Discussion chapter that could not be incorporated in the main text for lack of space. Here will be presented the data related to the plasma generation optimization study made in an argon atmosphere.

D. Plasma generation optimization study

D.1 Argon Atmosphere: Generator with FS paper

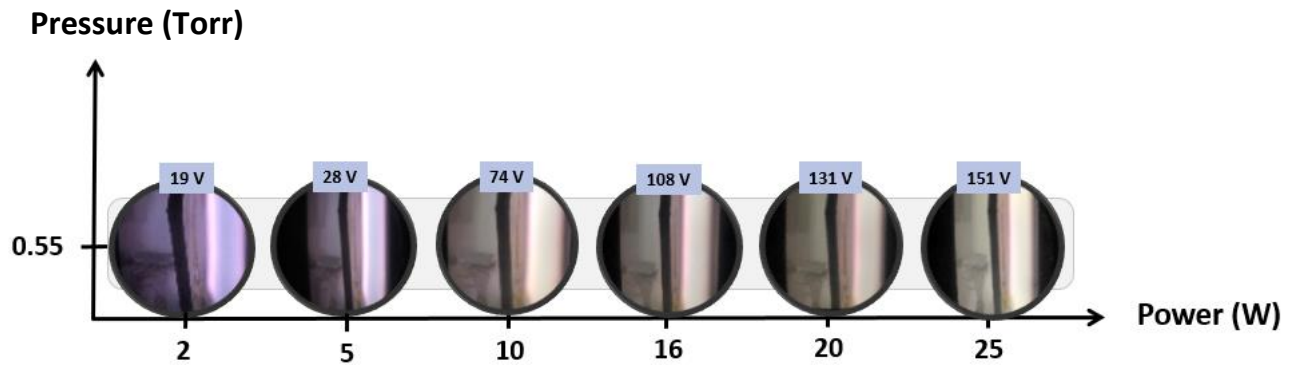


Figure D.1 - Plasma generation optimization test with an FS generator in an argon atmosphere. DC-bias represented in blue. Plasma time of 12 minutes.

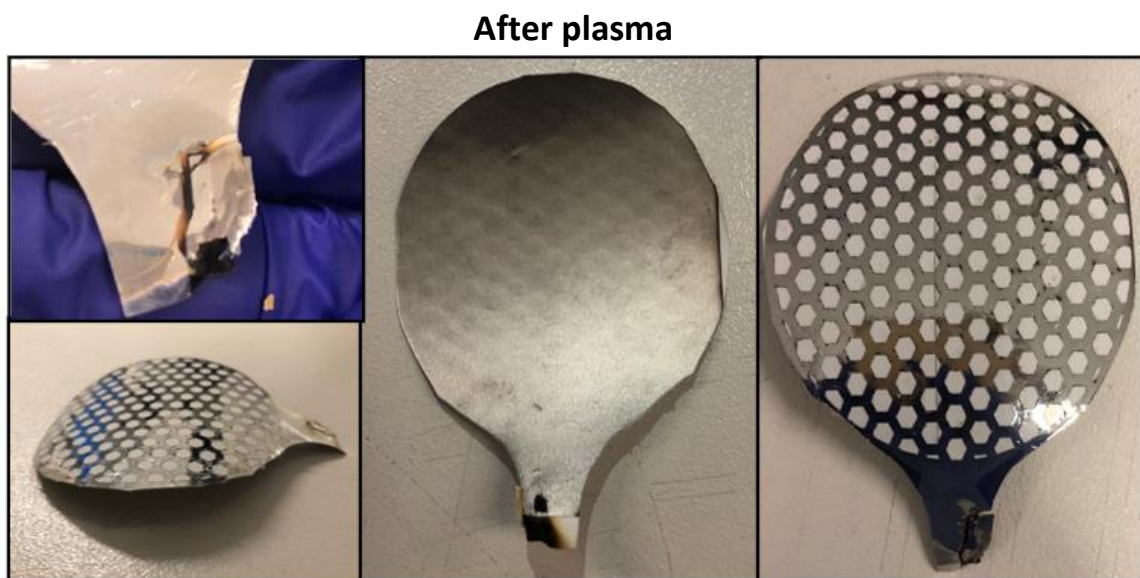


Figure D.2 - Photograph of the FS generator after the optimization test in an argon atmosphere.

D.2 Argon Atmosphere: Generator with VEG paper

Pressure (Torr)

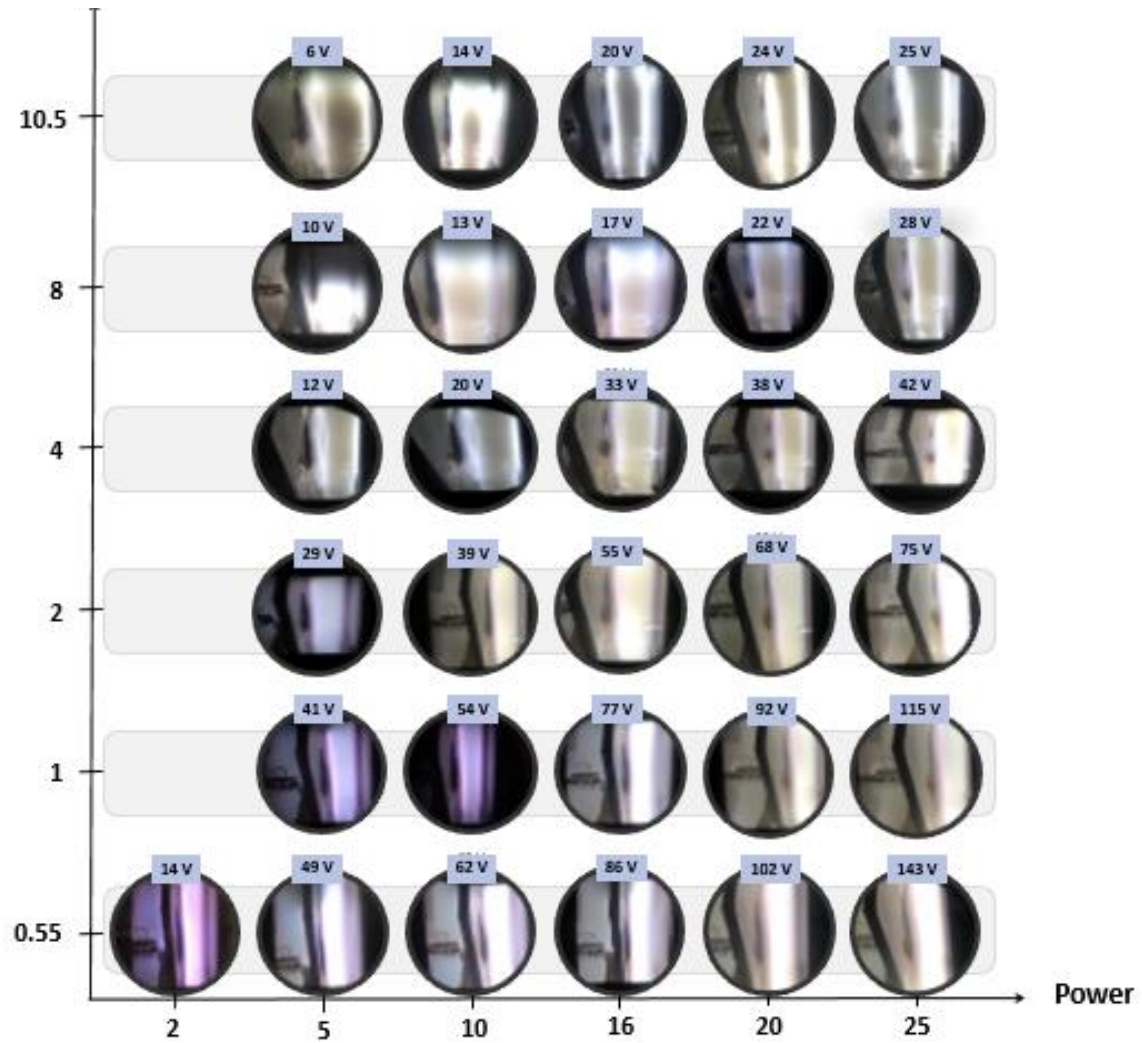


Figure D.3 - Plasma generation optimization test with a VEG generator in an argon atmosphere. DC-bias represented in blue. Plasma time of 62 minutes.

After plasma

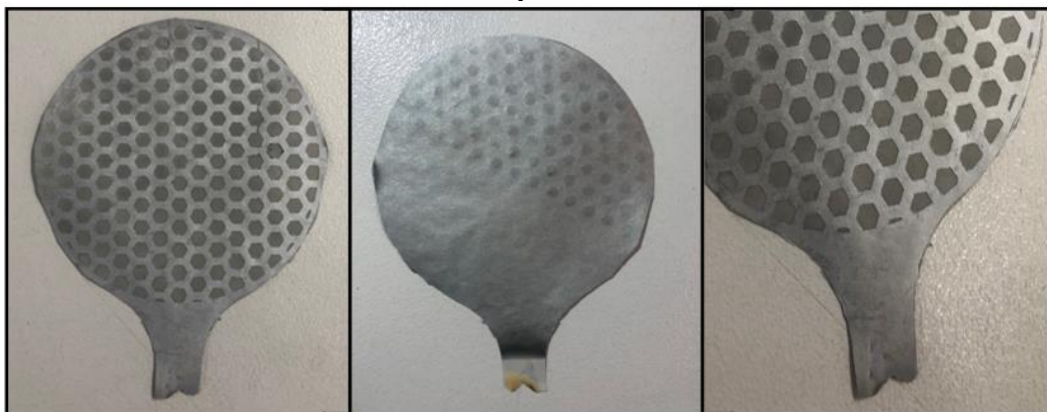


Figure D.4 -- Photograph of the VEG generator after the optimization test in an argon atmosphere.

D.3 Argon Atmosphere: Generator with XD paper

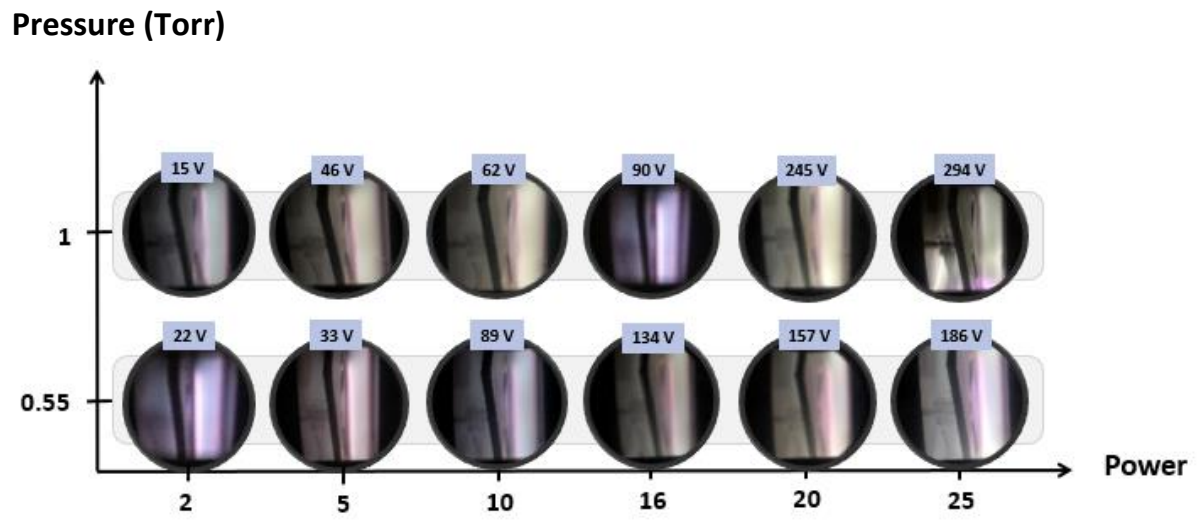


Figure D.5 - Plasma generation optimization test with an XD generator in an argon atmosphere. DC-bias represented in blue. Plasma time of 24 minutes.

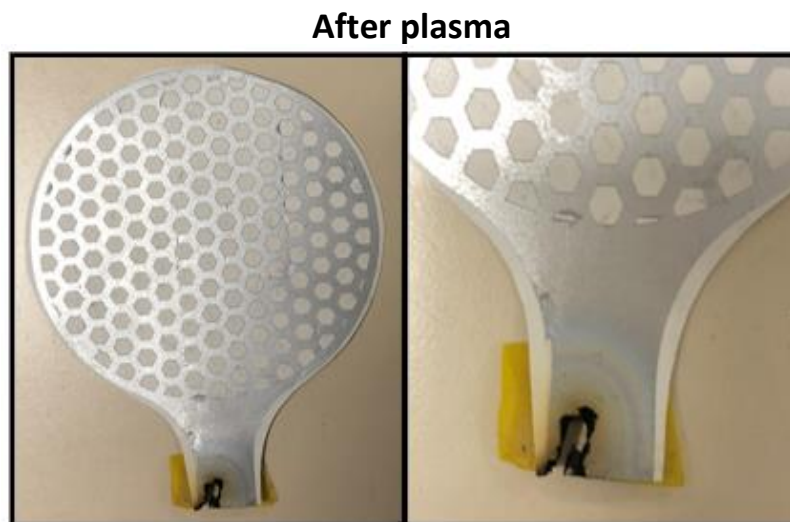


Figure D.6 - Photograph of the XD generator after the optimization test in an argon atmosphere.

E. | Annex

This annex will be provided additional information regarding the Results and Discussion chapter that could not be incorporated in the main text for lack of space. Here will be presented the data related to the plasma generation study, made in argon and then in an air atmosphere.

E. Plasma generation study

E.1 Argon Atmosphere: Generator with XD paper

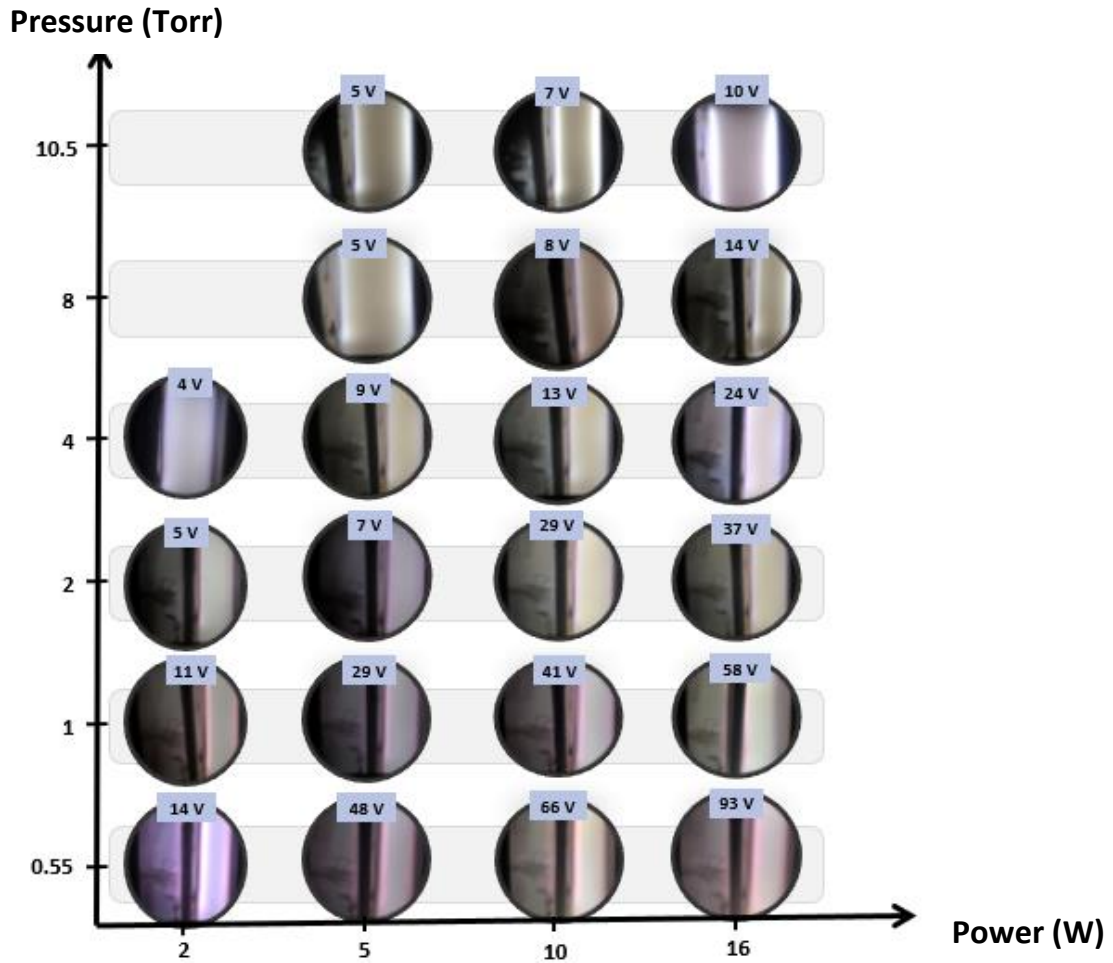


Figure E.1 - Plasma generation test with an XD generator in an argon atmosphere. DC-bias represented in blue. Plasma time of 38 minutes.

E.2 Air Atmosphere: SEM images from the generator with VEG paper

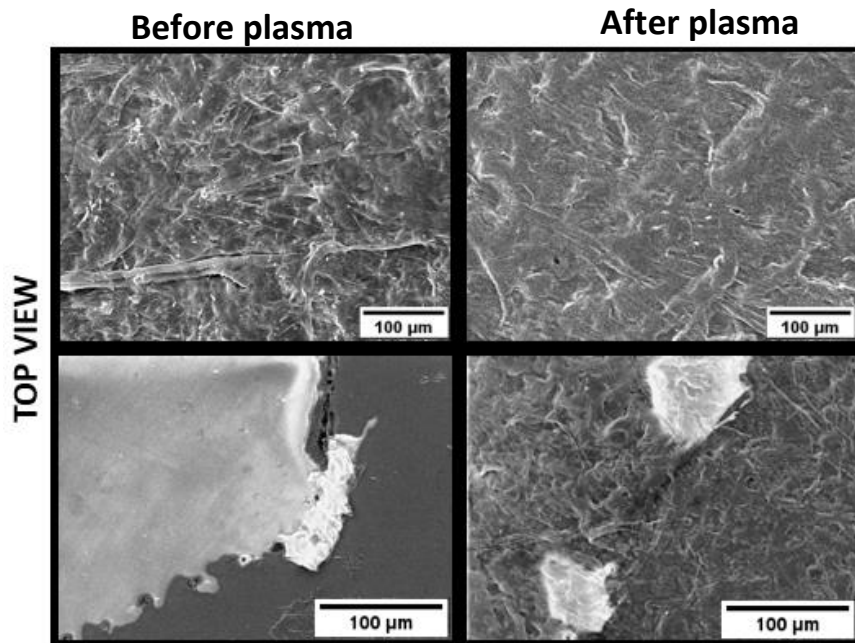


Figure E.2 - SEM images from VEG generator of the top view before and after the plasma generation in air atmosphere.

E.3 Air Atmosphere: SEM images from the generator with XD paper

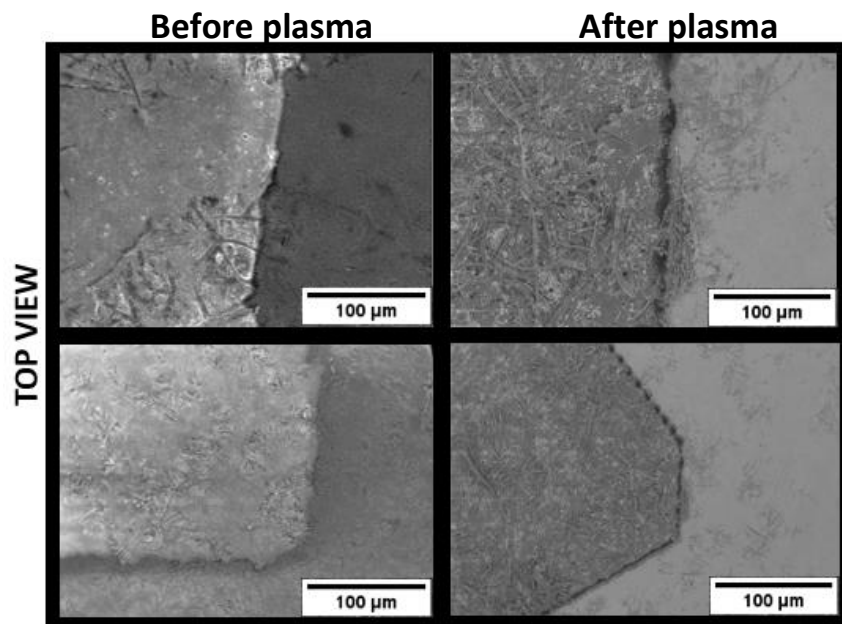


Figure E.3 - SEM images from XD generator of the top view before and after the plasma generation in air atmosphere.

E.4 Air Atmosphere: ATR-FTIR of the generators before and after plasma

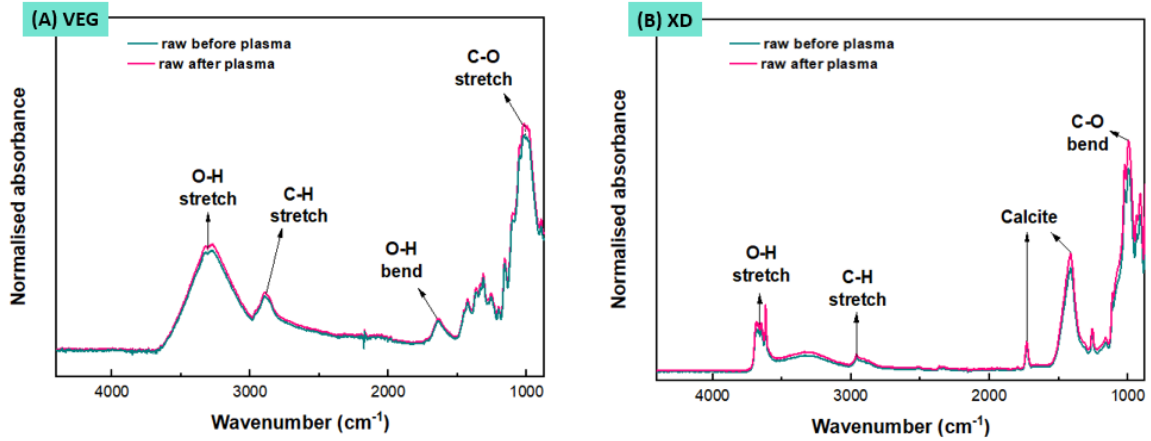


Figure E.4 - ATR-FTIR spectrum before and after the plasma generation in argon of the papers:

(A) VEG paper and (B) XD paper. Plasma time of 6 minutes.

E.5 Comparison between argon and air atmosphere: DC-bias versus Power graph

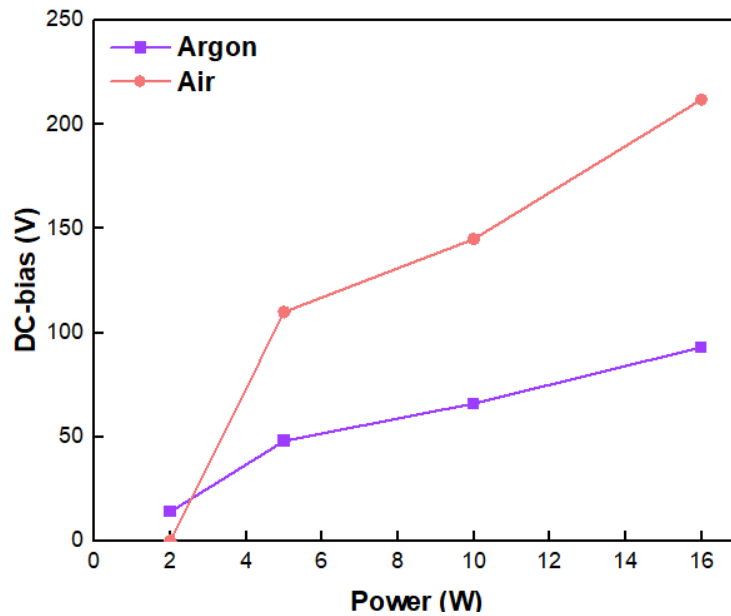


Figure E.5 - DC-bias vs Power graph: comparison between argon and air atmosphere.

F. | Annex

This annex will be provided additional information regarding the Results and Discussion chapter that could not be incorporated in the main text for lack of space. Here will be presented the data related to the plasma generation time tests and OES analysis, made in an argon atmosphere.

F. Plasma generation time tests and OES

F.1 Optical emission spectroscopy: Generator with *XD* paper

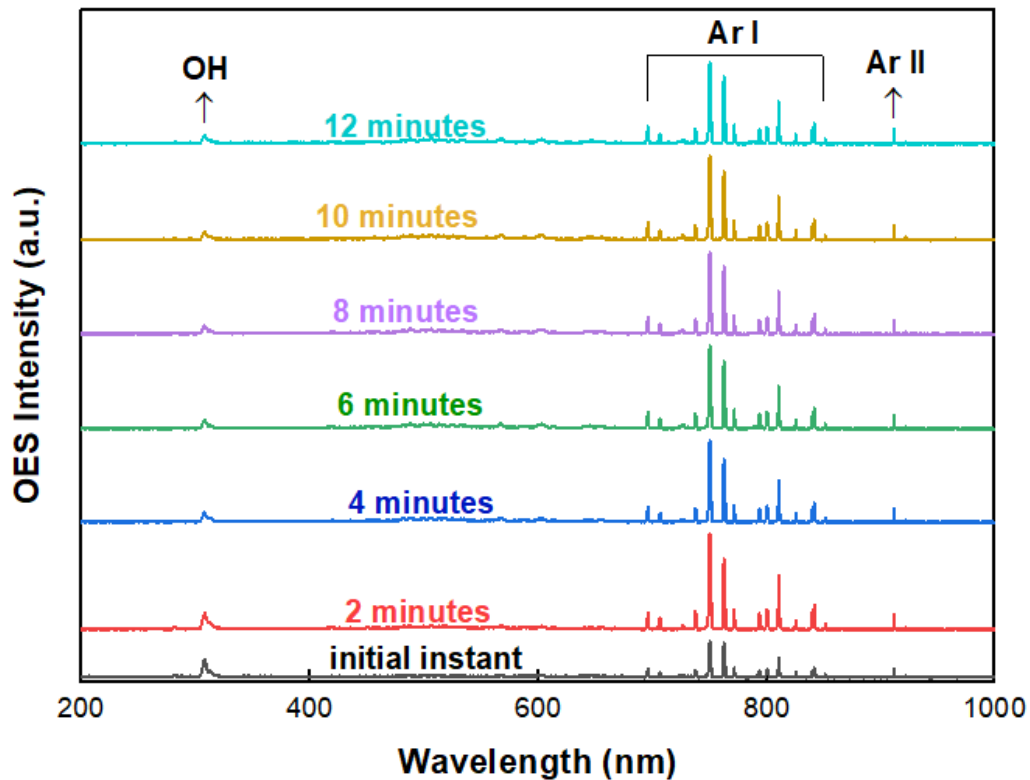


Figure F.1 - OES spectrum of XD generator during time tests.

G. Annex

This annex will be provided additional information regarding the Results and Discussion chapter that could not be incorporated in the main text for lack of space. Here will be presented the data related to the inkjet printing tests. Also, will be presented the tests with silvers generator made by the laser method. All the tests were made in an argon atmosphere.

G. Inkjet printing tests

G.1 (200DPI (first layer) and x2 300DPI (second layer))

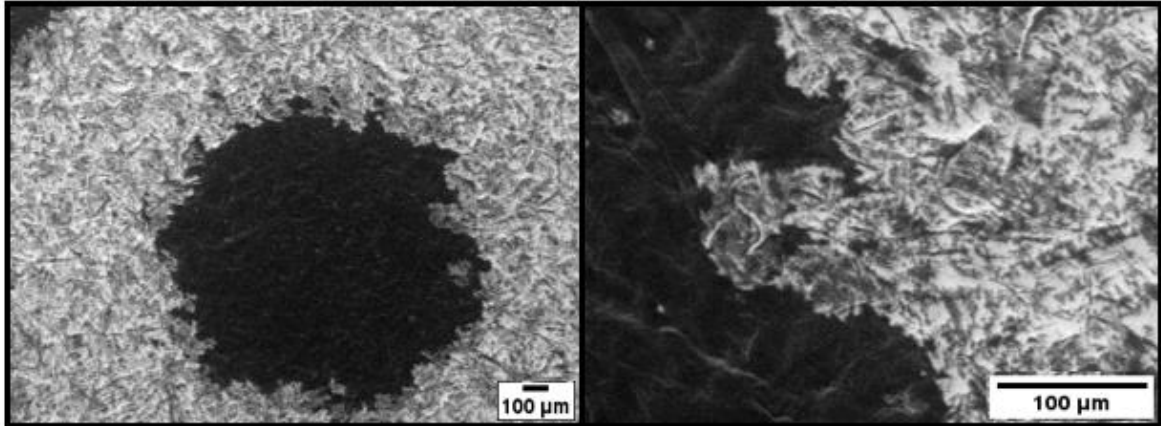


Figure G.1 - SEM images from VEG inkjet (200DPI and x2 300 DPI) generator of the top view before plasma generation.

G.2 400 DPI

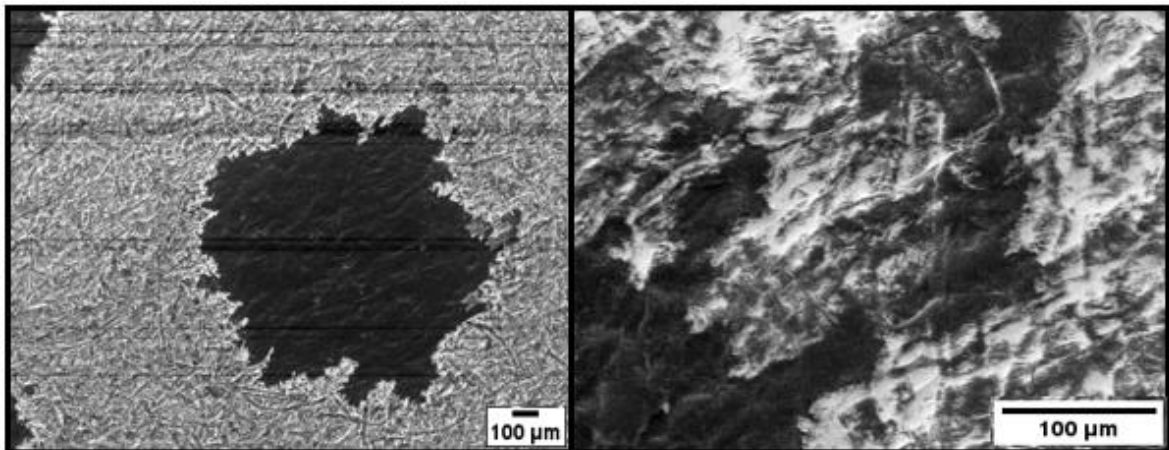


Figure G.2 - SEM images from VEG inkjet (400 DPI) generator of the top view before plasma generation.

G.3 SEM images from the inkjet generator with FS (700 DPI)

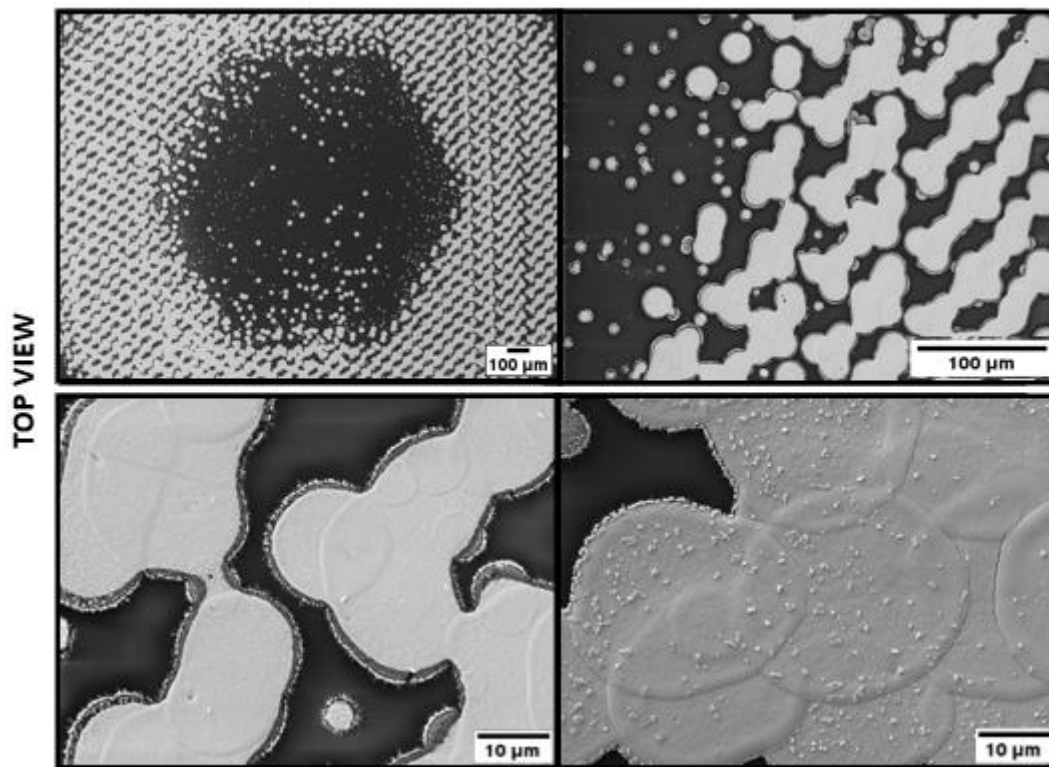


Figure G.3 - SEM images from inkjet generator FS (700DPI) of the top view after the plasma generation.

G.4 OES graphs from the inkjet generators with FS

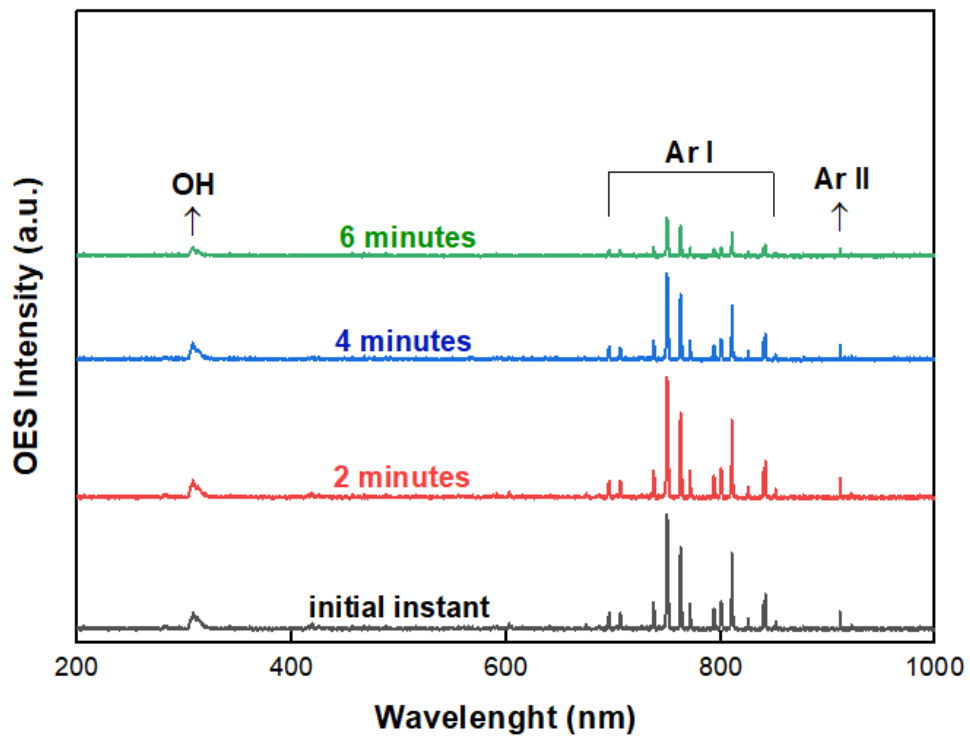


Figure G.4 - OES spectrum of FS inkjet generator 700DPI.

G.5 Test from silver laser-based pattern engraving generators

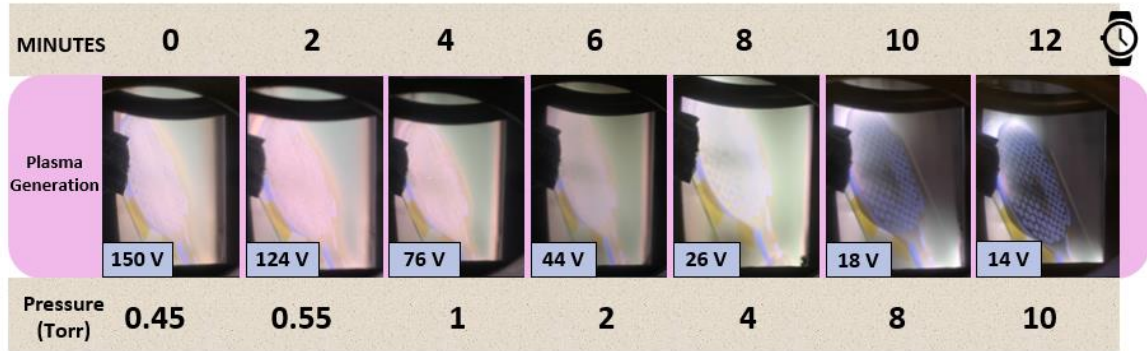


Figure G.5 - Plasma generation tests with the silver FS generator. DC-bias in blue.

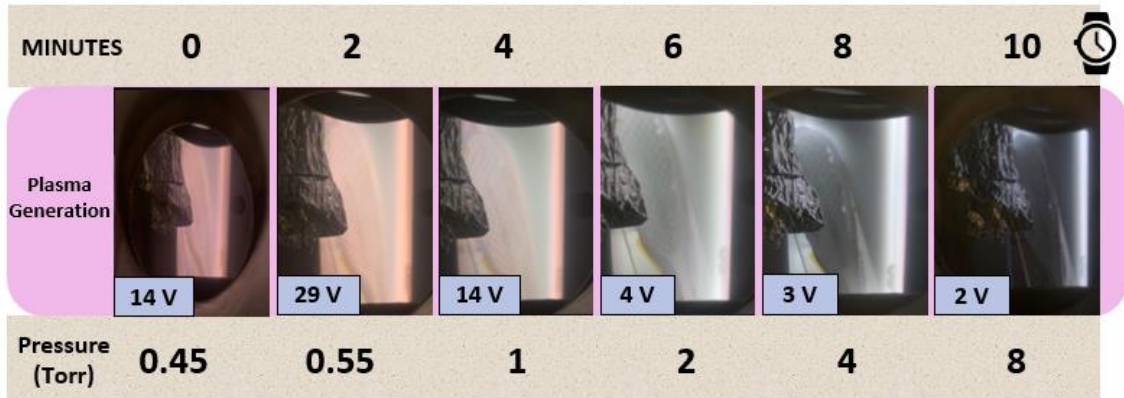


Figure G.6 - Plasma generation tests with the silver VEG generator. DC-bias in blue.

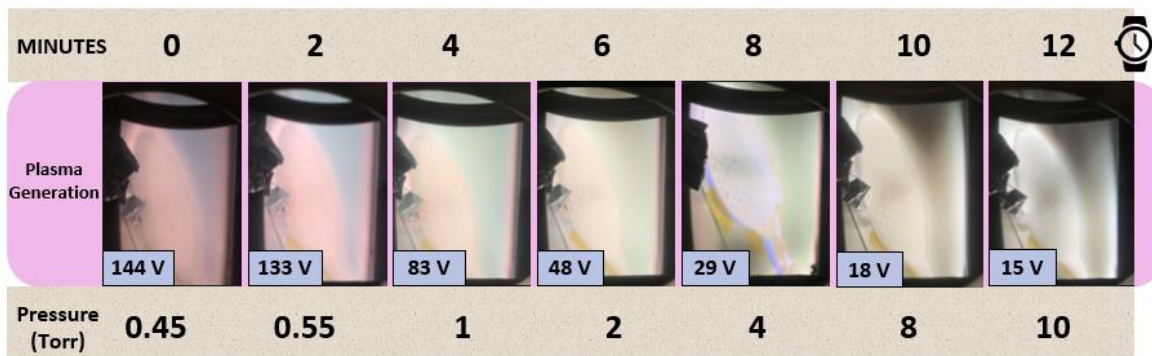


Figure G.7 - Plasma generation tests with the silver XD generator. DC-bias in blue.

G.6 SEM images from the top view of silver generators

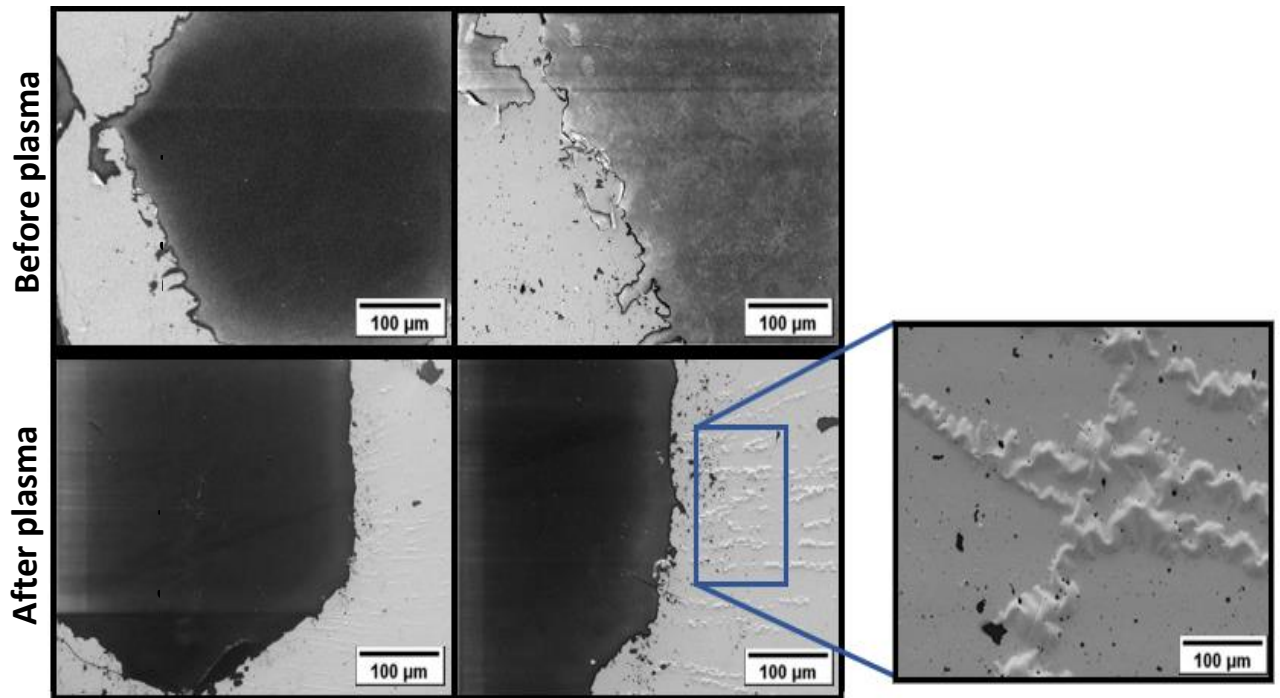


Figure G.8 - SEM images from silver FS generator of the top view before and after the plasma generation.

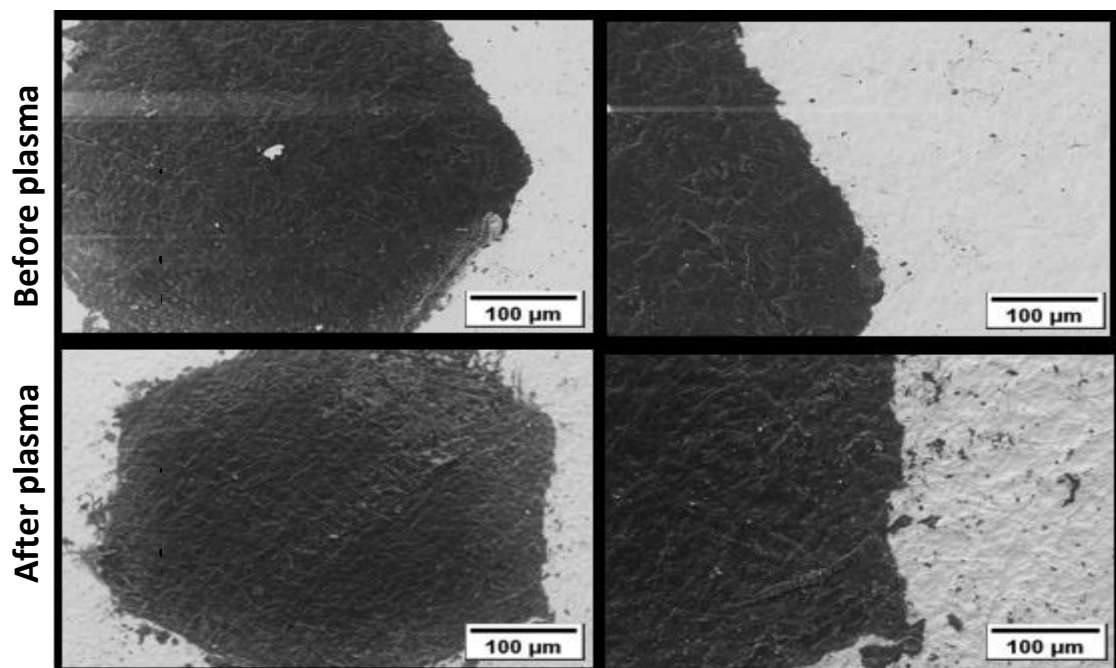


Figure G.9 - SEM images from silver VEG generator of the top view before and after the plasma generation.

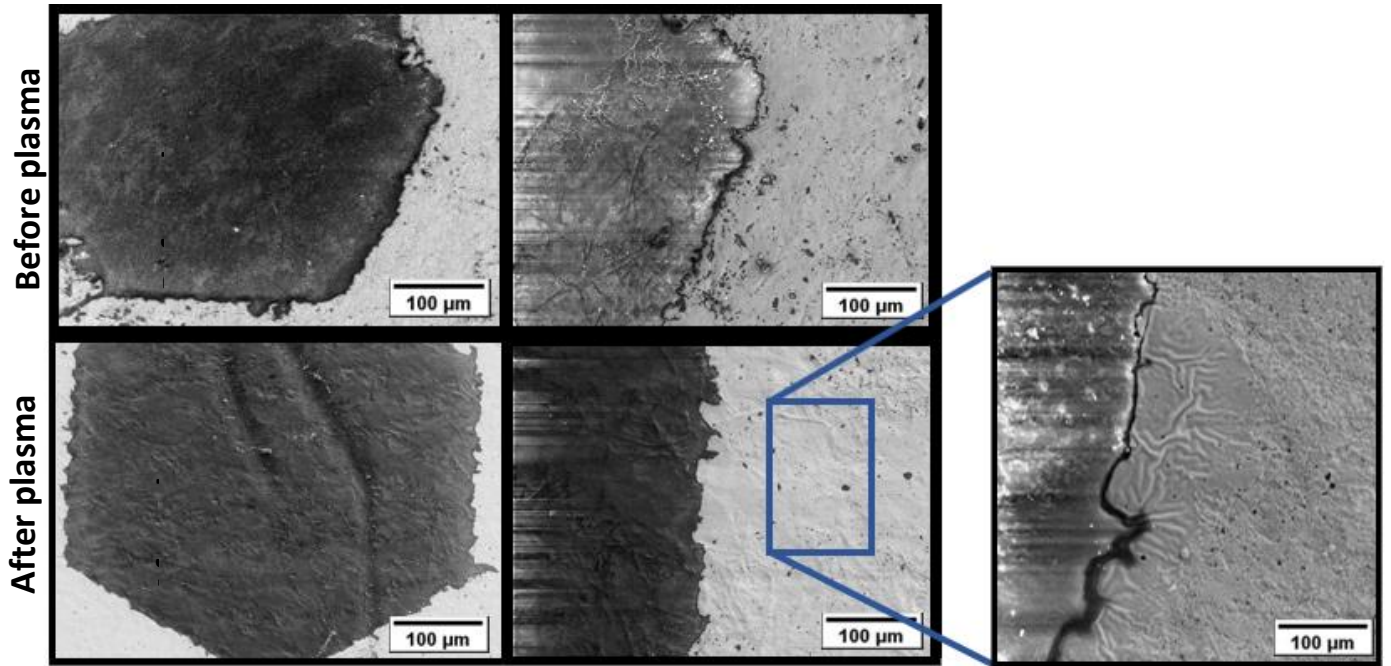


Figure G.10 - SEM images from silver XD generator of the top view before and after the plasma generation.

G.7 OES graphs from the silver generators

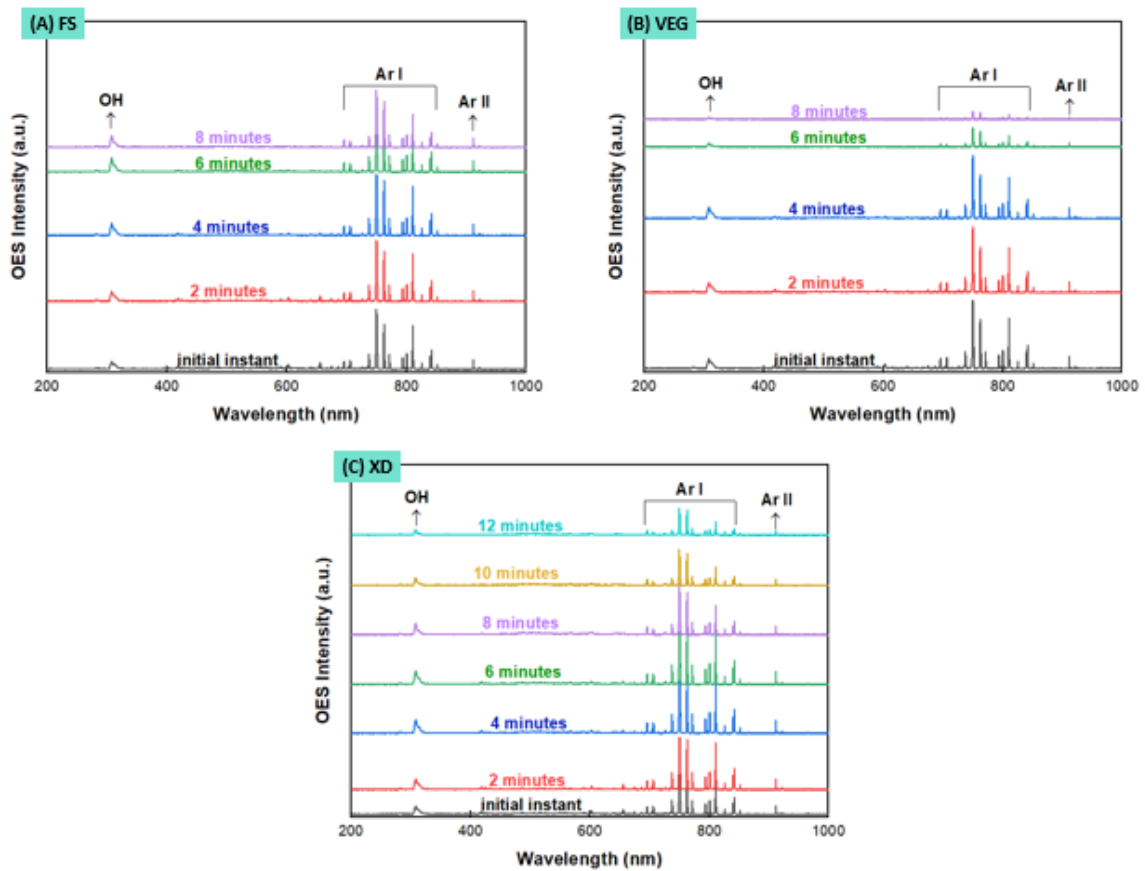


Figure G.11 - OES spectrum of silver generators: (A) FS, (B) VEG and (C) XD.

G.8 Photos of silver FS generator

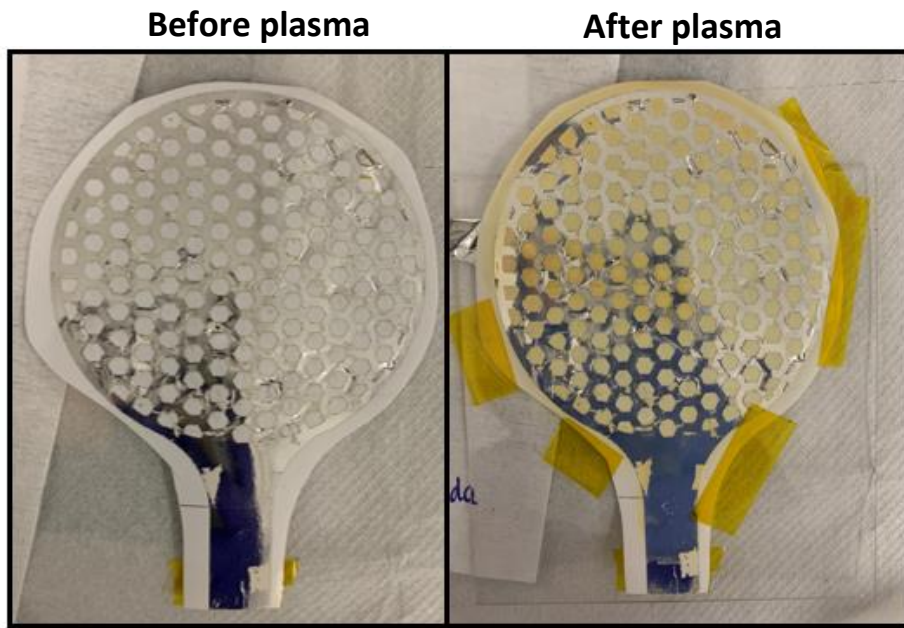


Figure G.12 - Photograph of silver FS generator before and after plasma generation.

G.9 Photos of silver VEG generator

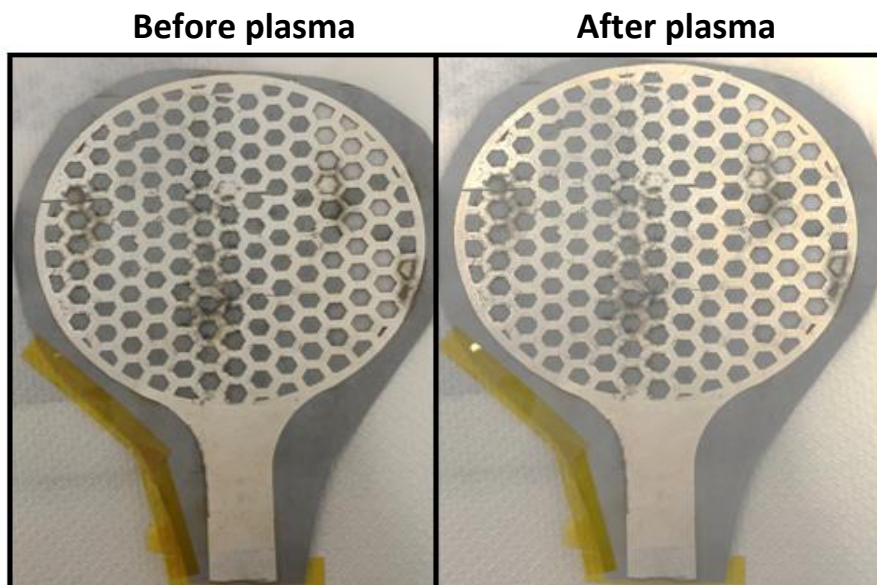


Figure G.13 - Photograph of silver VEG generator before and after plasma generation.

G.10 Photos of silver XD generator

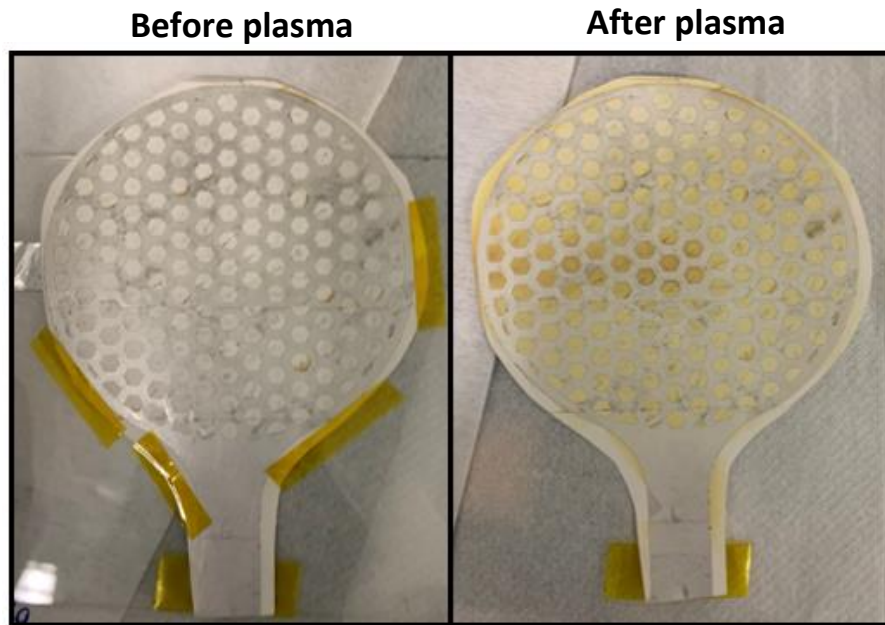


Figure G.14 - Photograph of silver XD generator before and after plasma generation.

H. | Annex

This annex will be provided additional information regarding the Results and Discussion chapter that could not be incorporated in the main text for lack of space. The data relating to the surface modification tests will be presented below.

H. Surface modification study

H.1 Photos of the surfaces studied in the vacuum chamber

Note that the fabric was not used because it was already hydrophilic, and because of that it was not possible to do the contact angle tests.

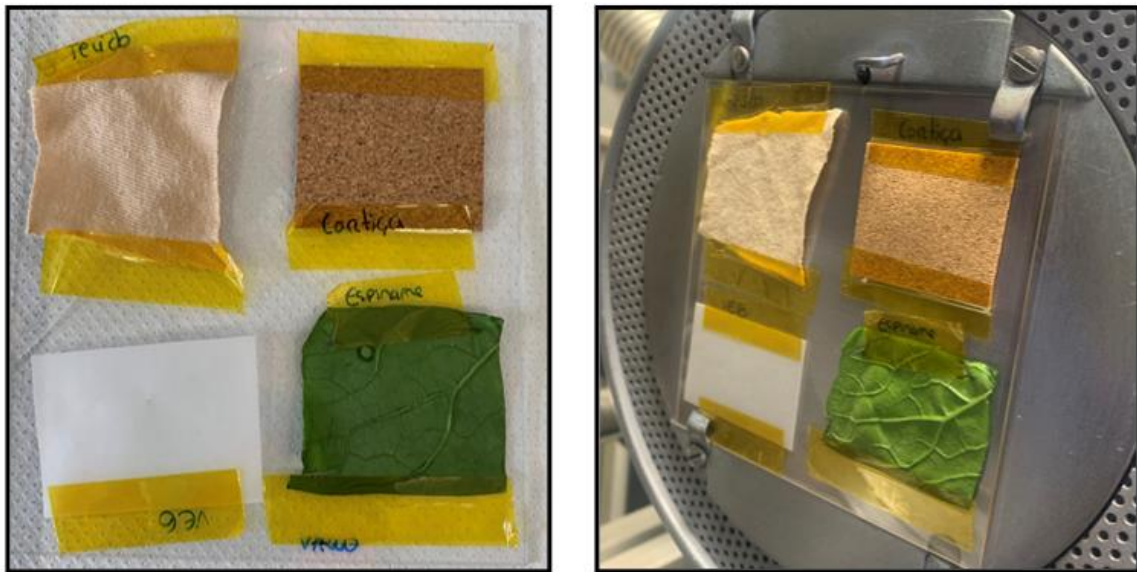


Figure H.1 - Photographs of the different surfaces in the support.

H.2 Time optimization tests on spinach leaf

Intending to understand whether the spinach leaf would undergo any change in its morphology due only to the vacuum's exclusive performance, a 5-minute test was carried out with a pressure of 1.18 Torr. Then, the generator and the spinach leaf were placed in the vacuum chamber's support, and a plasma generation test was executed for 2 minutes, at 3 Torr and 16W. This test is needed to understand what should be the generation time necessary for the following tests. It was realized that 2 minutes was too long because the spinach leaf was destroyed. Thus, 45 seconds were chosen as the maximum plasma generation time.

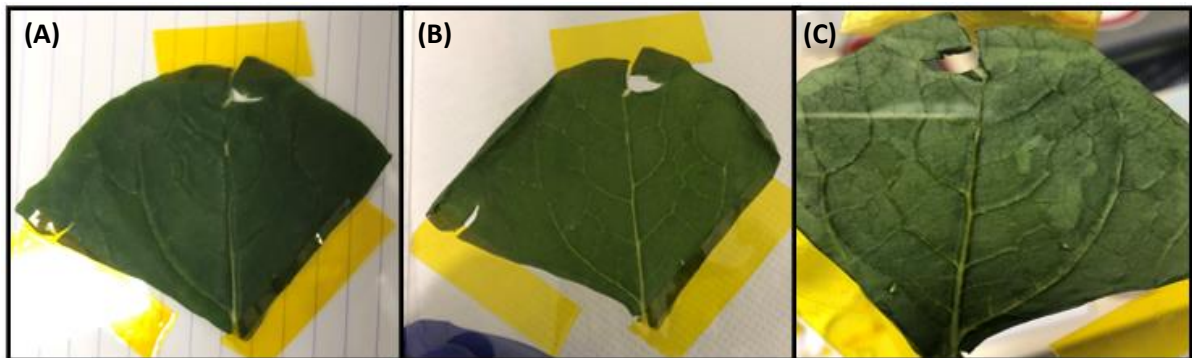


Figure H.2 - Photographs of spinach leaf: (A) Without treatment; (B) with 5 minutes of vacuum; (C) with 2 min of plasma treatment.

H.3 Contact angle as function of plasma treatment time graph

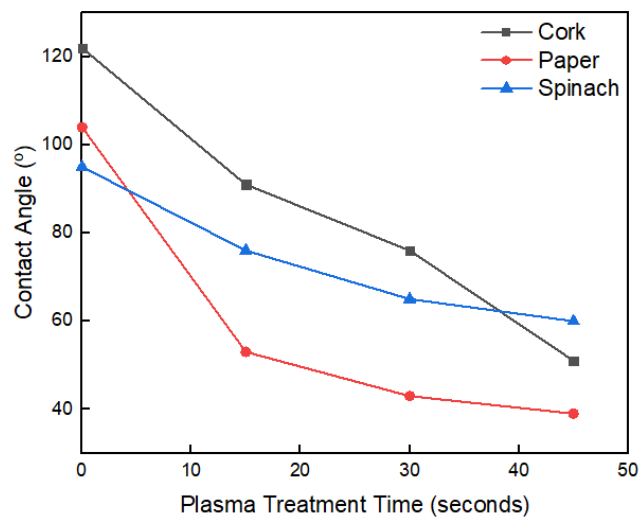


Figure H.3 - Graph of Contact angle in the function of plasma treatment time.